The Pennsylvania State University

The Graduate School

Department of Meteorology

A Method for Diagnosing Surface Parameters Using Geostationary Satellite Imagery and a Boundary-Layer Model

A Thesis in

Meteorology

by

Arthur C. Polansky

Submitted in Partial Fulfillment
of the Requirements
for the Degree of

Master of Science

November, 1982

The Pennsylvania State University

The Graduate School

Department of Meteorology

A Method for Diagnosing Surface Parameters Using Geostationary Satellite Imagery and a Boundary-Layer Model

A Thesis in

Meteorology

by

Arthur C. Polansky

Submitted in Partial Fulfillment
of the Requirements
for the Degree of

Master of Science

November, 1982

We approve the thesis of Arthur C. Polansky.

Date of Signature:

Sept 29, 1982

Toby N. Carlson, Professor of Meteorology, Thesis Advisor

4 Oct 1982

John A. Dutton, Professor of Meteorology, Chairman of the Department of Meteorology

Oct. 4, 1982

Alfred K. Blackadar, Professor of Meteorology

ABSTRACT

A method for diagnosing surface parameters on a regional scale via geosynchronous satellite imagery is presented. The method is a modification of one described by Carlson and Boland (1978). Moisture availability, thermal inertia, atmospheric heat flux, and total evaporation are determined from three infrared images obtained from the Geostationary Operational Environmental Satellite (GOES). The output fields compare favorably with fields generated by the Carlson et al. (1981) method, which uses HCMM data.

Three GOES images - early morning, midafternoon, and night - are obtained from computer tape. Two temperature-difference images are then created. The boundary-layer model of Carlson et al. (1981) is run, and its output is inverted via cubic regression equations. The satellite imagery is efficiently converted into output-variable fields. All computations are executed on a PDP 11/34 minicomputer. Output fields can be produced within one hour of the availability of aligned satellite subimages of a target area.

TABLE OF CONTENTS

TABLE OF CONTENTS (Continued)

LIST OF FIGURES

LIST OF FIGURES (Continued)

LIST OF FIGURES (Continued)

LIST OF TABLES

ACKNOWLEDGEMENTS

In many endeavors, there is an unsung hero, a person whose name is not associated with the final product but without whose effort there would be no final product. The unsung hero of this research is Eileen Perry. For the past year, she has spent at least eight hours per day, five days per week working on this project. She developed and now maintains important parts of the graphics routines used to prepare the figures of Section 4 of this thesis. She maintains the utility programs which select and align subimages from McIDAS satellite-image tapes. She performed the extremely tedious task of selecting the subimages used in this thesis. Were there any justice, this thesis would be hers.

I would also like to express my thanks to:

- The McIDAS facility at the University of Wisconsin through the facilities of the National Satellite Data Service, for supplying HCMM and GOES imagery for this project.
- Ms. A. Giedroc of Tek-Art, Inc., State College, for drafting the figures presented in Section 4.
- Michele Shawver, for a fine job of translating my first draft into readable typewritten copy.
- Professor A.K. Blackadar, for his critical reading of this work.

Finally, my sincere thanks to my thesis advisor, Professor Toby N. Carlson, who has managed to guide me through this research despite my best efforts to procrastinate, drift aimlessly, and become hopelessly lost.

This research was supported by the following grants from the National Aeronautics and Space Administration (NASA):

- Contract No. NAS5-26456 (NASA Heat Flux)
- Grant No. NAG 5-184 (NASA Moisture)

1.0 INTRODUCTION

1.1 THE PROBLEM

Remote sensing of the terrestrial environment has provided earth scientists with a wealth of data, and is beginning to yield economic benefits. Noteworthy are the economic and research benefits derived from weather satellite imagery and LANDSAT imagery. Weather satellites are valuable sources of timely meteorological data for operational forecasters, and are becoming significant data sources for operational numerical weather prediction (NWP). LANDSAT has provided valuable data to economic geologists, cartographers and land-use planners (Short et al., 1976).

The principal operational weather satellites are equipped with two types of sensors: visible-light detectors and detectors sensitive to the thermal emission of the earth (longwave IR). LANDSAT has detectors for visible light and solar infrared reflected from the earth (shortwave IR). Weather satellites may thus be able to study ground properties invisible to LANDSAT by detecting variations in surface infrared emission.

The longwave IR sensors on the Geostationary Operational Environmental Satellite (GOES) and Heat Capacity Mapping Mission (HCMM) satellite measure effective surface blackbody temperature. Several soil properties can be deduced from surface temperature and

temperature change during the daily heating and cooling cycle. A simple energy-balance equation for the earth's surface can be written:

$$S(1-A) + I\downarrow = H_o + LE_o + I\uparrow + G_o \qquad (1.1)$$

where:

S = shortwave flux incident on the surface (insolation)

A = albedo (visible and shortwave IR)

$I\downarrow$ = longwave IR flux from atmosphere, incident on surface

$I\uparrow$ = longwave IR flux emitted by surface

H_o = sensible heat flux from surface to atmosphere

L = latent heat of evaporation

E_o = evaporative flux (mass of water)

G_o = sensible heat flux into the ground

The longwave IR emissivity of the ground is assumed to be 1.

S is determined by geometry, the solar constant, and atmospheric moisture and turbidity. A can be estimated for most land-use categories. The satellite measures a flux related to $I\uparrow$. If the remaining terms can be estimated, soil moisture availability and thermal inertia can be determined.

Soil moisture availability (M) can be defined as the ratio of actual evaporation to the evaporation that would occur from a flat surface of pure water. M influences evaporation (E_o), since M is a direct parameterization of the amount of water available to evaporate. Thermal inertia (P), is defined by the equation:

$$P = (C_g \lambda_s)^{1/2} \qquad (1.2)$$

where:

C_g = ground heat capacity (volumetric)

λ_s = thermal conductivity of the soil

P is a measure of the ability of the ground to store heat during the day and release it at night. G_o is determined largely by P.

In this work, a numerical model is used to provide values of $I\downarrow$, H_o, E_o, and G_o. M and P are input parameters of the model, and are varied over a range of possible values. Model output is then compared with satellite data, and actual M and P values are diagnosed. H_o and E_o values are also obtained, at no extra cost.

1.2 HISTORY

The use of the longwave IR detection capability of weather satellites for remote sensing of soil characteristics is in its infancy. Wetzel and Atlas (1981) have developed a technique for diagnosing soil moisture from morning surface temperature change and windspeed. Dejace and Megier (1979), following Rosema et al. (1978), have mapped soil moisture, ground thermal inertia, and daily evaporation using aircraft measurements of longwave IR and HCMM imagery. Carlson et al. (1981), following Carlson and Boland (1978), diagnosed moisture availability, thermal inertia, and the surface energy budget over two cities, using HCMM data. The above approaches are similar to one another. A computer model of soil and lower atmosphere is run, using a variety of soil characteristics as initial conditions. A set of forecast surface temperatures is generated.

Observed data is then processed, and the model is inverted mathematically, to yield soil characteristics from the observed temperatures. Price (1980, 1982a, 1982b) has adopted a different approach. Surface temperature data are incorporated directly into the basic energy-budget equation for the surface, yielding estimates of soil parameters and evaporation.

This thesis is an extension of Dodd's work (Dodd, 1979), reported by Carlson et al. (1981). The method is similar to the Carlson and Boland (1978) method. Dodd used HCMM imagery to obtain surface temperatures; my work compares HCMM and GOES imagery. Dodd studied a small-scale phenomenon characterized by large differences in surface parameters: the urban heat island. I extend Dodd's technique to studies of regional-scale patterns of surface moisture variability, which I relate to antecedent rainfall differences and crop moisture index variability over agricultural regions.

The method of diagnosing soil parameters from satellite data developed by Carlson is described briefly in Section 2. Several modifications were made in this procedure when GOES imagery was incorporated. These modifications and their implications are discussed in Section 3. Of particular importance are the model sensitivity studies presented in Section 3.6. Two case studies are presented in Section 4. Conclusions and suggestions for future research are collected in Section 5.

2.0 THE CARLSON/DODD METHOD

Quoting from the abstract of Dodd (1979):

> A flexible analysis system has been developed which combines high-resolution satellite-derived radiometric ground temperature information with output from a numerical model of the boundary layer to infer the spatial variation of thermal inertia (P), moisture availability (M), and the surface energy budget.

The system consists of three basic phases:

1) Data acquisition and preprocessing

2) Numerical boundary-layer simulation

3) Production and display of output fields

Satellite images are received on magnetic tape. Utility programs LONLAT and REGGIE are run to select subimages of identical size, shape, and geographical location from a day-night HCMM image pair. Also, the raw satellite intensities are converted into effective surface temperatures, using atmospheric moisture values obtained from soundings.

A one-dimensional numerical model developed by Carlson and Boland (1978) is used to simulate atmospheric and ground response to insolation. The model and its use in Dodd's study is completely described in Section 2.1 of Dodd (1979), and will not be repeated here.

Model simulations are run for 16 ordered pairs of (M, P) values. Output from the model at simulated satellite overpass times is

passed to a regression routine. Regression equations for M, P, H_o, and total evaporation (E) are produced, using surface temperature at satellite overpass times as the predictors. Biquadratic regression equations omitting the cross-product term were used in Dodd (1979). The regression equations derived from the numerical model are then used to convert the satellite subimages into output images of M, P, H_o, and E. The output images are then plotted or displayed on a graphics terminal. For a complete discussion of this method, refer to Section 2 of Dodd (1979). Henceforth, this procedure will be abbreviated CD.

Note the following features of CD:

1) CD utilized HCMM data. Only two image times per day were used: approximately 1400 and 0200 local time.
2) The postprocessing phase produced biquadratic equations in midafternoon temperature (TD) and night temperature (TN). Higher-degree regression equations were not used.
3) CD was implemented on a mainframe computer, Penn State's IBM 370/3033. The numerical model and regression routines in particular had to be submitted as batch-processing jobs. Slow turnaround and the mechanics of batch job submission rendered interactive use of the model impossible.

These are the principal features of CD which have been modified to produce the system to be described in Section 3, the GOES method.

3.0 THE GOES METHOD

3.1 THE PROBLEM

CD uses HCMM polar-orbiter data to diagnose M, P, H_o, and E over small areas. Dodd (1979) studied the urban complex. Kocin (1979) estimated M over a small rural watershed. Carlson and DiCristofaro (1981) discussed the applicability of diagnosed H_o in estimating plume spread over urban and rural areas. In these studies, the target area was on the order of 10^3 to 10^4 km^2. For other applications, such as regional crop assessment, target areas on the order of 10^5 to 10^6 km^2 may need to be studied. Either CD should be demonstrated successfully on this larger scale (henceforth called 'regional scale'), or another method should be devised to handle regional-scale domains.

As Kocin (1979) noted, studies of the development of M and P anomalies with time are difficult using polar-orbiter data. Due to its orbital parameters, HCMM provides a day/night image pair only once per 16 days for target areas in midlatitudes. The situation is similar with TIROS N, but not quite as restrictive. Cloud cover at either image time can render the affected image pair unusable. Thus, diagnoses of M, P, H_o, and E derived from HCMM images, using the CD method, can have no better time resolution than 16 days. For studies of the time-dependent behavior of soil parameters, a different data source is desirable.

CD was restricted to two image times per day, since HCMM never scanned an area in midlatitudes more than twice in a day. However, the HCMM overpass times, approximately 1400 and 0200 local solar time, were close to ideal, given the restriction of only two image times per day (Carlson and Boland, 1978). These optimum times occur near the times of maximum and minimum surface temperature, respectively. If observations of surface temperature were available more frequently during the diurnal cycle, better diagnoses of M, P, H_o, and/or E might have been possible. Wetzel and Atlas (1981) suggest that the time derivative of temperature may be better correlated with M than the actual temperature. The possibility that additional data could improve the CD method is certainly worth investigating.

In this thesis, a modification of CD is presented which uses GOES images instead of HCMM images for surface temperature data. The greater spatial and temporal availability of GOES data addresses the problems cited above. The rationale behind the use of GOES imagery is described in Section 3.2. Theoretical justification is presented in Section 3.3, and practical considerations are considered in Section 3.4. Section 3.5 discusses the image-differencing feature of the GOES method. An extensive series of quality and sensitivity tests were run on the GOES method; the results are reported in Section 3.6.

3.2 WHY USE GOES IMAGERY?

CD is theoretically valid only when:

1) HCMM provides a day/night image pair of the target area

2) nonadvective conditions prevail

3) skies are clear

Obtaining all three conditions simultaneously over an area of interest can be a major challenge. Obtaining all three simultaneously on a regular basis over a period of months is a forlorn hope. Even fulfilling condition (1) alone is difficult. Dodd (1979) used a night/day image pair in both his urban complex cases. Kocin (1979) used an image pair (June 9-10) in which the night overpass time was 36 hours before the day overpass time -- a departure of 48 hours from the modeled night overpass time. GOES imagery is available every day; HCMM image pairs are available only once per 16 days. If GOES data are used, the assumption that nonadvective conditions last more than a day is never necessary; if HCMM data must be used, this assumption of stationarity must often be made (as in Kocin, 1979). If GOES data are used, no one day is crucial. If clouds cover the sky or advection is significant on any particular day, the next day's data can be used. With HCMM data, clear skies and nonadvective conditions on a day/night overpass-pair day are crucial: the next day/night pair is not available for over two weeks. Even under the restriction that we must use images at 1400 and 0200 local standard time (LST), GOES imagery provides sixteen times the chance of meeting the three criteria listed above.

GOES imagery is produced every 30 minutes. This greater availability of imagery adds another dimension of flexibility to the diagnostic technique. GOES imagery can be used to diagnose relevant variables even if:

1) skies are partly cloudy
2) the clouds do not cover enough of the sky long enough to invalidate the energy budget calculations of the model
3) the clouds are moving fairly rapidly

HCMM imagery would almost certainly fail under these conditions. With either source of imagery, areas obscured by clouds at any image time used must be discarded. With HCMM, only two image times exist, and both are needed for CD. Soil parameters could not be diagnosed at any point where there were clouds at either HCMM overpass time. With GOES imagery, there is flexibility in choice of image times. If a crucial spot is covered by clouds at one image time, a previous or subsequent image could be used (but see Sections 3.4 and 3.6). Also, if hardware or software failure causes one GOES image to be lost, a subsequent or previous image could be used. Such a failure could cause a HCMM case to be discarded.

The greater availability of GOES data allows a more fundamental change in CD. There is no need to restrict the diagnostic method to two images or to any particular image times if GOES data are used. There are 48 GOES image times per day; in principle, there are 2^{48} possible sets of image times which could be used.

Incorporating GOES data into the CD diagnostic method provides the following advantages:

1) more days with images at convenient times

2) greater flexibility in selecting image times.

3) the option to use more than two images in the method

These advantages must be weighed against the disadvantages of using a geostationary platform instead of a platform in low earth orbit:

1) poorer resolution (larger pixel size)

2) greater distortion of the image, due to the curvature of the earth

For regional-scale studies, the advantages outweight the disadvantages. For high-resolution, small-scale studies, HCMM data probably should be used, if available. The greater flexibility resulting from the use of GOES data may be important even for small-scale studies.

3.3 THE GOES METHOD: THEORETICAL JUSTIFICATION

CD used two images per day because only two were available. Wetzel and Atlas (1981) implied that the choice of image times and particularly the number of images used in CD may not be optimal. With the greater data base provided by the GOES satellite, the restrictions on image times encountered in CD are removed. Consideration of the effects of M and P on the daily march of surface temperature suggests that three or four images per day should produce superior diagnoses. The reasoning leading to this conclusion is outlined in this section.

M is a measure of the amount of water available for evaporation. It therefore plays an important role in the partitioning of energy between sensible heat flux and latent heat flux during the day. A high M value implies more evaporation, and less sensible heat to be distributed between ground and air. Carlson and Boland (1978) and Wetzel and Atlas (1981) showed that the effect of M on surface temperature is greatest during the morning. In the morning, available moisture will be evaporating, and the mass of the air beneath the decaying nocturnal inversion will be small. A relatively small change in the ratio of latent to sensible heat can produce a relatively large change in the morning temperature rise, since the heat capacity of a thin layer of air is small. In the afternoon, the boundary layer reaches its greatest thickness. Temperature rise is slower, since the thick layer has a larger heat capacity. The magnitude of the temperature rise becomes less sensitive to M. At night, evaporation ceases or becomes negative; M becomes indeterminate and its effect is inconsequential.

P is a measure of the ability of the ground to store heat during the day and release it at night. The effect of P on surface temperature should be most pronounced during early evening. As insolation decreases and the surface begins to cool, atmospheric convection subsides. The atmosphere tends to decouple from the surface, particularly if the wind is light. The surface cools more rapidly than the atmosphere, since the surface is a better radiator than the air. During the evening, stored heat from below must supply

most of the energy radiated from the surface to space. A large P value implies relatively large amounts of heat will be stored in the soil, and that there is sufficiently large thermal conductivity to allow the heat to reach the surface from below. Large P implies slow cooling of the surface. Later at night, the downward thermal emission from the relatively warm atmosphere partially compensates for the radiative loss from the surface. If wind and stability conditions are right, an increase in wind speed above the surface layer will occur. Low Richardson-number conditions will develop, producing turbulent transfer of heat to the surface. P remains important in determining surface temperature throughout the night, but its relative importance decreases as the night progresses.

The analysis of the effect of P on surface temperature during the day is more difficult. Certainly, if energy is released at night, it must be stored during the day. As the sun rises and insolation increases rapidly, P must have a strong effect on surface temperature. However, as surface temperature rises, the atmosphere becomes convectively coupled to the ground. This coupling enhances evaporation and atmospheric heat flux. Each flux increases at its own rate as the morning progresses. In the early morning, when surface temperature is most sensitive to variations in the magnitude of heat sinks, latent heat flux and atmospheric heat flux are both significant and both varying. Ground heat flux tends toward a minimum during this period (Sellers, 1965). The effect of P tends to be masked by the effects of M and H_o. CD model simulations

(Carlson and Boland, 1978) show that P is more closely correlated with night temperature than with midafternoon temperature.

3.4 GOES METHOD: PRACTICAL AND NUMERICAL CONSIDERATIONS

As stated in Section 3.3, M is closely related to morning temperature rise; P is probably closely related to evening temperature fall. With only two image times available, it is not possible to express both these rates of change. The success of the CD method under the data-availability restrictions of HCMM is encouraging. With GOES imagery, we have the freedom to use more images and different combinations of image times, to capture any portions of the diurnal march of temperature that might be useful. Three image times could be used:

1) early morning, just after sunrise
2) midafternoon
3) near midnight

Alternatively, four images could be used to isolate the two temperature changes which should be most closely related to M and P:

1) early morning
2) late morning
3) midafternoon
4) near midnight (late evening)

In principle, all 48 GOES images for a given day could be used. There are several fundamental problems with the use of multiple imagery in CD-type models. These problems are linked to uncertainties, errors, and approximations characteristic of all numerical models and

remote-sensing instrumentation. In this section, we consider the practical and numerical restrictions on the use of imagery in the diagnostic model.

Although the HCMM and GOES satellites both have high-quality radiometers, both have limitations in resolution and accuracy. These limitations are more severe for GOES. Both must view the earth through an atmosphere containing a variable amount of water vapor and a variable vertical temperature profile. Corrections for water-vapor absorption are applied to the raw satellite data, greatly reducing errors but not eliminating them. The effect of thin cirrus clouds on the quality of satellite imagery is difficult to assess.

The satellites detect thermal infrared radiation (longwave IR) incident from below. A narrow band of wavelengths is measured to minimize atmospheric interference. The emission is converted to a temperature by inverting the blackbody radiation equation (Goody, 1964, Sec. 2.2, Eq. 2.35-2.37):

$$B_\lambda = \frac{C_1 \lambda^{-5}}{e^{C_2/\lambda\theta} - 1} \tag{3.1}$$

where:

B_λ = Planck function at wavelength λ (energy flux per unit of wavelength)

$C_1 = 2\pi hc^2$

$C_2 = hc/k$

h = Planck's constant

c = speed of light

k = Boltzmann's constant

θ = thermodynamic (absolute) temperature

This temperature is assumed to be the surface temperature. True surface temperature is the temperature of the earth's surface: the temperature of the infinitesimal layer of condensed-phase matter forming the lower boundary of the atmosphere. True surface temperature, unlike the conventional surface air temperature, is difficult to measure. A thermometer placed in a standard instrument shelter 1.3 meters above the ground measures the surface air temperature, by definition. The reading will be fairly independent of the construction of the thermometer and the shelter, within reasonable limits. If a thermometer is placed in direct sunlight on the surface of the earth, a temperature can be recorded. However, this temperature will be influenced as much by the properties of the thermometer as by the temperature of the surface which the thermometer obscures and possibly deforms. In a vegetated region, surface temperature is hard to define; its measurement may be an intractible problem. One could debate where or what the 'surface' is: is the surface the top of the plants in a particular area, or is it at some level in the canopy? Hand-held IR radiometers can be used to measure surface temperature. They reveal significant small-scale variability. Cooper (1981) reports that a single point on a vegetated surface will have a range of 'observed' temperatures: observed IR temperature is a function of the orientation of the instrument and configuration of the canopy in many cases.

The boundary-layer model used in CD is comparable to many one-dimensional models, but is nevertheless only an approximation. It is one-dimensional; the atmosphere is three-dimensional. The model is discrete in space and time; the atmosphere is continuous. The atmosphere is not limited by approximate physics, and is not subject to truncation error and closure assumptions. The model output is converted into regression equations, to invert the model mathematically. These regression equations represent the model well, but not perfectly.

The problem of diagnosing the surface parameters reduces to the problems encountered in using:

- regression equations instead of actual model runs
- an imperfect numerical model
- imperfect satellite measurements
- 'surface temperature' - a quantity which may not be definable, and therefore, not measurable

In addition, we must assume that the 'surface temperature' used in the numerical model is the same physical quantity as the 'surface temperature' observed by the satellite. The errors and uncertainties inherent in these problems have significant numerical implications.

These uncertainties place several restrictions on the choice of image times and analysis techniques which may be used in a GOES-based diagnostic model. The principal restrictions involve the interval of time between image times, and the total number of images which can be used.

To obtain an estimate of the midmorning time-derivative of surface temperature, it is necessary to use a pair of image times

bracketing midmorning. In theory, the smaller the time interval between the two images, the better the approximation to the derivative. In practice, with uncertain data and uncertain model output, a short time interval between images will produce a very poor estimate of the derivative. Refer to Appendix I, Section 1 for details. Image times several hours apart are needed, to guarantee a large temperature change between image times. Errors in the estimate of the derivative introduced by the nonlinearity of temperature as a function of time must be accepted. Figure 3.1 (from Wetzel and Atlas (1982) after Schmugge et al. (1978)) shows that morning temperature rise and evening temperature fall are close enough to linear to permit finite-difference approximations to derivatives using data times several hours apart.

The temperatures at the image times become the predictors in a multivariate polynomial regression equation foe each diagnosed variable. Numerical constraints on the number of image times and the permissible degree of the regression equations are discussed in Appendix I, Section 2. To avoid overfitting the model output, it is necessary to restrict the total number of regression coefficients and the degree of the regression equations.

To maximize the actual temperature differences between images while minimizing the total number of images used, the following image times were selected:

1) early morning;

2) midafternoon (near daily temperature maximum);

3) around or after midnight.

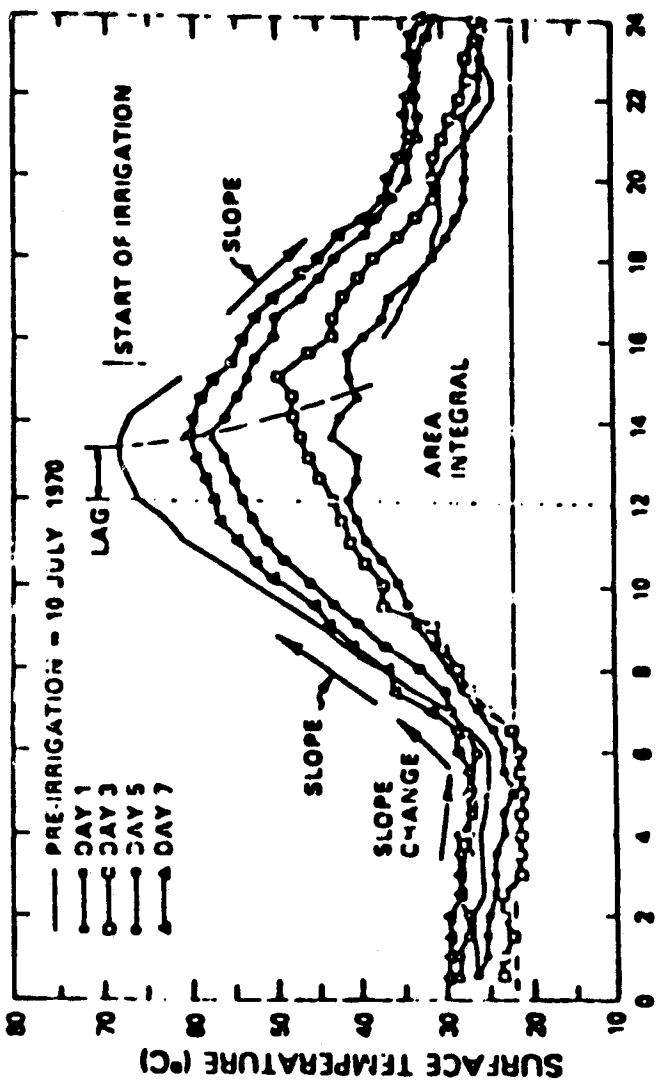

Diurnal variation of surface temperature over a bare soil field as measured by a Thermocouple. Indicated are some of the parameters measurable from geosynchronous satellites which are sensitive to soil moisture. Data reproduced from Schmugge et al. (1978).

Figure 3.1: Wetzel and Atlas (1981), Fig. 1.

Preliminary testing was done, simulating the use of two images (CD) and four images, as well as simulating the above image times. The three-image simulation was superior to the two-image simulation. A four-image simulation, using late-morning and mid-late-afternoon instead of the midafternoon time, provided no improvement over the three-image simulation. Since numerical difficulties and cost increase as the number of images increases, the three-image method was adopted.

3.5 IMAGE DIFFERENCING

The three images used as input to the GOES method are differenced, producing two temperature-change fields:

DTD = (midafternoon temperature) - (early-morning temperature)

DTN = (midafternoon temperature) - (night temperature)

There are three reasons for performing this difference, as will be explained in this section:

1) to approximate the derivative of temperature
2) to reduce numerical errors
3) to correct for large-scale temperature variability across the target area

It has been shown that M and P are strongly correlated with $\frac{\partial T}{\partial t}$. DTD is a crude approximation to $\frac{\partial T}{\partial t}$ at midmorning. DTN is a crude approximation to $\frac{\partial T}{\partial t}$ in the early evening. In Section 3.4, it was shown that these crude approximations are adequate and that better approximations may be unattainable. If $\frac{\partial T}{\partial t}$ is to be used to

diagnose M and P, $\frac{\partial T}{\partial t}$ itself must be estimated from satellite data. Numerically, DTD and DTN are probably the best estimates of $\frac{\partial T}{\partial t}$ obtainable from satellite data at the present time.

Using DTD and DTN as predictors, a bicubic regression equation of the following form can be used:

$$X = a_{00} + a_{11}DTD + a_{12}DTN + a_{21}DTD^2 + a_{22}DTN^2 + a_{31}DTD^3 + a_{32}DTN^3 \quad (3.2)$$

There are seven regression coefficients. Were three temperatures to be used, ten coefficients would be needed for a cubic regression equation. It is unclear whether the additional coefficients could be added to the regression equation without overfitting the data. Using differenced fields appears to be the best way of taking advantage of a higher-order regression equation.

When three quantities are mapped into two, some information is inevitably lost. In this case, when three temperatures are mapped into two differences, the information discarded contain a potential source of error. The information discarded when computing DTD and DTN is contained in the mean: $1/3\ (T_1 + T_2 + T_3)$.

The target areas for the studies presented in Section 4 are several hundred km in longest dimension. Over distances that large, it would not be unusual to find systematic temperature differences, even in relatively uniform air masses. The numerical model used to simulate the boundary layer over these areas is one-dimensional. Horizontal temperature differences cannot be modeled. Only one initial surface temperature and only one initial sounding can be used. If the target area is dominated by a relatively uniform air

mass, the vertical structure of the lower atmosphere will be similar throughout the region. Soundings from various points in the target area would have similar profiles when plotted on skew-T/log-P charts. In the absence of advection, any two points in the region with identical surface characteristics should experience the same temperature rise and fall during a 24-hour period. However, one of these points could be a few degrees cooler or warmer than the other point throughout the period. Consider an extreme example. Let the surface temperature be 300 K at point A in the region, and let the surface temperature be 305 K at point B in the region, several hundred km from A. Assume identical surface characteristics at the two points. Also assume clear skies and negligible advection throughout the region. Assume that the soundings at the two points have similar shapes in the lower 200 mb: sounding A is uniformly 5 K cooler than sounding B. Let both points receive the same total insolation. Will the surface temperature difference between point A and point B vary significantly with time?

The term in the surface energy budget equation (Eq. 1.1) most directly dependent on surface temperature is $I\uparrow = \sigma T^4$. G_o and H_o depend on vertical temperature gradients in ground and air, respectively. E_o depends on surface temperature, vertical temperature gradient, relative humidity, and vertical moisture gradient. We will ignore the absolute-temperature dependency of E_o here, with ample justification. The 5 K temperature difference between points A and B represents a difference of $(305/300)^4$, or a factor of 1.068 in

total radiation emitted from the surface. If we make the reasonable assumption that vertical gradients of temperature and moisture are the same at A and B, we can ignore effects due to G_o, H_o, and E_o. As a rough estimate, assume that DTD is directly proportional to energy surplus at the surface. A 7 percent change in I↑ might then produce a 7 percent change in DTD. If DTD = 35 K at point B, then DTD at point A would be 1.07(35) = 37.45 K, a difference of about 2.5 K.

It is important to note that I↑ is not the only term in Eq. 1.1 which depends on absolute temperature. I↓ depends on an effective average temperature of the atmosphere. If we assume that this average atmospheric temperature ($\overline{T}_a$) at B is 5 K higher than at A, I↓ at B will be larger than I↓ at A. The compensation will not be perfect, since $\overline{T}_a < T$ in most cases, and the effective emissivity of the atmosphere differs from the effective emissivity of the surface. The compensation will be significant. In a numerical simulation, using the boundary-layer model, lowering all input temperatures by 5 K lowered all output temperatures by about 5 K. DTD and DTN changed by about 0.5 K.

Since a temperature gradient on the order of 1 K/100 km produces a variation of only about 0.5 K in modeled surface temperature change in a regional-scale study, the effect of large-scale temperature gradients on the GOES method is unimportant. If there is a large enough temperature difference across the target area to produce unacceptable errors in modeled DTD and DTN due to radiative effects, the nonadvective assumption will be invalid and the GOES method cannot be used.

3.6 GOES METHOD: SENSITIVITY AND ACCURACY STUDIES

In any 24-hour period, there are 17296 distinct ordered triplets of GOES times. Even if the choice of GOES-time triplets is restricted to a morning image, midafternoon image, and a night image around or before local midnight, there are nearly 1000 possible triplets. This section describes the selection of GOES time triplets which can be used in the GOES method, subject to the data quality and numerical restraints considered in Section 3.4. A method for evaluating GOES triplets is presented in Part 1. The results of the evaluation are tabulated in Table 3.1 and are discussed in Part 2.

3.6.1 An Evaluation Method for GOES Time Triplets

The best way to evaluate the performance of a numerical model is to test it against actual data:

- Gather accurate data for several contrasting situations
- Simulate each situation numerically
- Compare numerical results with observations

This procedure could not be followed for the GOES method. M, P, H_o, and E are difficult to measure. It would be logistically impossible to measure them on the regional scale. Even a set of local measurements in several selected locations would have proven economically infeasible. The difficulties in measuring (or even defining) surface temperature have been mentioned in Section 3.4. The numerical difficulties described in Section 3.4 must also be considered. A model simulation which provides satisfactory results with high-quality ground-based temperature measurements might fail when

Table 3.1A

Sensitivity Testing Summary: M

GOES Times (LST) 1	2	3	Output Value M=.5	$\frac{\partial M}{\partial DTD}$	$\frac{\partial M}{\partial DTN}$	Worst Storage Error M=0.5	r^2 Percent
06	14	23	.5541	-.1593	.1029	.1043	98.0
07	14	23	.4726	-.1387	.0674	.0808	95.3
08	14	23	.4972	-.1383	.0135	.0595	90.2
09	14	23	.4996	-.1992	-.0191	.0861	94.1
10	14	23	.4901	-.2714	-.0389	.1216	92.6
11	14	23	.4997	-.3689	-.0333	.1603	89.4
07	09	23	.6034	-.2739	.1428	.1652	89.5
07	10	23	.5839	-.2269	.1238	.1393	91.4
07	11	23	.5764	-.1930	.1079	.1195	93.4
07	12	23	.5406	-.1709	.0938	.1048	95.2
07	13	23	.5510	-.1520	.0885	.0948	96.1
07	14	23	.4726	-.1387	.0674	.0808	95.3
07	15	23	.4803	-.1454	.0419	.0743	91.7
07	16	23	.4933	-.1553	.0249	.0714	93.2
07	17	23	.5109	-.1958	-.0125	.0829	92.9
07	18	23	.5613	-.2113	-.0141	.0909	87.5
07	19	23	.5217	-.2225	-.0735	.1073	86.3
09	12	23	.5093	-.2167	.0188	.0942	91.3
09	13	23	.5061	-.2078	.0003	.0832	92.8
09	14	23	.4996	-.1992	-.0191	.0873	94.1
09	15	23	.4932	-.2044	-.0406	.0980	92.9
09	16	23	.5028	-.2093	-.4170	.2505	91.5
07	14	16	.5736	-.0912	.1236	.0964	93.6
07	14	17	.5907	-.0966	.0945	.0800	94.1
07	14	18	.5384	-.1119	.0787	.0772	93.7
07	14	19	.5523	-.1169	.0748	.0762	93.4
07	14	20	.4789	-.1323	.0622	.0769	94.4
07	14	21	.5186	-.1273	.0696	.0776	93.9
07	14	22	.4507	-.1739	.1090	.1117	94.8
07	14	23	.4726	-.1387	.0674	.0808	95.3
07	14	24	.5417	-.1371	.0726	.0821	95.6
07	14	25	.4528	-.1491	.0673	.0847	95.8
07	14	26	.4945	-.1069	.0258	.0511	96.0
07	14	29	.5009	-.1409	.0564	.0758	96.1

Table 3.1A (Continued)

Sensitivity Testing Summary: M

GOES Times (LST) 1	2	3	Output Value M=.5	$\frac{\partial M}{\partial DTD}$	$\frac{\partial M}{\partial DTN}$	Worst Storage Error M=0.5	r^2 Percent
08	11	23	.5596	-.2129	.0733	.1106	95.3
08	12	23	.5090	-.1540	.0533	.0793	94.9
08	13	23	.4951	-.1521	.0295	.0715	89.7
08	14	23	.4972	-.1383	.0135	.0695	90.2
08	15	23	.5021	-.1638	-.0082	.0684	92.9
08	16	23	.4802	-.1875	-.0415	.0911	93.0
08	17	23	.5190	-.2090	-.0435	.1003	91.7
08	18	23	.5230	-.1708	-.0798	.0964	90.9

Table 3.1B

Sensitivity Testing Summary: P

GOES Times (LST) 1	2	3	Output Value M=.5	$\frac{\partial M}{\partial DTD}$	$\frac{\partial M}{\partial DTN}$	Worst Storage Error M=0.5	r^2 Percent
06	14	23	.06529	.00589	-.01140	.00700	99.3
07	14	23	.06709	.00469	-.00989	.00584	98.4
08	14	23	.06556	.00472	-.00824	.00523	98.1
09	14	23	.06549	.00807	-.00722	.00723	99.5
10	14	23	.06817	.01034	-.00618	.00666	99.7
11	14	23	.06699	.01326	-.00614	.00781	99.5
07	09	23	.06159	-.00595	-.00453	.00389	99.6
07	10	23	.06131	-.00162	-.00590	.00286	99.5
07	11	23	.06388	.00121	-.00673	.00326	99.5
07	12	23	.06252	.00285	-.00813	.00445	99.4
07	13	23	.06422	.00398	-.00915	.00528	99.1
07	14	23	.06709	.00469	-.00989	.00584	98.4
07	15	23	.06978	.00579	-.00996	.00637	97.1
07	16	23	.06946	.00687	-.01120	.00731	96.5
07	17	23	.06771	.01140	-.01314	.01015	98.4
07	18	23	.06861	.01323	-.01747	.01274	99.0
07	19	23	.06938	.00833	-.03391	.01715	98.5
09	12	23	.06188	.00397	-.00741	.00460	99.4
09	13	23	.06160	.00648	-.00765	.00575	99.4
09	14	23	.06549	.00807	-.00722	.00623	99.5
09	15	23	.06636	.00941	-.00750	.00687	99.6
09	16	23	.06574	.00970	-.00920	.00767	99.3
07	14	16	.05235	-.00054	.02752	.01055	95.7
07	14	17	.05787	.00184	-.01872	.00863	96.5
07	14	18	.05510	.00290	-.01473	.00729	97.2
07	14	19	.06200	.00303	-.01133	.00586	97.8
07	14	20	.06125	.00311	-.00966	.00581	98.1
07	14	21	.06503	.00340	-.00983	.00535	98.0
07	14	22	.06685	.00423	-.00992	.00569	98.3
07	14	23	.06709	.00469	-.00989	.00584	98.4
07	14	24	.06770	.00499	-.00958	.00583	98.4
07	14	25	.06805	.00523	-.00930	.00581	98.5
07	14	26	.06835	.00539	-.00904	.00576	98.6
07	14	29	.06791	.00574	-.00869	.00575	98.8

Table 3.1B (Continued)

Sensitivity Testing Summary: P

GOES Times (LST) 1	2	3	Output Value M=.5	$\frac{\partial M}{\partial DTD}$	$\frac{\partial M}{\partial DTN}$	Worst Storage Error M=.05	r^2 Percent
08	11	23	.06359	.00166	-.00676	.00348	99.4
08	12	23	.06320	.00289	-.00754	.00421	99.4
08	13	23	.06574	.00408	-.00765	.00475	98.9
08	14	23	.06556	.00472	-.00824	.00523	98.1
08	15	23	.06648	.00841	-.00865	.00698	98.9
08	16	23	.06537	.01008	-.00978	.00812	99.3
08	17	23	.06845	.01071	-.01189	.00922	99.1
08	18	23	.06667	.00512	-.01612	.00883	97.6

less-acurate GOES imagery is used. Since the preferred testing strategy cannot be used, another strategy must be devised.

Previous work (Carlson and Boland, 1978, Dodd, 1979) indicates that the numerical boundary layer model used in CD and the GOES method provides acceptable surface temperature values for a wide range of soil parameters. It was decided to use the numerical model to simulate temperature data for GOES method testing. Since M and P are input parameters of the model, GOES method testing was restricted to diagnosing M and P. A master run of the numerical model was executed to provide surface temperatures at 48 GOES times for 63 ordered pairs of (M, P) values. Meteorological and geographical initializations were obtained from a St. Louis case studied by Carlson et al. (1981) and Kocin (1979). The output from the master run was used to represent GOES imagery of a fictitious target area exhibiting considerable variability in M and P. A test run was then executed, using the 16 (M, P) pairs to be used in the subsequent GOES method case studies (Section 4). The M and P values in the test run differed from those used in the master run. GOES time triplets were selected, and DTD and DTN were computed from the output of the test run. Bicubic regression equations were produced for M and P from the output of the test run. These regression equations were applied to appropriate DTD and DTN values obtained from the master run output. The resulting M and P values were then compared to the M and P inputs used to generate the master run output.

3.6.2 Sensitivity Studies Results

The results of the sensitivity and accuracy studies are presented in Table 3.1.

Actual values of M and P from the test-data regression equations and master-data temperatures are presented in Column 4 of Table 3.1. Relatively little importance is attached to these figures. The temperatures passed to the regression-evaluation routine were not observed temperatures; they were model-output simulated temperatures from the master run. Actual data could produce different results, due to differing amounts and types of error in model output and GOES imagery. If the results tabulated in Column 4 were perfect, all one could conclude is that the regression routine represents the model perfectly at (M, P) = (0.5, 0.065). Although the ability of the GOES method to represent itself is highly desirable, that ability is not essential to the work at hand. The quantities tabulated in Column 5 and 6 are more important to the current study than the values tabulated in Column 4.

Columns 5 and 6 contain the partial derivatives of the regression equation with respect to the predictands DTD and DTN respectively. These partials were evaluated with simulated temperatures from the (M, P) = (0.5, 0.065) master model run. They represent the sensitivity of the GOES method to small perturbations (or errors) in model output and/or data. In a typical model run, when (M, P) varies from (0.05, 0.0125) to (0.95, 0.125), DTD and DTN vary by about 20 K. A value of $\frac{\partial M}{\partial DTD}$ of 0.05/K or $\frac{\partial P}{\partial DTN}$ of 0.005/K is sufficient to account

for the real variation of M and P as functions of DTD and DTN. The tabulated values are generally larger, indicating possible numerical difficulties.

Column 7, labeled 'worst storage error,' contains $0.4 \left|\frac{\partial M}{\partial DTD}\right| + \left|\frac{\partial M}{\partial DTN}\right|$ or $0.4 \left|\frac{\partial P}{\partial DTD}\right| + \left|\frac{\partial P}{\partial DTN}\right|$. This quantity is the maximum error incurred by storing GOES temperatures in single bytes of computer storage. The GOES imagery used in this thesis was obtained from the McIDAS facility at the University of Wisconsin in Madison, WI. Each pixel of the satellite image was allocated one byte of magnetic tape storage. The raw intensity levels are converted into Kelvin temperatures by a preprocessing routine. The temperatures generally fall into a 100 K range: from 243 to 343 K. If the mapping from raw intensities to temperatures is nearly linear and nearly the entire domain of intensities is mapped into nearly the entire 243-343 K range, the temperatures can be no more accurate than $\pm$ 0.2 K. The subtraction step to form DTD and DTN doubles this error range. If the numerical model and the satellite data were completely error-free, the GOES method could still have errors as large as the values in Column 7, due to the method of storing data on the McIDAS input tapes.

Column 8 displays the multiple regression coefficient, r^2, a statistic generated by the MINITAB statistical package (Ryan, Joiner, and Ryan, 1976). It is a measure of the quality of the regression equation. r^2 is the square of the correlation coefficient between the M (or P) values in the input to MINITAB and the M (P)

values obtained by substituting the DTD and DTN values in the MINITAB input into the regression equation for M (P) produced by MINITAB. r^2 is the fraction of variance explained by the regression equation. A value of r^2 close to 100 percent indicates that the regression equation can be used to invert the model without appreciable error.

The results of the GOES times screening study were evaluated subjectively. Three objective criteria were applied, but these criteria were selected subjectively:

- avoid time triplets wehre r^2 for M is less than 90 percent
- avoid worst-storage-errors for M exceeding 0.10
- avoid worst-storage errors for P exceeding 0.010

GOES time triplets were rejected when r^2 began to decrease significantly as one of the times was varied away from its optimum. Triplets were rejected when sensitivities (Column 5, 6, and 7) began to increase rapidly as one GOES time was changed. Also considered, but not shown in Table 3.1 was the performance of the method at extreme values of (M, P). Pronounced difficulties were occasionally encountered for ($M \geq 0.8$; $P \geq 0.10$), where the inversion of the model is numerically least stable.

The results of the sensitivity study are summarized below:

1) The preferred midday GOES time is after local noon, preferably between 1300 and 1500 but no later than 1600 local standard time (LST). The time of surface temperature maximum is optimum.
2) Acceptable morning GOES times are after sunrise, but before 1000 LST. The optimum is about 1 1/2 h after sunrise.

Times after 0900 will provide marginally acceptible results, if afternoon and evening times are optimal.

3) The night GOES time should be at least 2 h after sunset. Performance of the method improves slowly as the night GOES time is made later than 2300 LST. Model execution time (hence, cost) also increases as the night time is made later. The marginal improvement in performance probably does not justify the expense of selecting night images after local midnight in an operational setting.

4) If the midday image time deviates more than 30 minutes from optimum, flexibility in the choice of morning image time is reduced.

These results were obtained from model simulations performed on the St. Louis case used in Carlson et al. (1981) and Kocin (1979). They may not have general applicability. Rose (1982, personal communication) reports poor results with the Kansas case study (Section 4), using GOES times of 0830, 1400, and 0100 LST. The sensitivity studies of the St. Louis simulation indicate that (0830, 1400, 0100) should be suboptimal but acceptible. This failure may be related to the choice of M and P values used in the model. Rose is using a smaller P range and a more sophisticated algorithm for generating (M, P) pairs for model initialization. Additional experimentation with the GOES method should lead to refinements in the criteria cited above.

Another restriction on the choice of GOES times was discovered during the processing of the Kansas case study (Section 4):

5) If possible, the model should be initialized to start after effective sunrise, about 1 h after astronomical sunrise. The morning GOES time should be at least 30 minutes after model-initialization time. If this is impossible (due to limited imagery or adverse cloud conditions), then:
   a. Initialize the model to start at the selected GOES time
   b. Use the model initial conditions (the initial surface temperature, etc.) as the model output for the first GOES time

Effective sunrise of radiation sunrise is defined as the time at which the surface first receives an excess of input energy (incident radiation plus G_o) over emitted radiation. At effective sunrise, H_o becomes positive. If the model is initialzed to start before effective sunrise, the model enters the nocturnal mode and produces a very shallow, spurious nocturnal inversion. Modeled surface temperatures are unreliable until this inversion is destroyed by heating. Use of model initial conditions as model output is not desirable, but it is better than the use of purely erroneous data resulting from the nocturnal-mode computations encountered if the model is started before effective sunrise.

For a few GOES time triplets in the sensitivity study, MINITAB produced the diagnostic message: VARIABLE . . . OMITTED FROM

REGRESSION EQUATION. This message implies that the model output for that GOES time triplet is overfit by a bicubic. One of the cubic terms is discarded by MINITAB. When this occurs, r^2 decreases and the sensitivity measures (Column 5, 6, 7) increase. There is no a priori way of determining which GOES time triplets will suffer from this overfitting. It has not been observed to happen in an optimal GOES time triplet; it occurs infrequently in suboptimal but acceptable triplets. The problem is almost certainly situation-dependent: different geographical and/or meteorological initializations imply different GOES time triplets having this property. MINITAB is most likely not in error. By coincidence, the model output has essentially no cubic component in one of the predictors, DTD or DTN. To eliminate this case of impaired performance, possible GOES triplets could be prescreened by the routine used in the sensitivity study:

1) Initialize the model with the appropriate geographical and meteorological parameters, including the M and P values to be used in the actual operational run.
2) Prepare a test dataset spanning all GOES times which are available for use.
3) Select a GOES time triplet from the available GOES times, subject to the constraints mentioned above in this section. Select the most nearly-optimal first.

4) Compute regression equations for any predictand, for the GOES triplet in question.

5) If the 'VARIABLE . . . OMITTED . . .' message appears, return to Step 3. Otherwise, accept the GOES time triplet.

4.0 RESULTS OF TEST CASES

4.1 INTRODUCTORY REMARKS

This thesis is an attempt to answer two major questions:

1) Can M, P, H_o, and/or E be diagnosed on the regional scale via satellite imagery?

2) Can GOES imagery be incorporated into the CD method?

Preliminary work (Section 3) indicates that both questions can be answered in the affirmative. It is necessary, however, to demonstrate the GOES method on actual regional data before making any meaningful claims.

Two test cases were considered:

1) Indiana/Illinois/Kentucky, 22 August 1978

2) Eastern Kansas, 27 July 1978

These cases were selected because both GOES and HCMM data were available. The Kansas case was also selected as a pilot for a future study of time-variability of M and P anomalies (Rose, 1983). Since none of the diagnosed variables could be measured on the regional scale, verification of the results of the test cases is difficult. The output of the two competing methods, CD and the GOES method, will be presented, along with crop-moisture-index and the preceding three week's rainfall. To the extent that both methods agree and are consistent with the available ground measurements, the GOES method can be judged a useful method.

The Indiana/Illinois/Kentucky case (henceforth called the Indiana case) is discussed in Section 4.2; the Kansas case, in Section 4.3. Figures 4.1 through 4.25, illustrating the Indiana and Kansas cases, are collected in Section 4.4 for convenience. General conclusions are presented in Section 5.1.

4.2 THE INDIANA CASE: 22 AUGUST 1978

So many things I could have done/But clouds got in my way

Judy Collins

Showers and thunderstorms left many bands and patches of cloud over the Indiana study area. At four of the five image times used in the study, there were clouds obscuring significant portions of the study area. The only clear image was the HCMM night image, 0748 Z, 21 August 1978, 48 hours before the modeled image time. Under these circumstances, the extra image used in the GOES method is a disadvantage. Whenever clouds appear on any image used, output values are meaningless. The third GOES image introduces a third set of clouds into the diagnostic method, obscuring more of the region. Only about 25 percent of the GOES/Indiana domain was not obscured by heavy clouds; thin clouds may affect about 10 percent more of the domain. About 50 percent of the HCMM/Indiana domain is usable.

Data results for the Indiana case are presented in Figures 4.1 through 4.11. There is evidence that both methods successfully diagnosed large-scale moisture-availability patterns, despite the interference by clouds. The three-week rainfall charts (Figures 4.2

and 4.7) show a marked antecedent precipitation minimum near the intersection of the Wabash and Ohio Rivers. Three-week precipitation and crop-moisture index[1] both indicate greater moisture to the north and east; the variation in crop moisture index values is less dramatic than that of the antecedent precipitation. Figures 4.4 and 4.9 show M as diagnosed from HCMM and GOES data, respectively. Both have dry values in the southwest quadrant. Neither is quantitatively accurate: M of 0.25 would indicate wilting vegetation, while M of 1.00 represents a wet surface or open water. The pattern of values correlates with the antecedent precipitation adequately, considering the masking due to clouds.

The diagnosis of P, H_o, and E in the Indiana case will not be discussed. The reader may discern for himself the degree of correlation between HCMM and GOES fields, and their relationship to three-week precipitation, crop moisture, and/or land-use patterns. P, H_o, and E will be discussed in the Kansas case (Section 4.3), where interference by cloudiness is markedly less evident.

The HCMM E field (Figure 4.6) contains a curious and counter-intuitive feature which will be discussed. A band of minimum E almost exactly parallels the Ohio River. One might expect high evaporation rates over bodies of water, all other conditions being equal. A definitive explanation for this minimum in E is not available. The river was probably cooler than the surrounding

---

[1]Operational product of NOAA/USDA Joint Agricultural Research Facility; broadcast as NAFAX map N118 and DIFAX map D262.

land during the daylight hours, although the satellite imagery failed to resolve a temperature anomaly. Evaporation from cool water could be lower than evaporation from warm land. The night HCMM image indicates a temperature maximum in the Ohio River Valley. This temperature maximum apparently was transformed into the E minimum by the regression routine. If total evaporation was actually lower over the river than over the land due to cool daytime water temperatures, the model has obtained a correct result for the wrong reason. If the evaporation minimum actually did not exist, the model has generated a spurious feature.

4.3 THE KANSAS CASE: 27 JULY 1978

The Kansas data are much better than the Indiana data. Clouds obscured less than 25 percent of the image area. As a result, all output fields could be obtained and compared. Data and results for the Kansas case are presented in Figures 4.12 to 4.25.

Meteorological conditions over the eastern Kansas study area were favorable. At 2100 Z, 27 July 1978, winds were generally 5-10 knots from the north to northeast. The pressure gradient was weak. By 0900 Z, 28 July 1978, winds had shifted to southerly, but had decreased to 0-5 knots over the area of interest. The temperature and wind patterns shown in Figure 4.13 are consistent with an approximate nonadvective assumption. Cloud conditions are not plotted in Figure 4.13 but satellite imagery shows relatively few patches of clouds over the study area. The three-week antecedent precipitation maps (Figures 4.14 and 4.20) indicate a dry region in

the southwest quadrant of the study area. Crop moisture index shows a similar dry area, displaced a bit eastward. A region of high crop moisture is found in the northwest quadrant of the region, consistent with the three-week precipitation but not entirely explained by it.

Several differences between HCMM and GOES temperature fields are evident in Kansas case imagery. The superior resolution of the HCMM satellite is clearly demonstrated. None of the GOES images (Figure 4.21A-C) displays any temperature feature which can be identified with any of the lakes in the study area. Both HCMM images (Figure 4.15A-B) show one or more lakes. Note in particular Perry Reservoir, the lake in the northeast quadrant of both the HCMM and the GOES domains. It appears as a distinct temperature minimum on the 1934 Z HCMM image and as a distinct maximum on the 0823 Z HCMM image. The high effective P of open water implies that lakes should be cooler than the surrounding land during the day and warmer than the land at night. For small bodies of water HCMM is able to observe this distinction; GOES is not. The 8 km resolution of GOES may explain its inability to see the lakes; Perry Reservoir, however, is larger than 8 km in dimension.

The temperature patterns displayed on the 1934 Z HCMM image (Figure 4.15A) and the 2000 Z GOES image (Figure 4.21B) are similar, but the HCMM image is about 10 C (10 K) warmer than the GOES image. The HCMM image was collected on 28 July 1978; the GOES, on 27 July 1978. A 10 C change in surface temperature between the two image

times seems excessive, considering the fairly stable weather pattern over the region. Both images are considerably warmer than the surface air temperatures displayed in Figure 4.13A. This is to be expected: the actual surface of the earth, exposed to direct sunlight, should be considerably warmer than the air inside an instrument shelter 1.3 m above the heated surface. A difference of about 25 C, as implied by the HCMM imagery, is possible; intuitively, 25 C seems extreme.

The land-use patterns (Figure 4.12) are not well correlated with the temperature fields. Most of the region consists of some mix of unirrigated cropland and rangeland. The principal crop in eastern Kansas is wheat. Wheat is a grass. The distinction between wheat and range grass is obvious to the farmer and the cartographer; the distinction may be much less obvious to the longwave-IR sensor of a weather satellite. Unfortunately, there was no significant area of irrigated cropland in the study area. Irrigated cropland would be expected to differ in surface temperature from unirrigated land.

The four output fields show good agreement between HCMM and GOES methods, good consistency among field types, and good agreement with three-week antecedent precipitation. The agreement with crop moisture index is adequate, but not as good as the relationship with antecedent rainfall. The output fields are not to be interpreted as exact values, though. The range of M displayed in

Figures 4.16 and 4.22 is unrealistically large, for example. This qualitative accuracy and quantitative inadequacy also occurred in the Indiana case (4.1).

Both M fields clearly show the dry region in the southwest of the HCMM domain and in the west of the GOES domain. Clouds unfortunately obscure the region of highest M gradient in the HCMM domain. The HCMM M field (Figure 4.16) resolves the Perry Reservoir as an M maximum; the lake on the northwest edge of the domain may be resolved.

The P fields show low values of P in the dry region, as would be expected. The HCMM P field (Figure 4.17) resolves two lakes as P maxima; the GOES field (Figure 4.23) does not resolve the lakes.

The H_o fields (Figures 4.18 and 4.24) show high heat flux over dry terrain.

The E fields (Figures 4.19 and 4.25) show the expected result: low evaporation in the dry region. Neither HCMM nor GOES E field resolves either lake. The E fields correlate better with previous three-week rainfall than with crop moisture index.

The reader is encouraged to study the output fields, the input fields, and the meteorological and physiographic data and reach his own conclusions about the relative merits of the GOES method and the CD method for diagnosing M, P, H_o and/or E.

4.4 FIGURES DEPICTING CASE STUDY RESULTS

Figures 4.1 through 4.25 depict initial conditions and results of the two case studies described in Sections 4.2 and 4.3. The figures are presented in the following order:

Indiana case: Figures 4.1 through 4.11

- 4.1: Base map and land-use data
- 4.2 through 4.6: Indiana-case HCMM:
  - 4.2: Three-week rainfall and crop moisture index
  - 4.3: Satellite images (temperature fields)
  - 4.4 through 4.6: Output fields (M, P, E)
- 4.7 through 4.11: Indiana-case GOES:
  - 4.7: Three-week rainfall and crop moisture index
  - 4.8: Satellite images
  - 4.9 through 4.11: Output fields (M, P, E)

Kansas case: Figures 4.12 through 4.25

- 4.12: Base map and land-use data
- 4.13: Surface weather analyses
- 4.14 through 4.19: Kansas-case HCMM:
  - 4.14: Three-week rainfall and crop moisture index
  - 4.15: Satellite images
  - 4.16 through 4.19: Output fields (M, P, H_o, E)
- 4.20 through 4.25: Kansas-case GOES:
  - 4.20: Three-week rainfall and crop moisture index
  - 4.21: Satellite images
  - 4.22 through 4.25: Output fields (M, P, H_o, E)

On all satellite imagery and output fields, areas affected by cloud cover are indicated by scalloped lines; contours are omitted in cloudy areas.

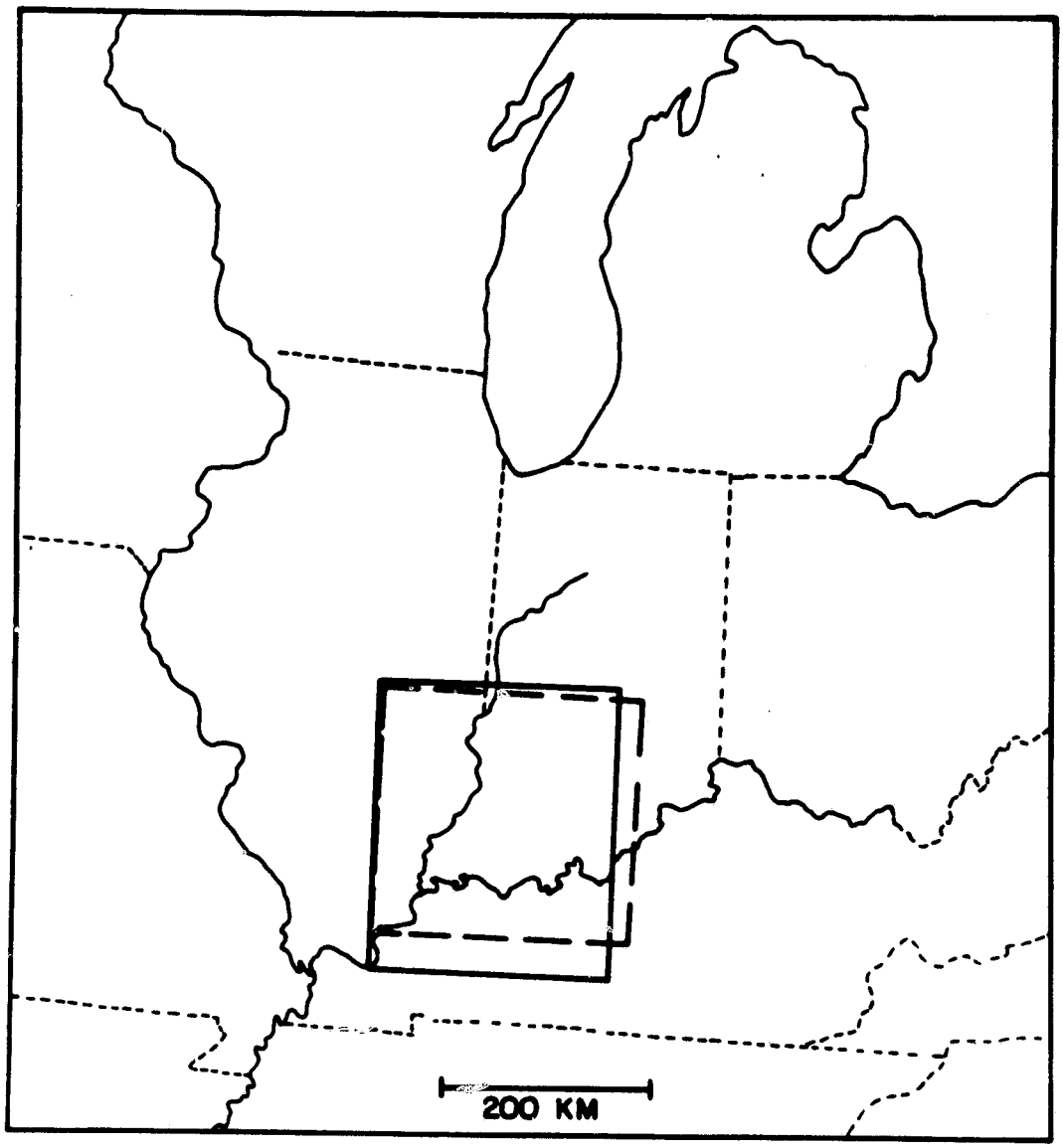

Figure 4.1A: Geographical location of GOES and HCMM domains for the Indiana test case.

Heavy solid lines: GOES domain
Heavy dashed lines: HCMM domain
Light solid lines: Rivers and lake shores
Light dashed lines: State boundaries

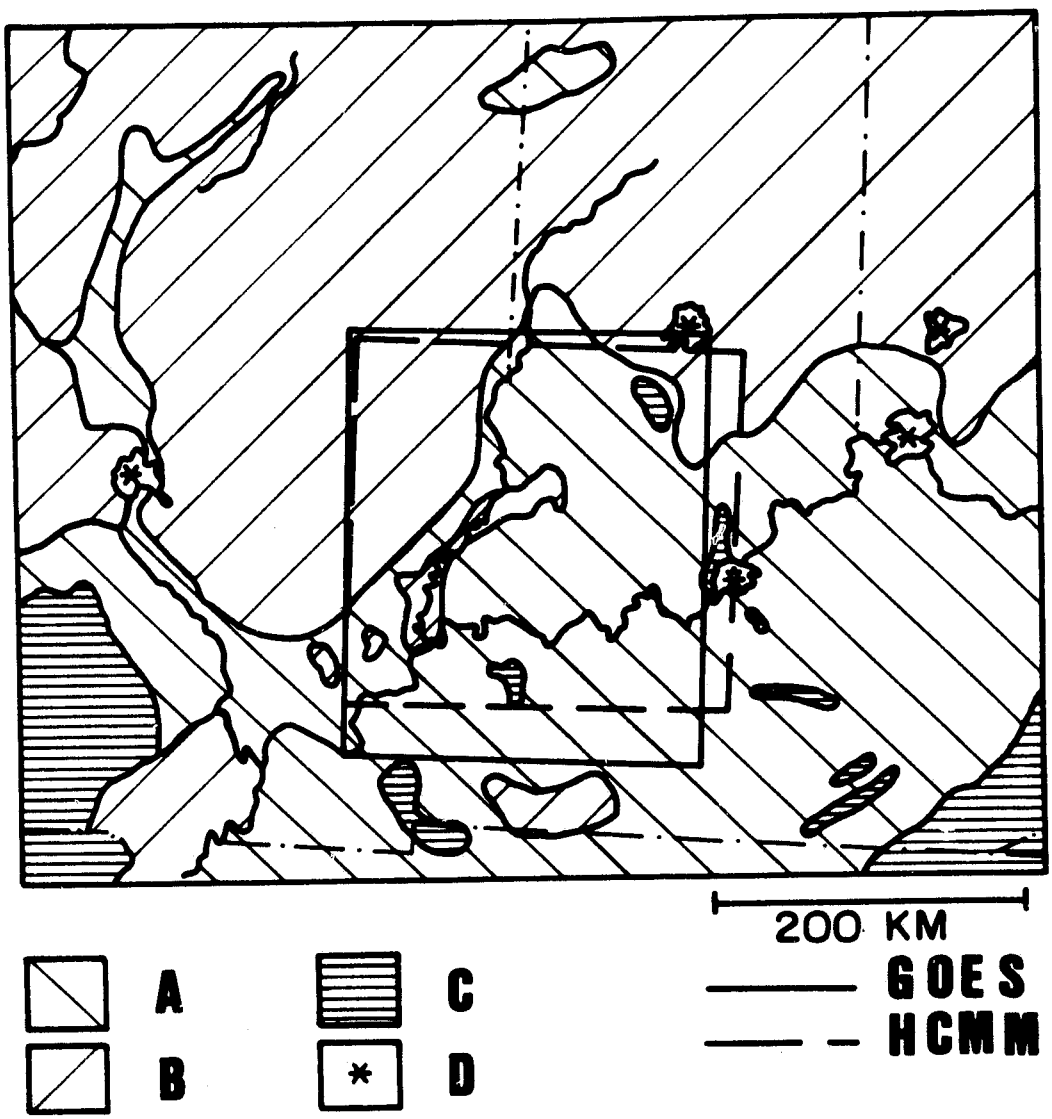

Figure 4.1B: Land use map for the Indiana case.

A: Cropland and woodland
B: Cropland
C: Forest woodland
D: Urban

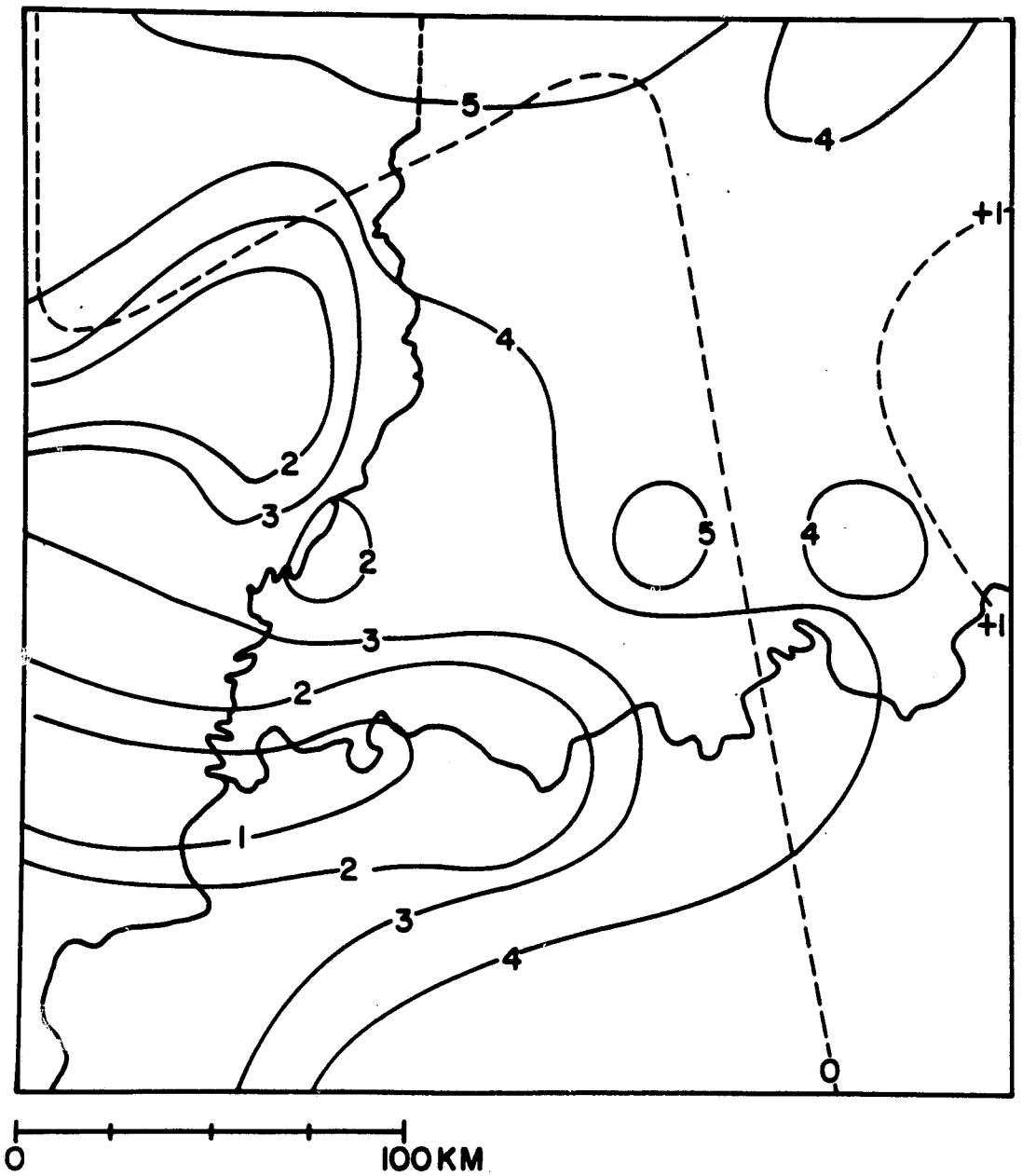

Figure 4.2: Three-week antecedent rainfall and crop moisture index for the Indiana case HCMM domain.

Solid contours: Preceding three-week precipitation (inches)
Dashed contours: Crop moisture index

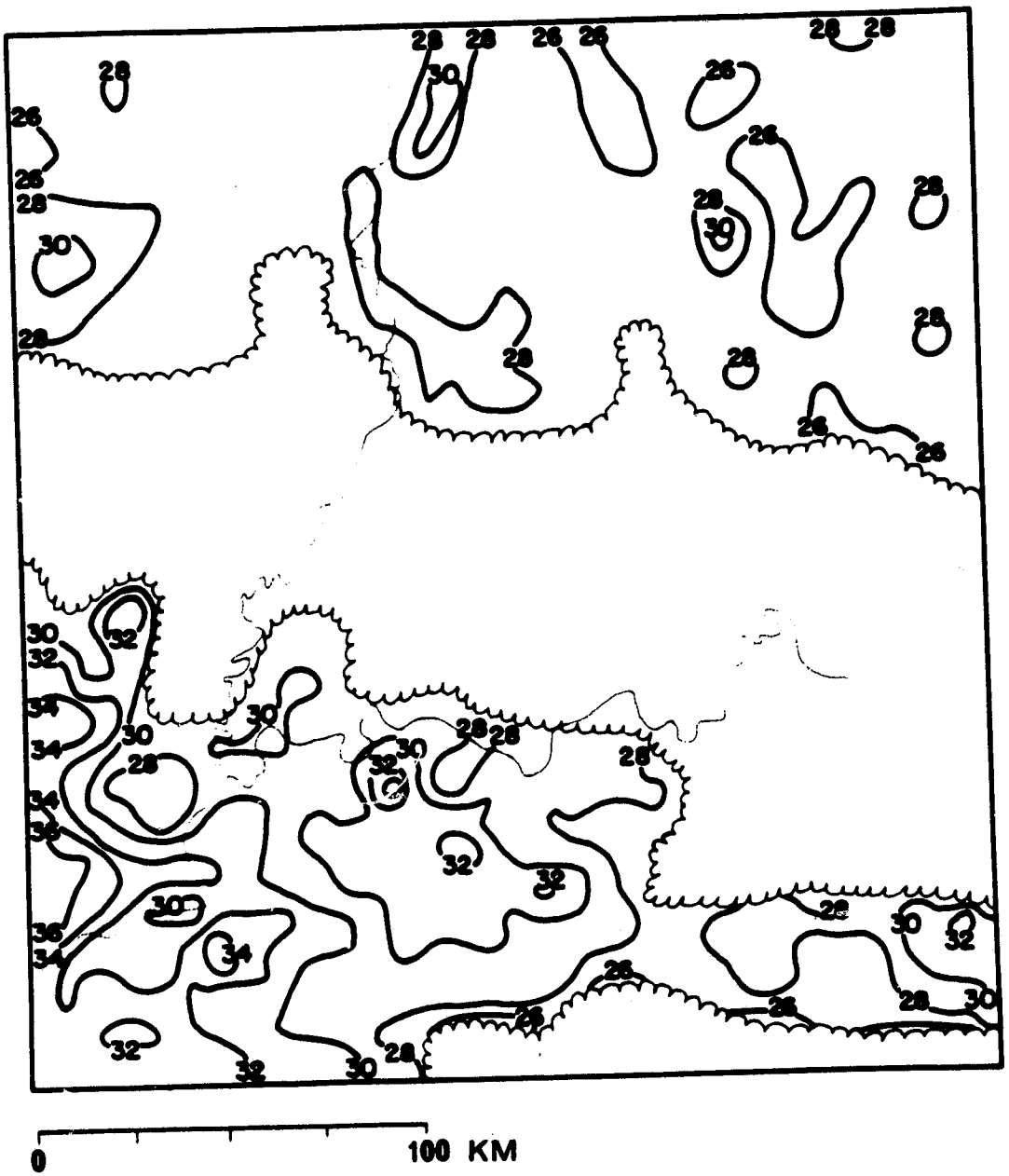

Figure 4.3A: Indiana-case HCMM image, 1858Z, 22 August, 1978. Contours are satellite-derived surface temperatures, in °C, corrected for atmospheric water vapor.

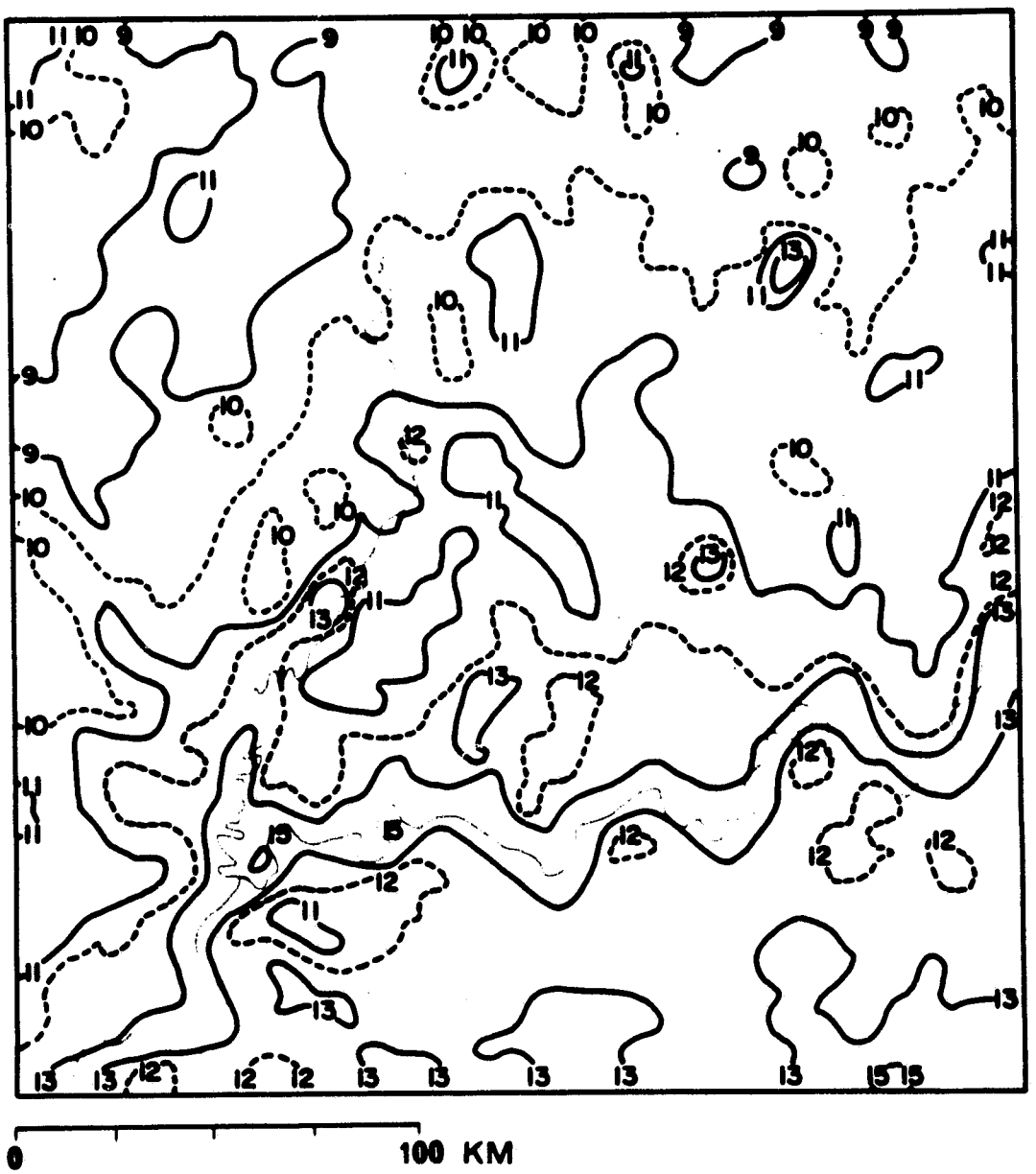

Figure 4.3B: Indiana-case HCMM image, 0748Z, 21 August, 1978. Contours as in Figure 4.3A.

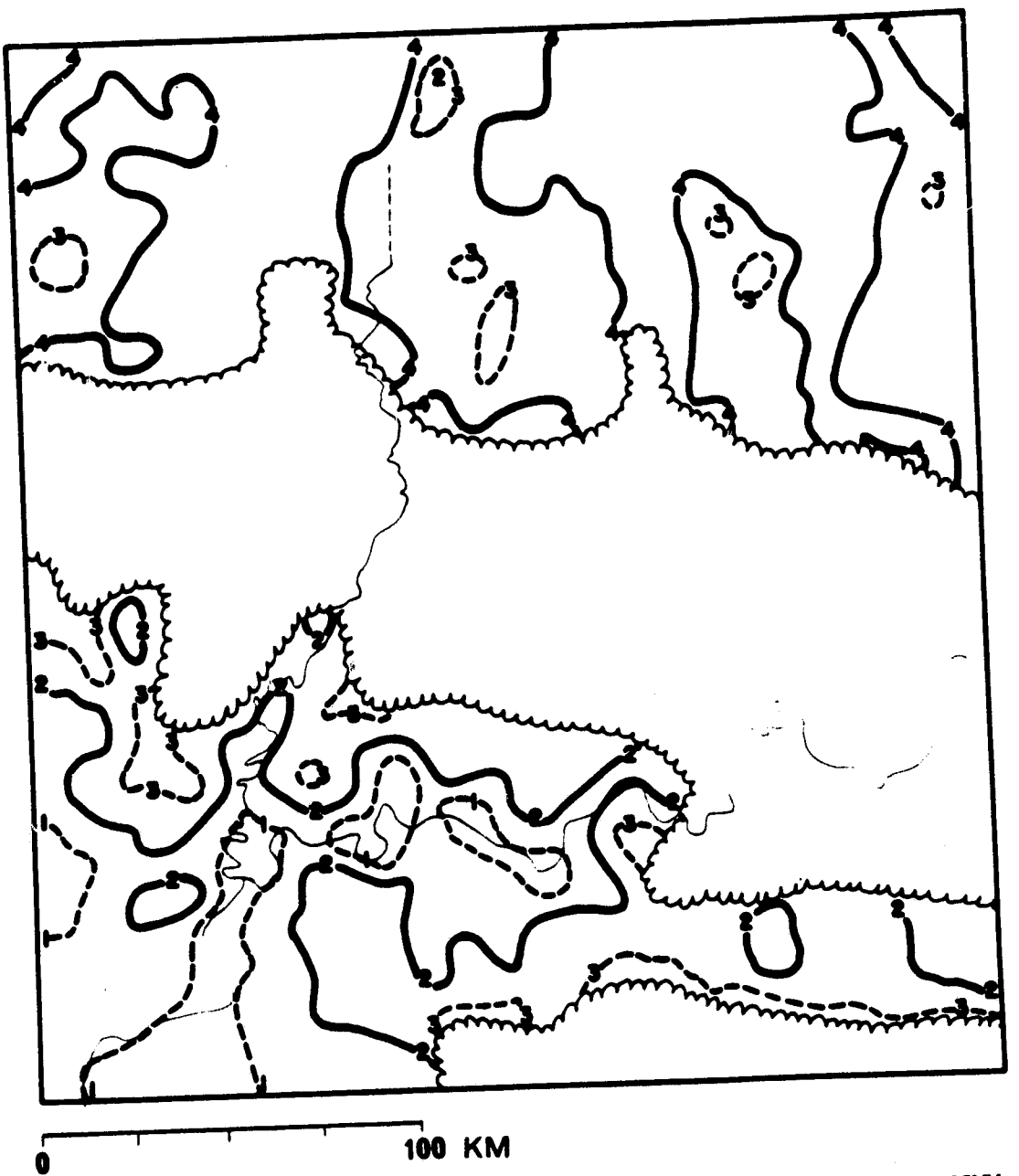

Figure 4.4: Indiana-case moisture availability diagnosed from HCMM data. Contour interval: 0.25.

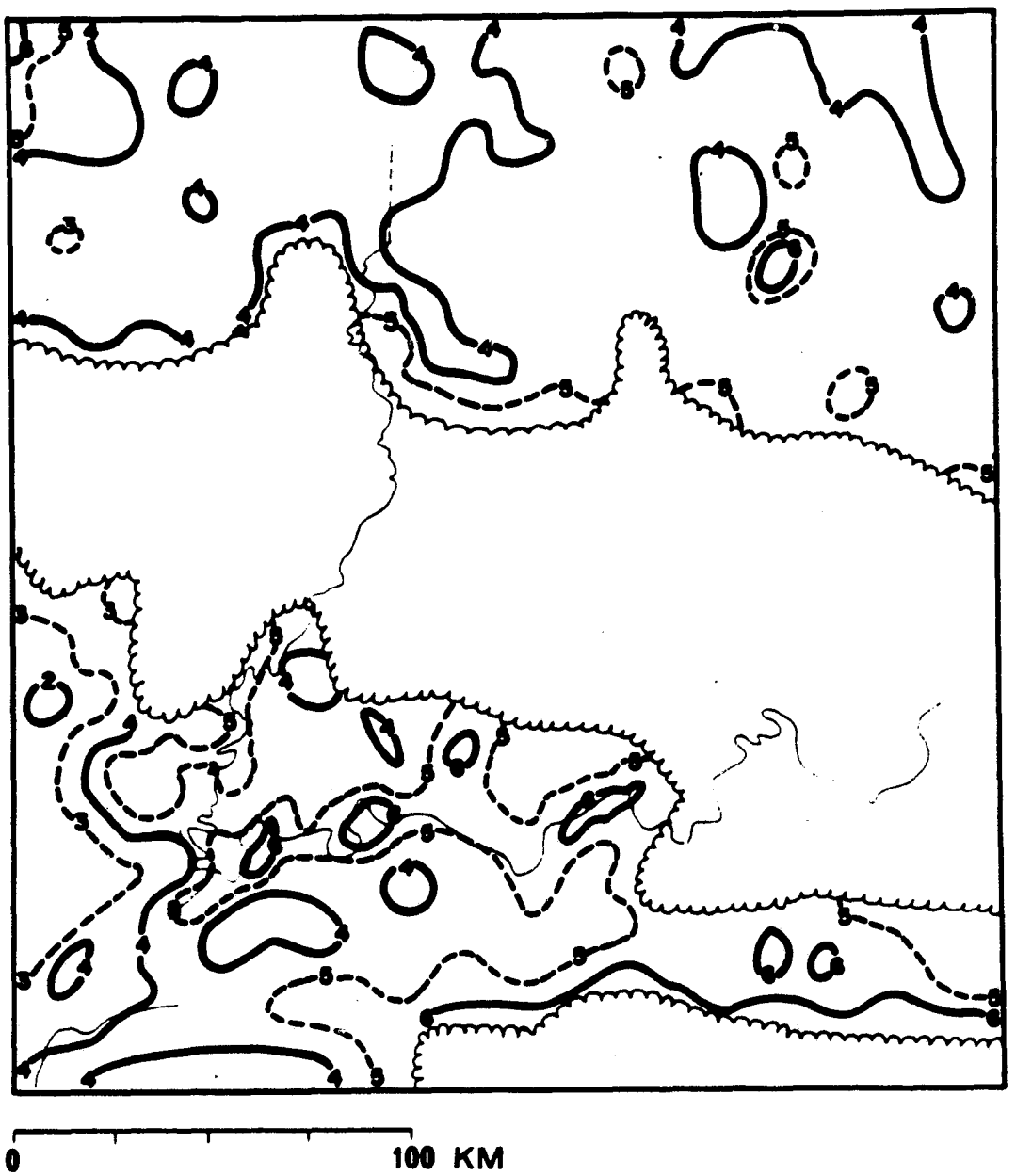

Figure 4.5: Indiana-case thermal inertia (P) diagnosed from HCMM data. Contour interval: 0.02 cal cm^{-1} K^{-1} $sec^{-1/2}$.

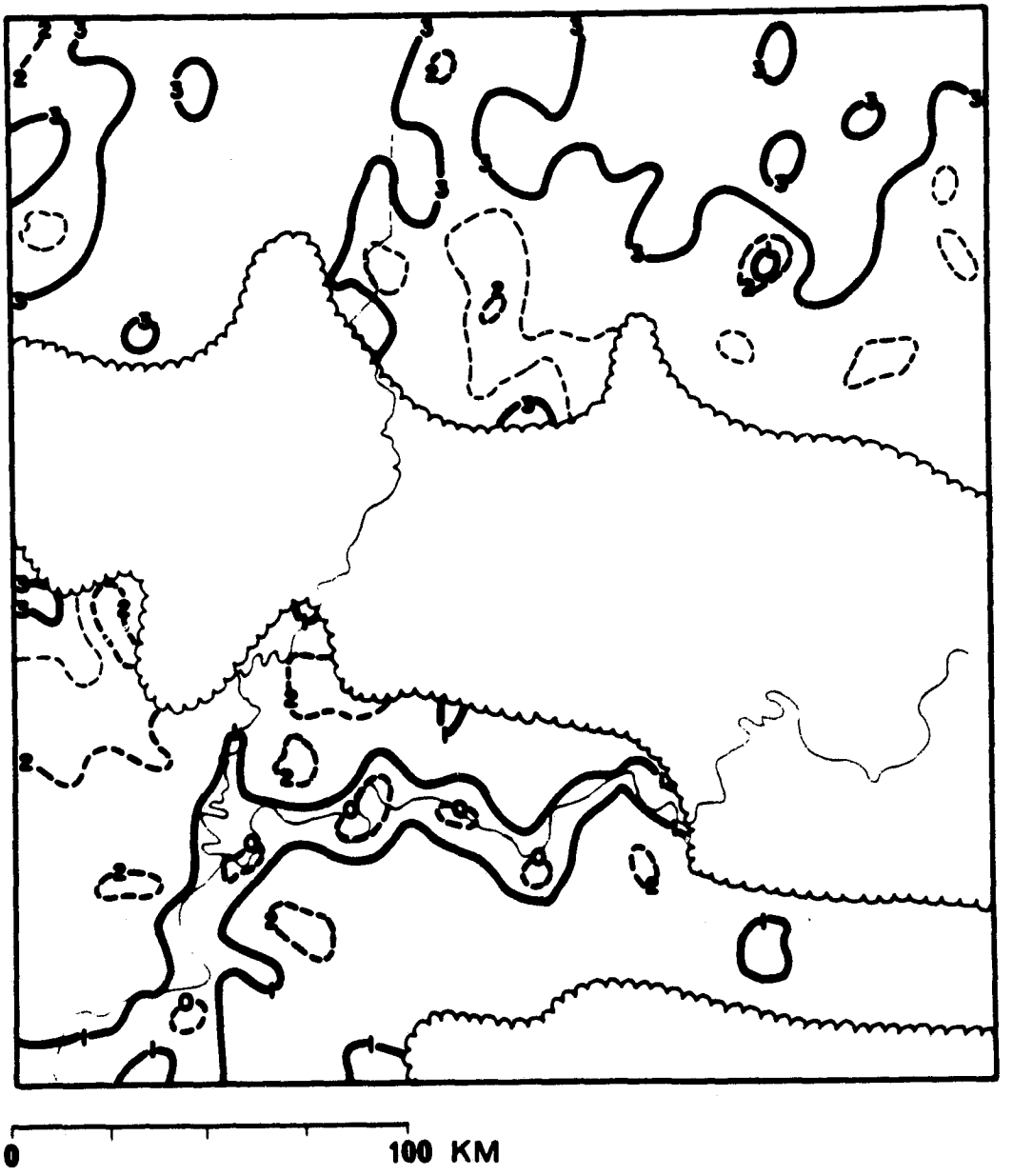

Figure 4.6: Indiana-case total evaporation diagnosed from HCMM data.

0: 0.05 cm 1: 0.15 cm 2: 0.25 cm
3: 0.35 cm 4: 0.45 cm

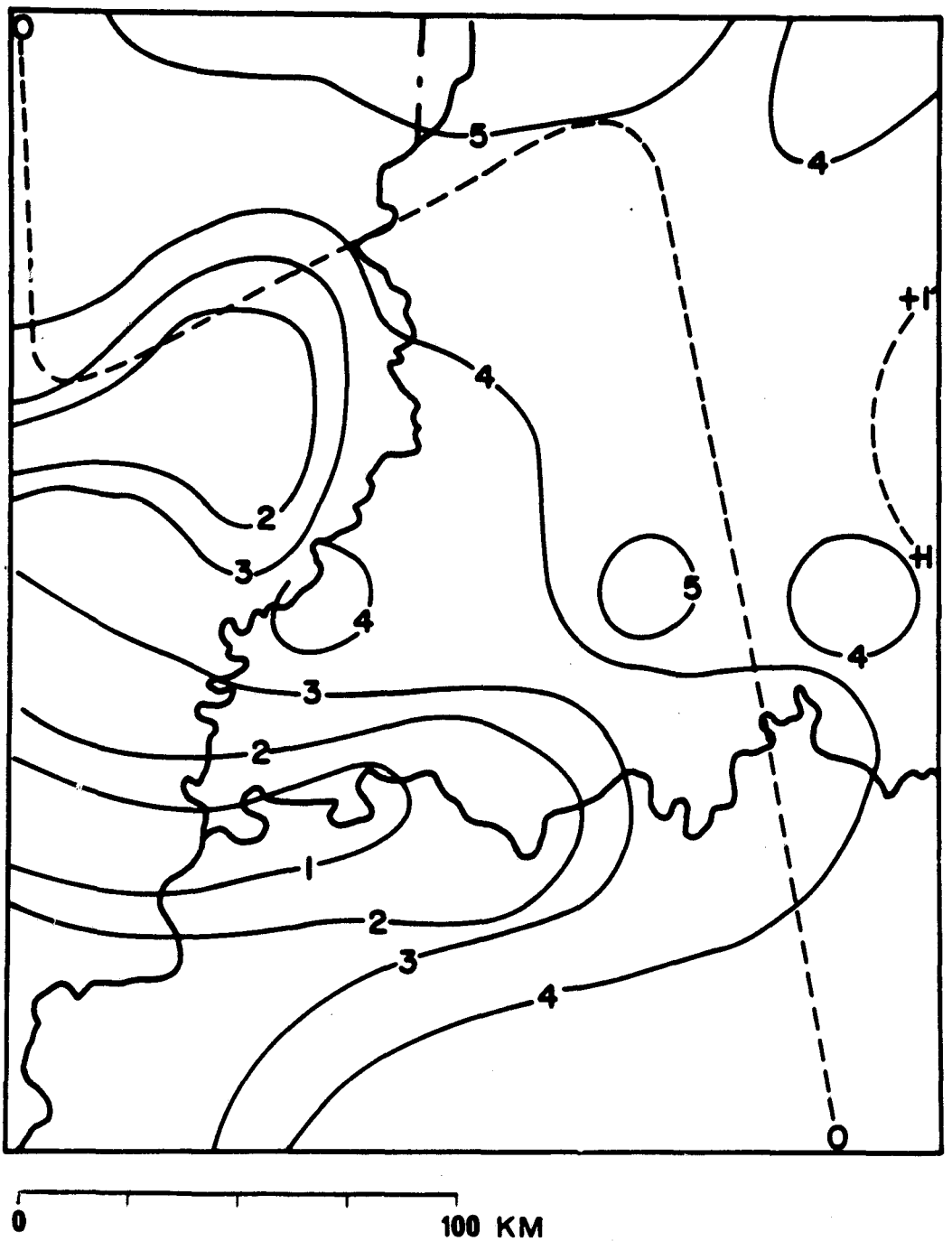

Figure 4.7: Three-week antecedent precipitation and crop moisture index for the Indiana case GOES domain. Contours as in Fig. 4.2.

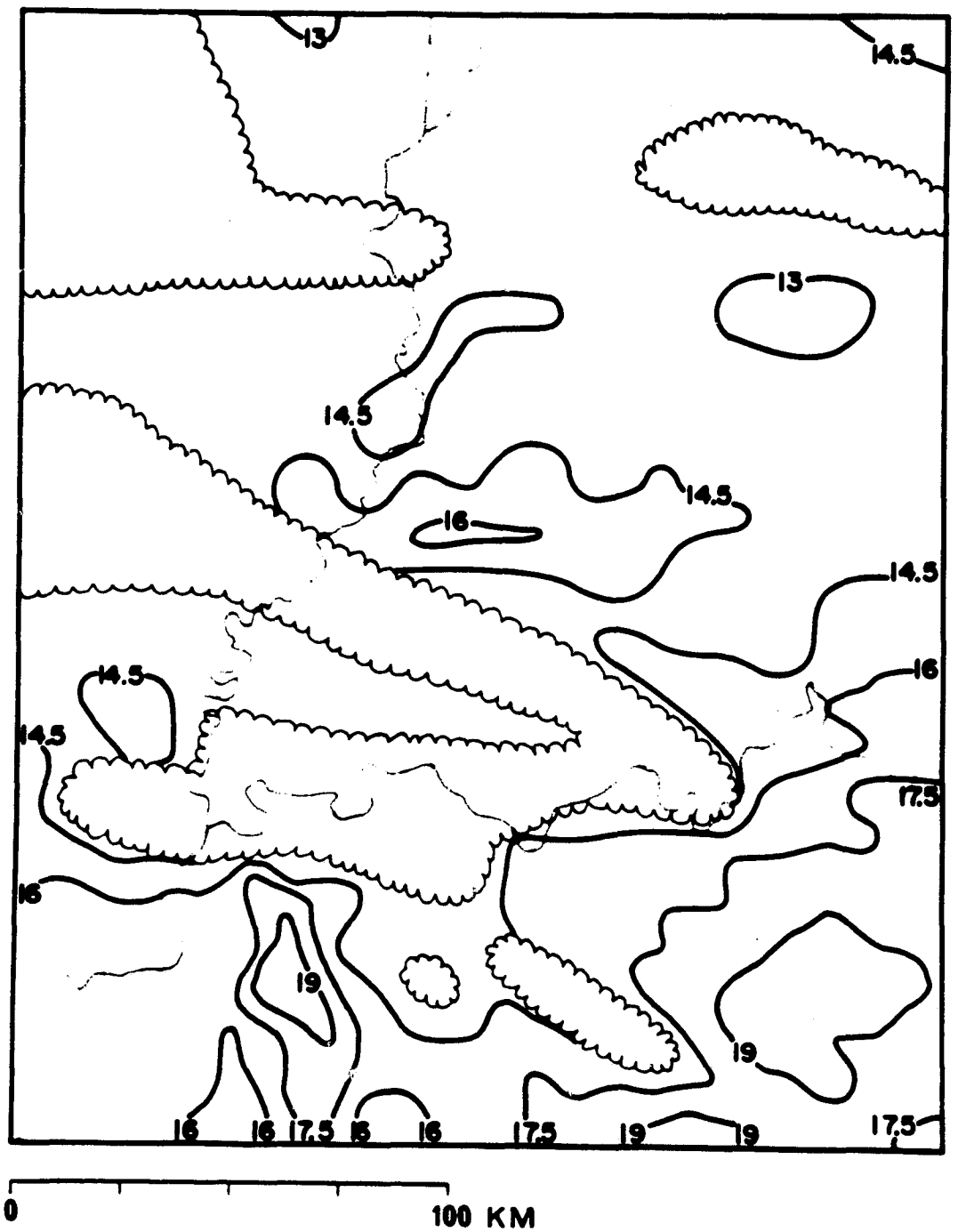

Figure 4.8A: Indiana-case GOES image, 1230Z, 22 August 1978. Contours as in Fig. 4.3A.

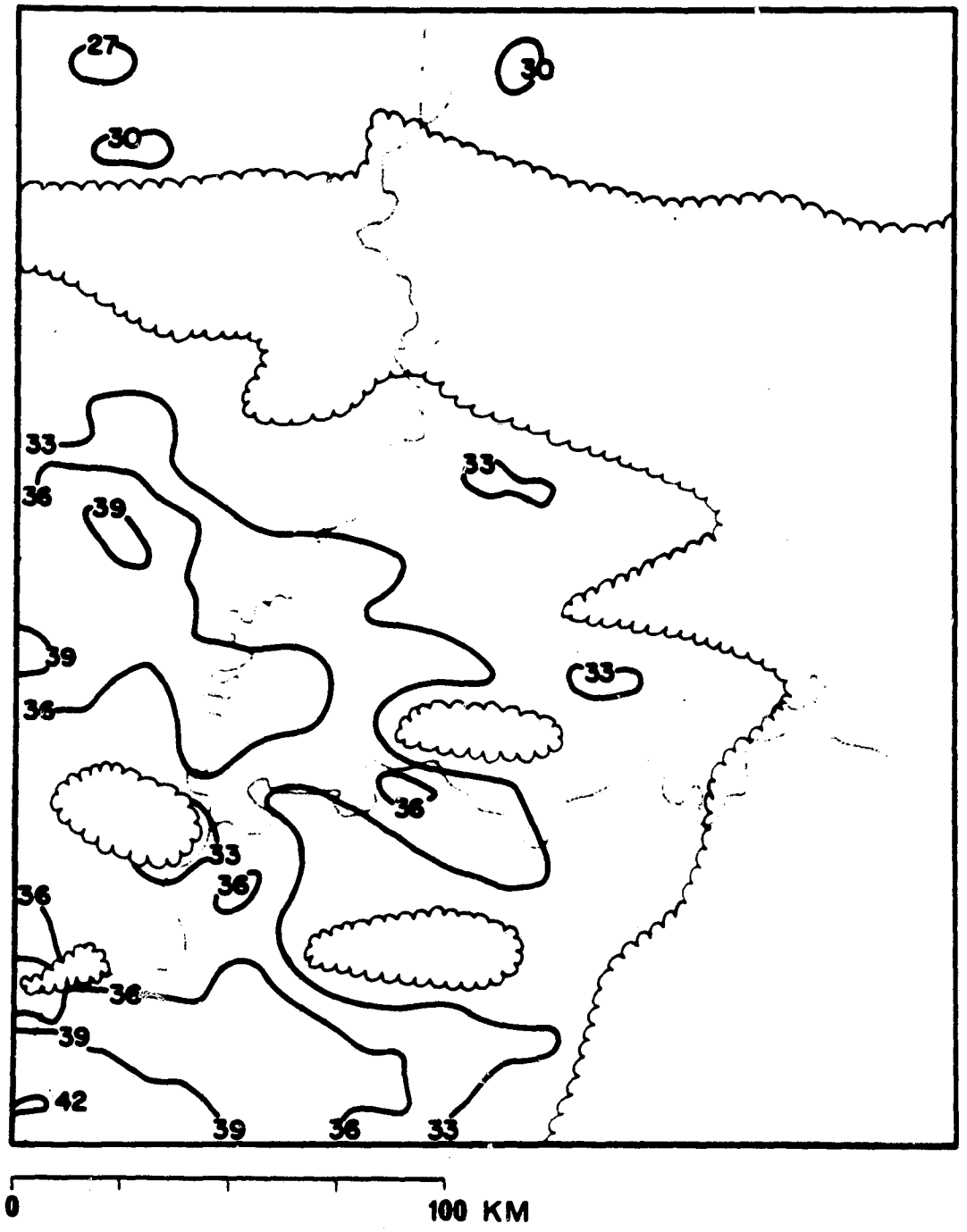

Figure 4.8B: Indiana-case GOES image, 1900Z, 22 August 1978. Contours as in Fig. 4.3A.

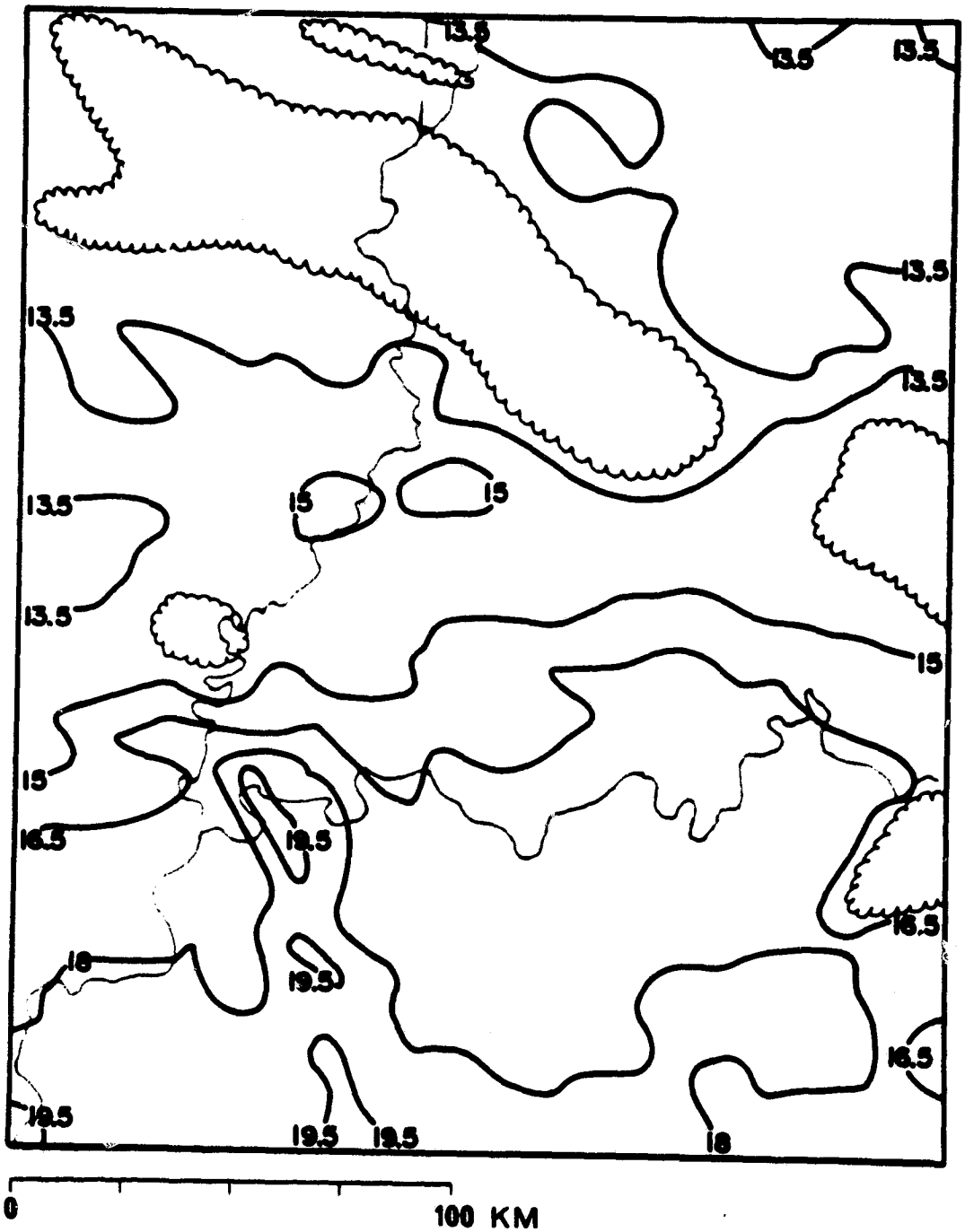

Figure 4.8C: Indiana-case GOES image, 0600Z, 22 August 1978. Contours as in Fig. 4.3A.

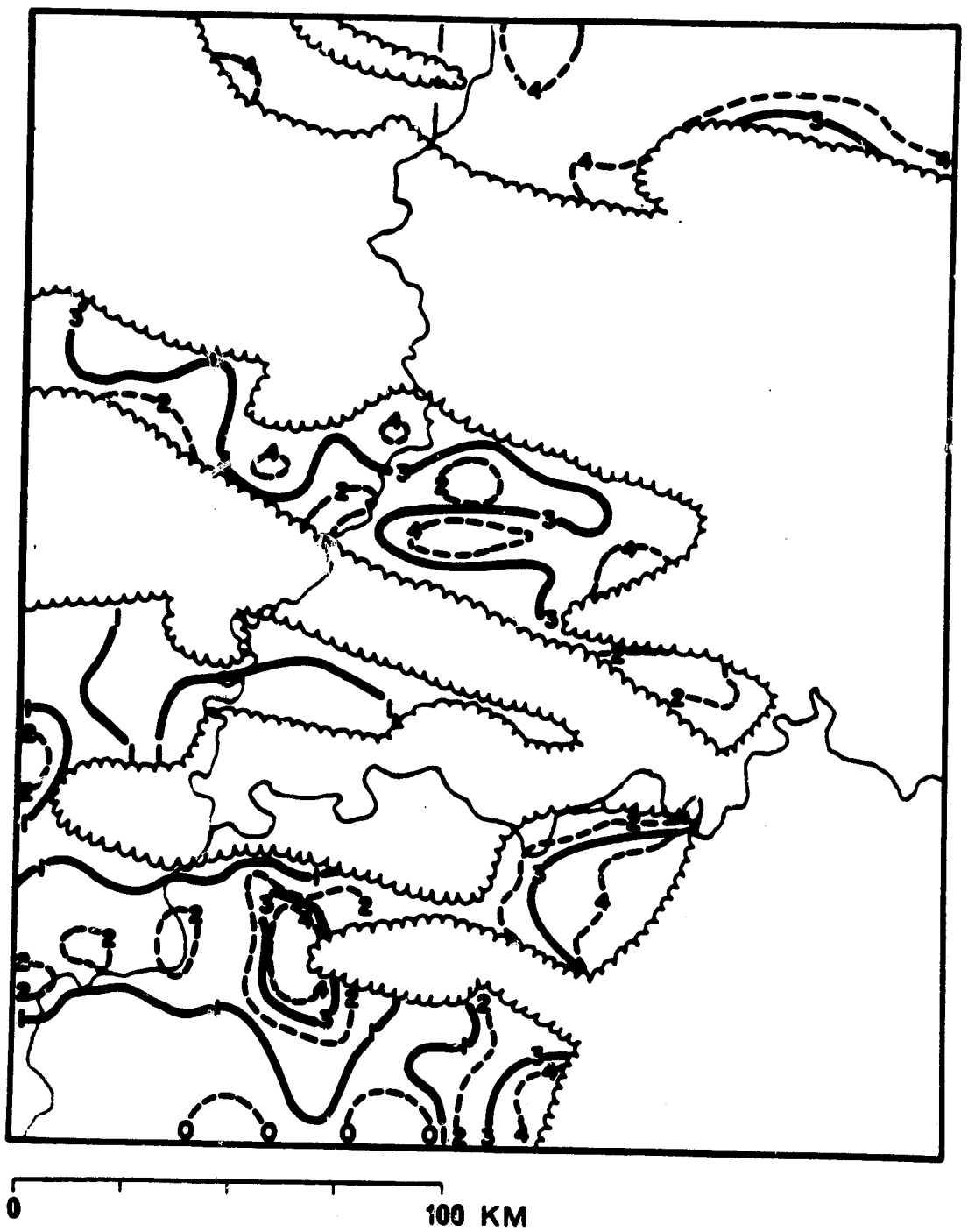

Figure 4.9: Indiana-case moisture availability (M) diagnosed from GOES data. Contours as in Fig. 4.4.

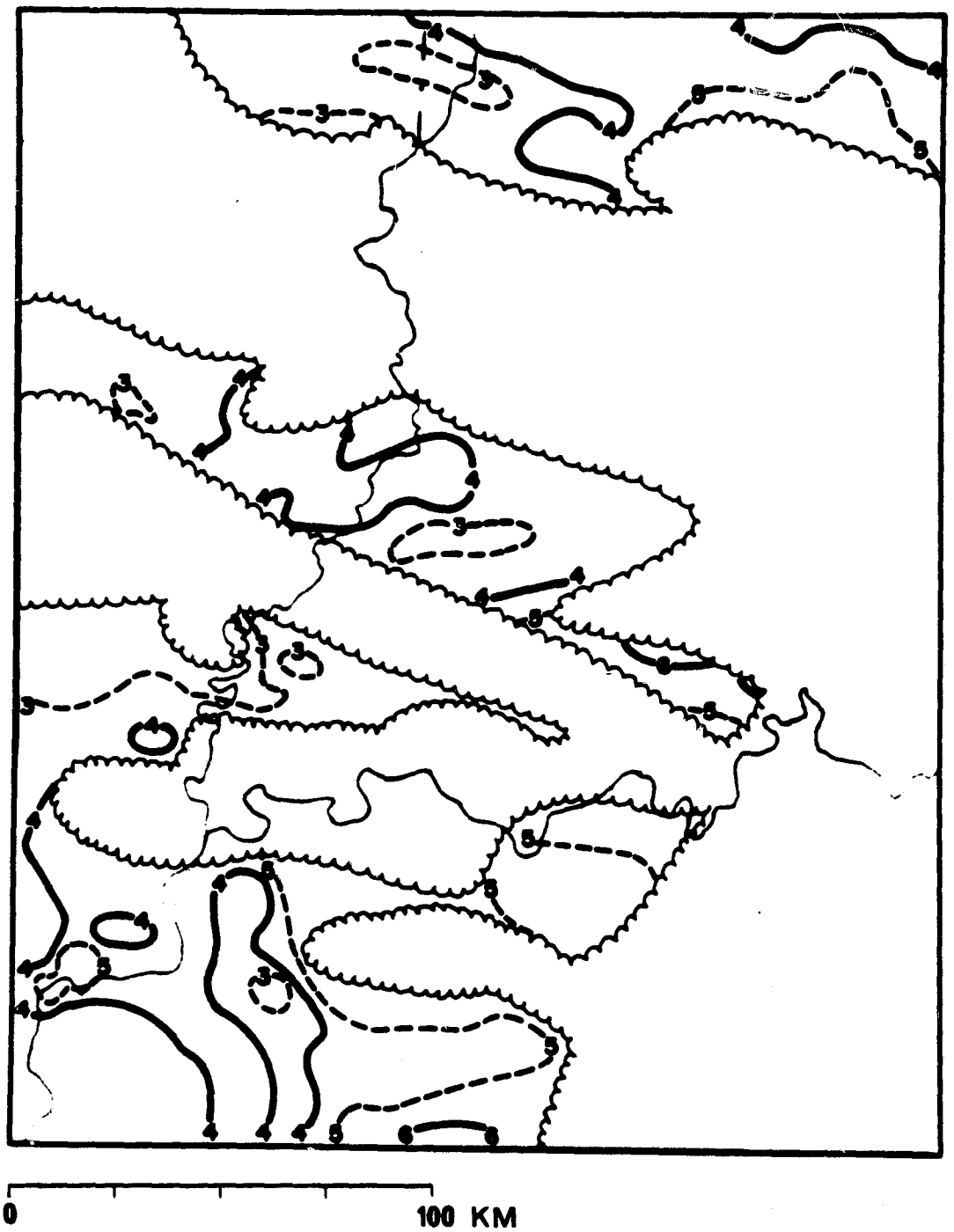

Figure 4.10: Indiana-case thermal inertia (P) diagnosed from GOES data. Contours as in Fig. 4.5.

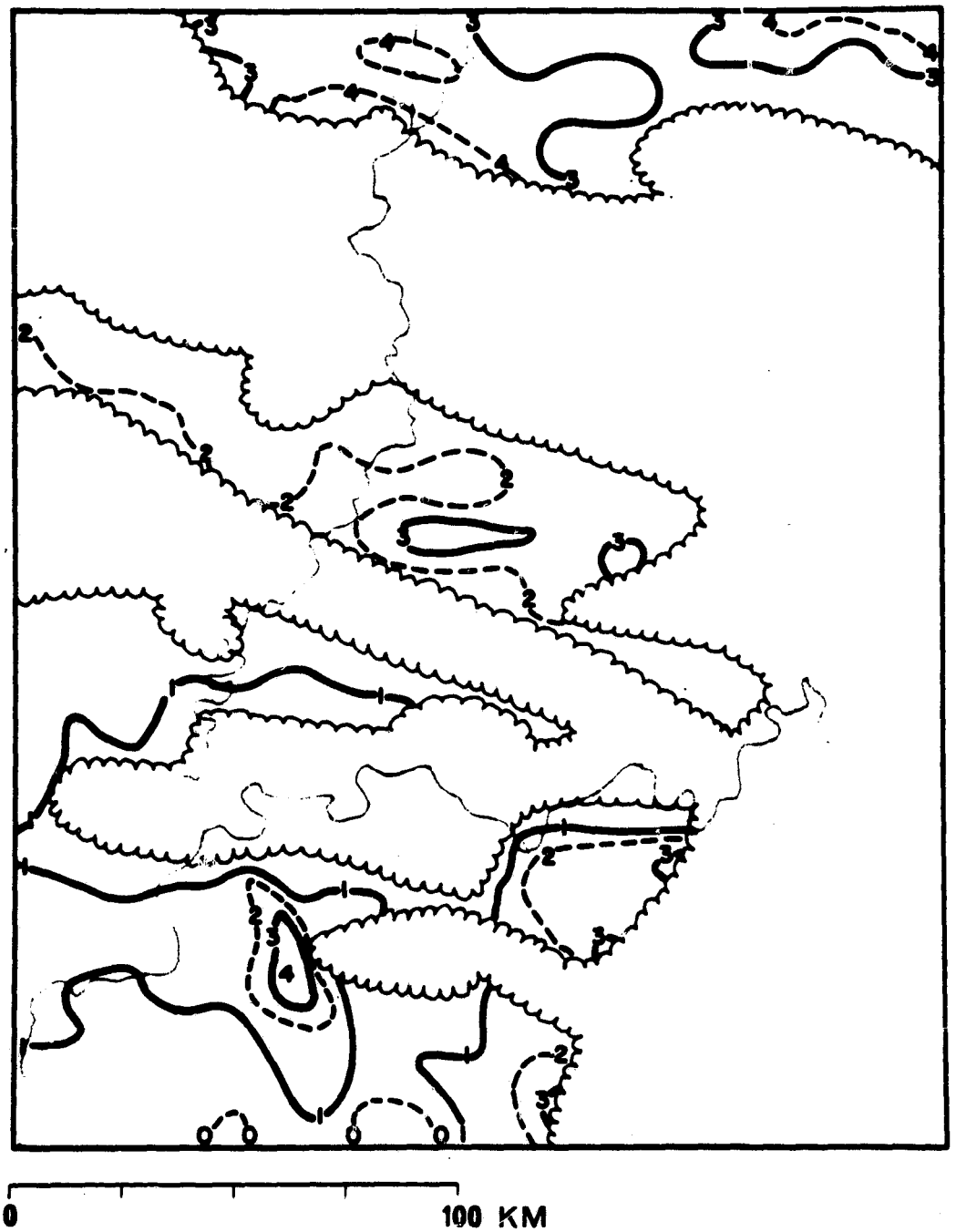

Figure 4.11: Indiana-case total evaporation (E) diagnosed from GOES data. Contours as in Fig. 4.6.

Key for Figure 4.12

A: Urban

B: Unirregated cropland - areas 60% or more unirrigated cropland

C: Unirregated cropland with rangeland - areas 50-60% unirrigated cropland and 30-50% grassland

D: Unirrigated cropland with irrigated cropland - areas with 50-80% unirrigated cropland and 20-30% irrigated cropland

E: Rangeland - areas with 80% or more grassland

F: Rangeland with unirrigated cropland - areas with 50-80% grassland and 30-40% unirrigated cropland

G: Woodland - areas with 70% or more woodland, but omitting minor streambank woodland

H: Water - major reservoirs and permanent semi-natural water bodies

I: Irrigated cropland - areas with 50% or more irrigated cropland

Reference: Kansas Land Use Patterns, Summer 1973. Donald L. Williams and Bonnie L. Barker. Space Technology Laboratories, University of Kansas in Cooperation with Planning Division, Kansas Department of Econ. Development.

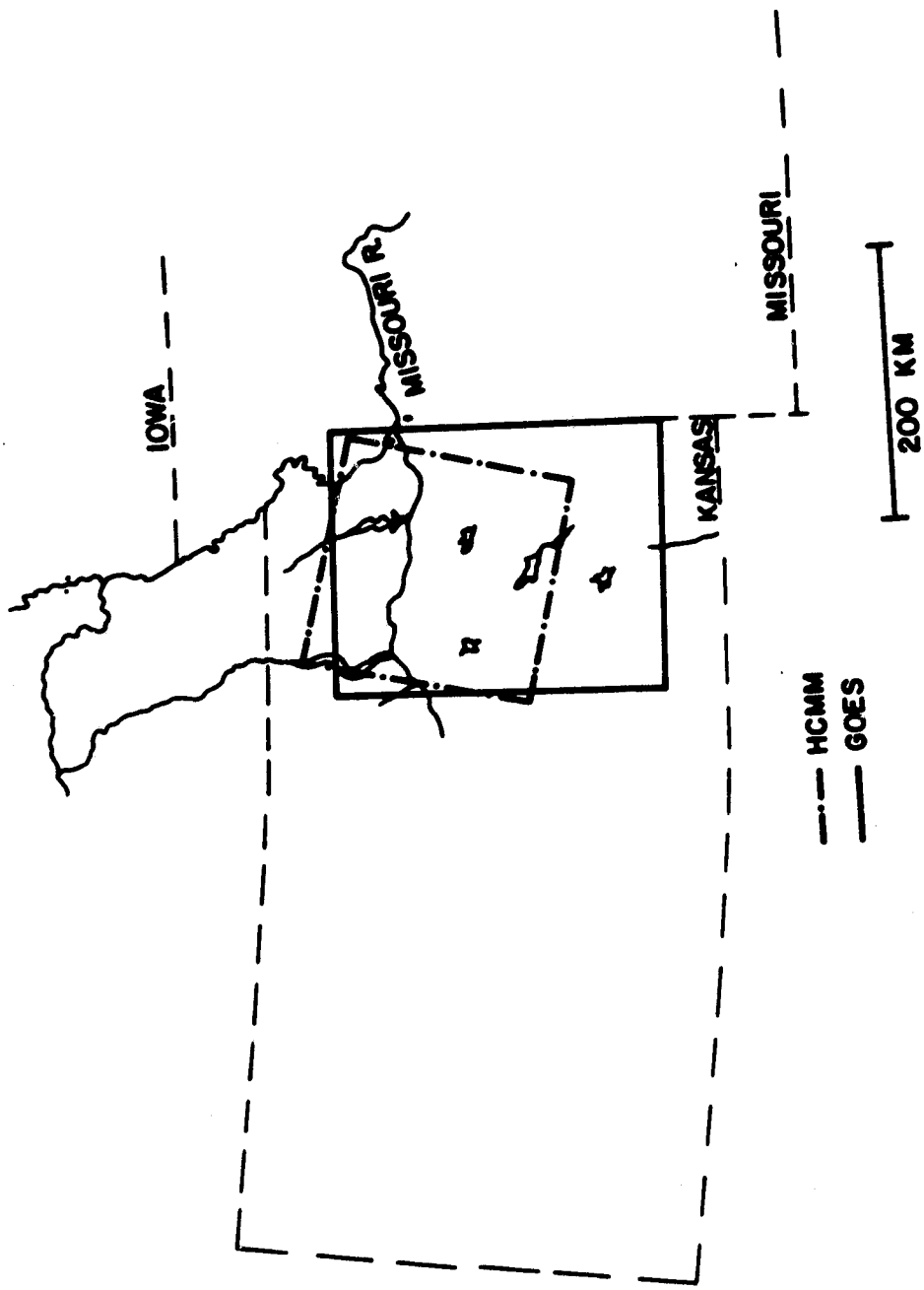

Figure 4.12A: Kansas-case base map.

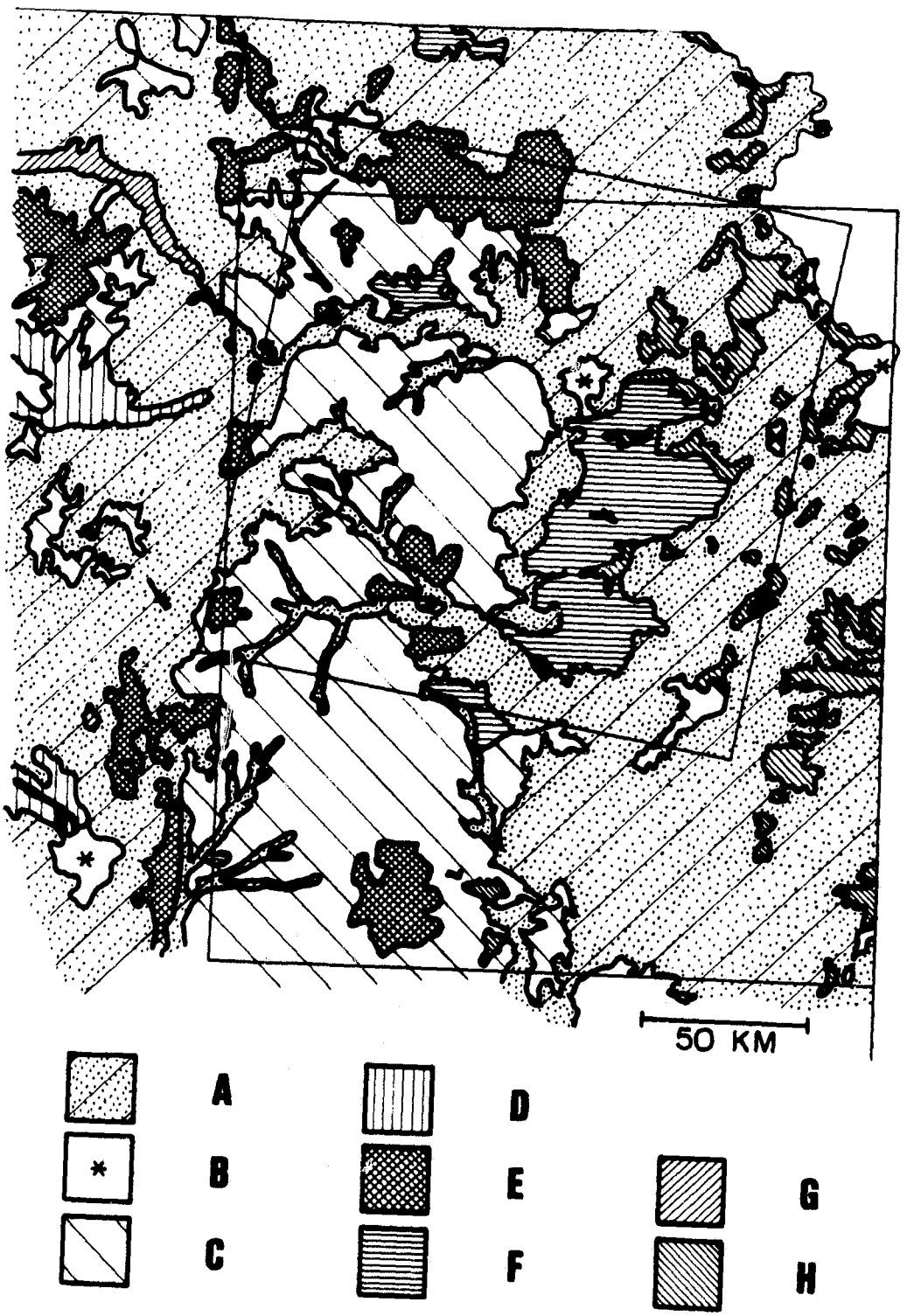

Figure 4.12B: Land use for the Kansas case.

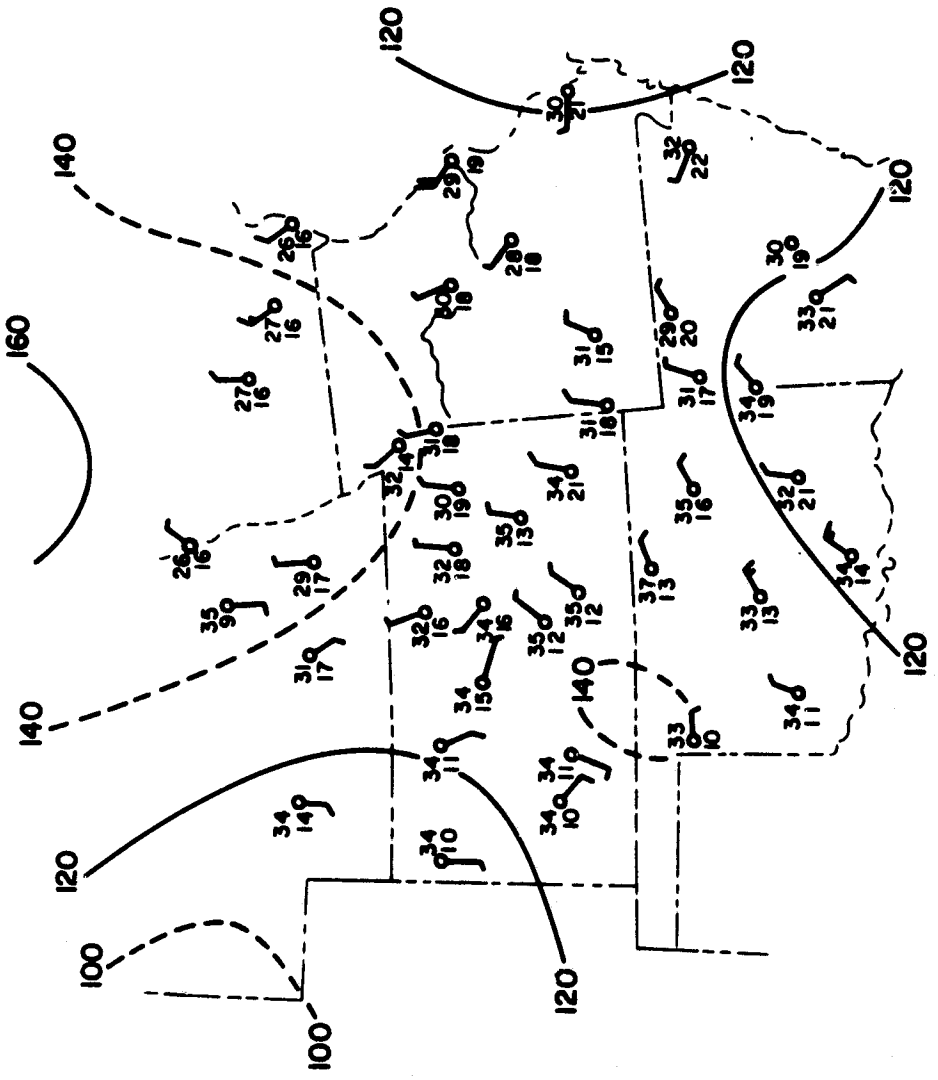

Figure 4.13A: Surface weather analysis. Contours: pressure in mb. and tenths; thousands and hundreds digits omitted.

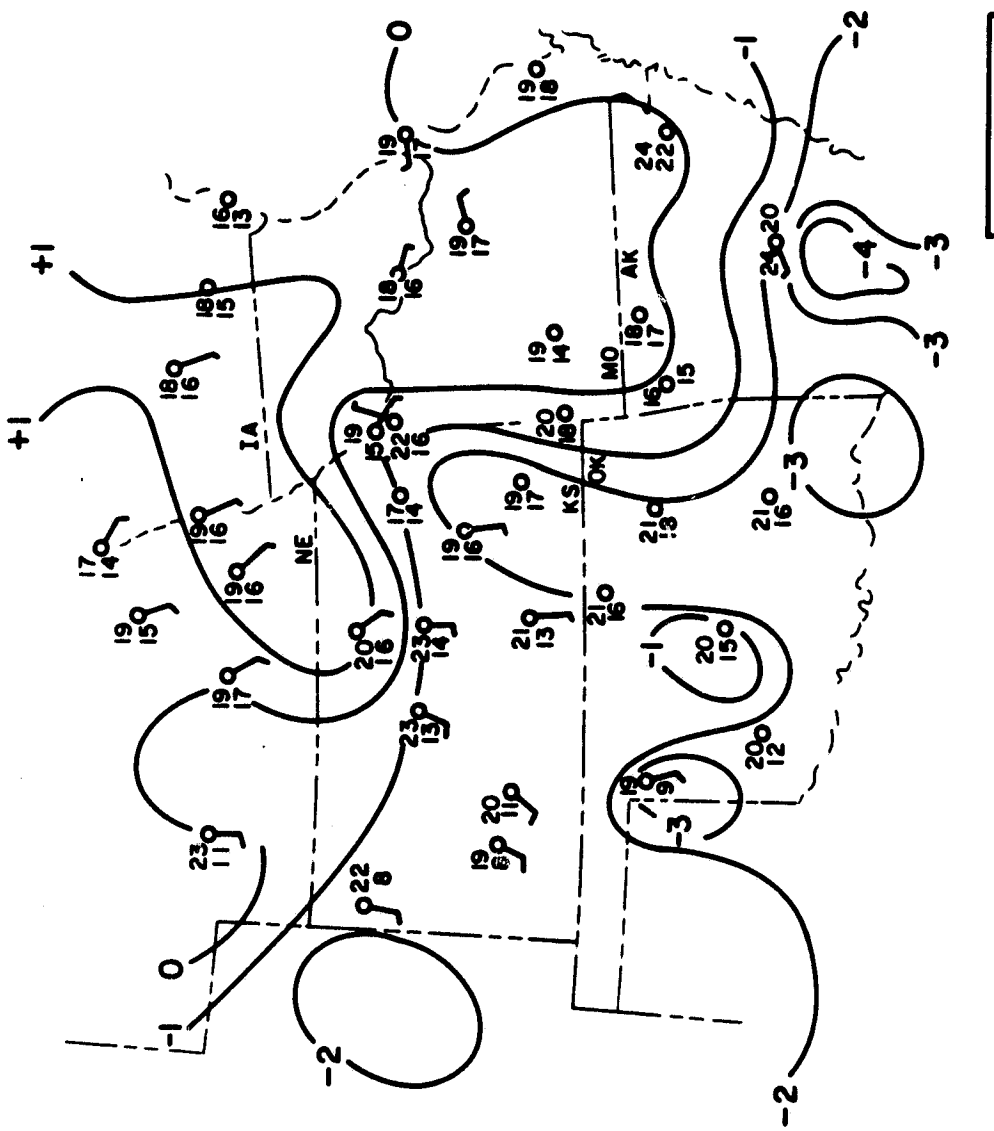

Figure 4.13B: Surface weather analysis. Contours: crop moisture index.

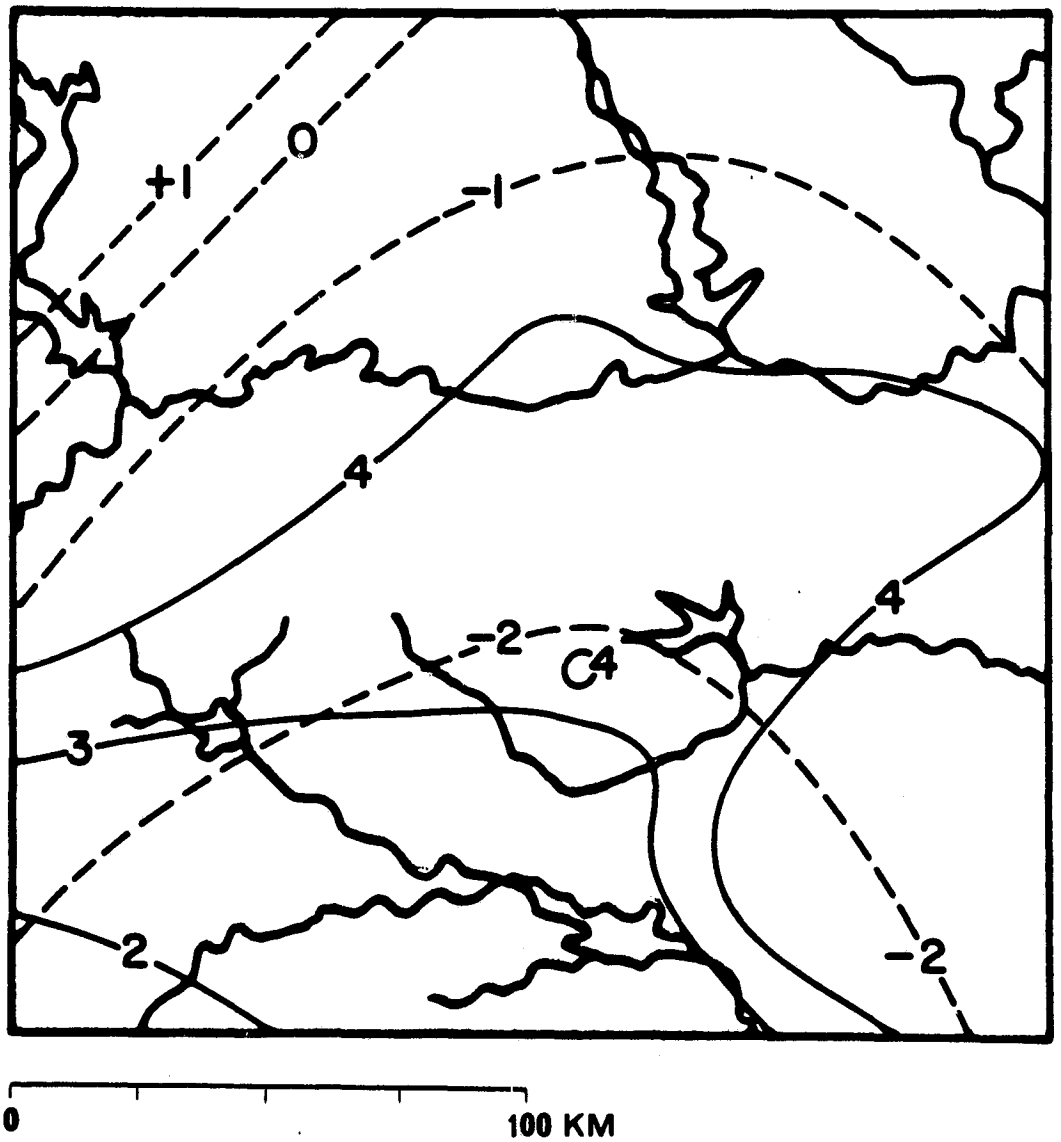

Figure 4.14: Three-week antecedent rainfall and crop moisture index for the Kansas case HCMM domain. Contours as in Fig. 4.2.

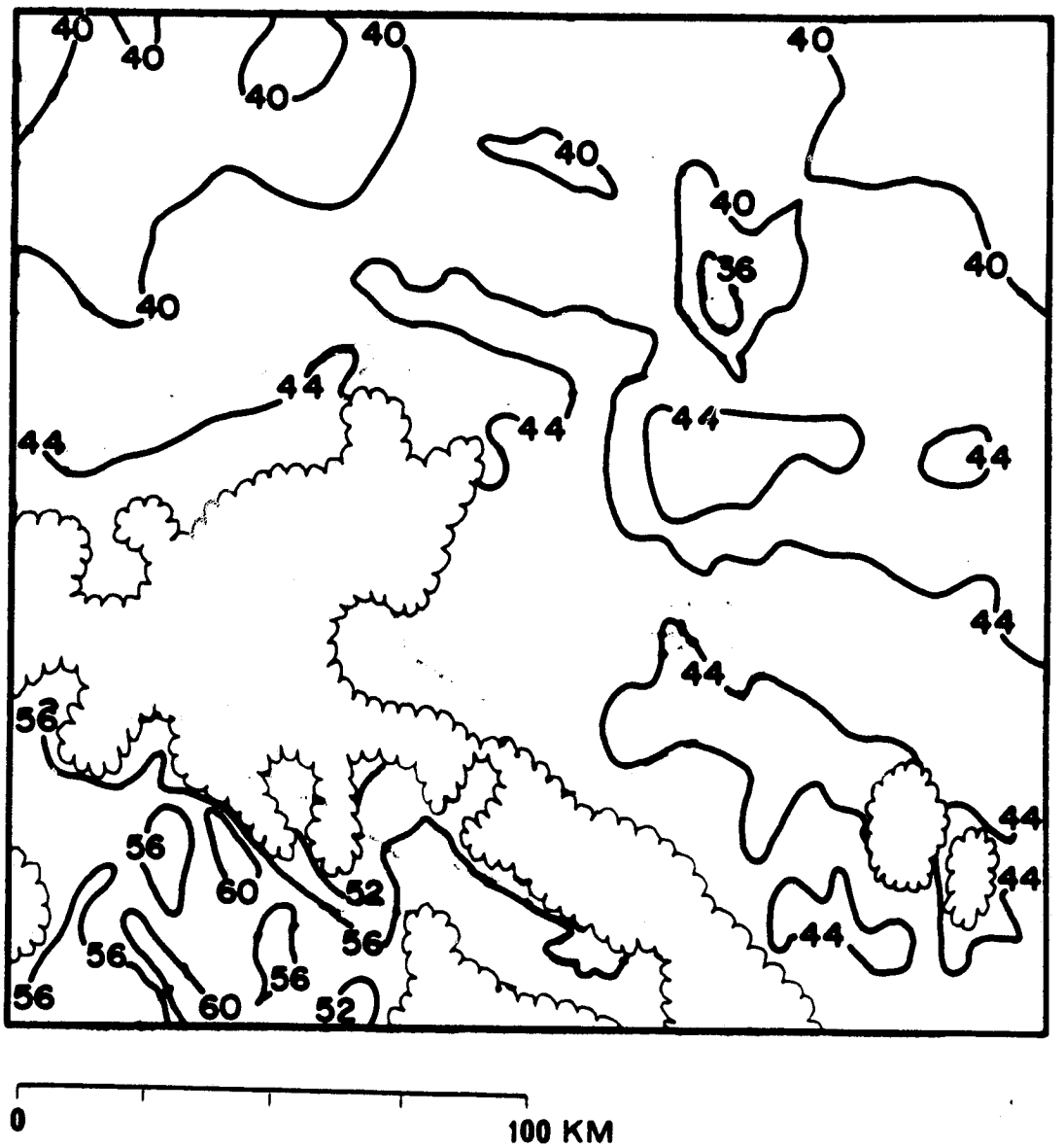

Figure 4.15A: Kansas-case HCMM image, 1934Z, 28 July 1978. Contours as in Fig. 4.3A.

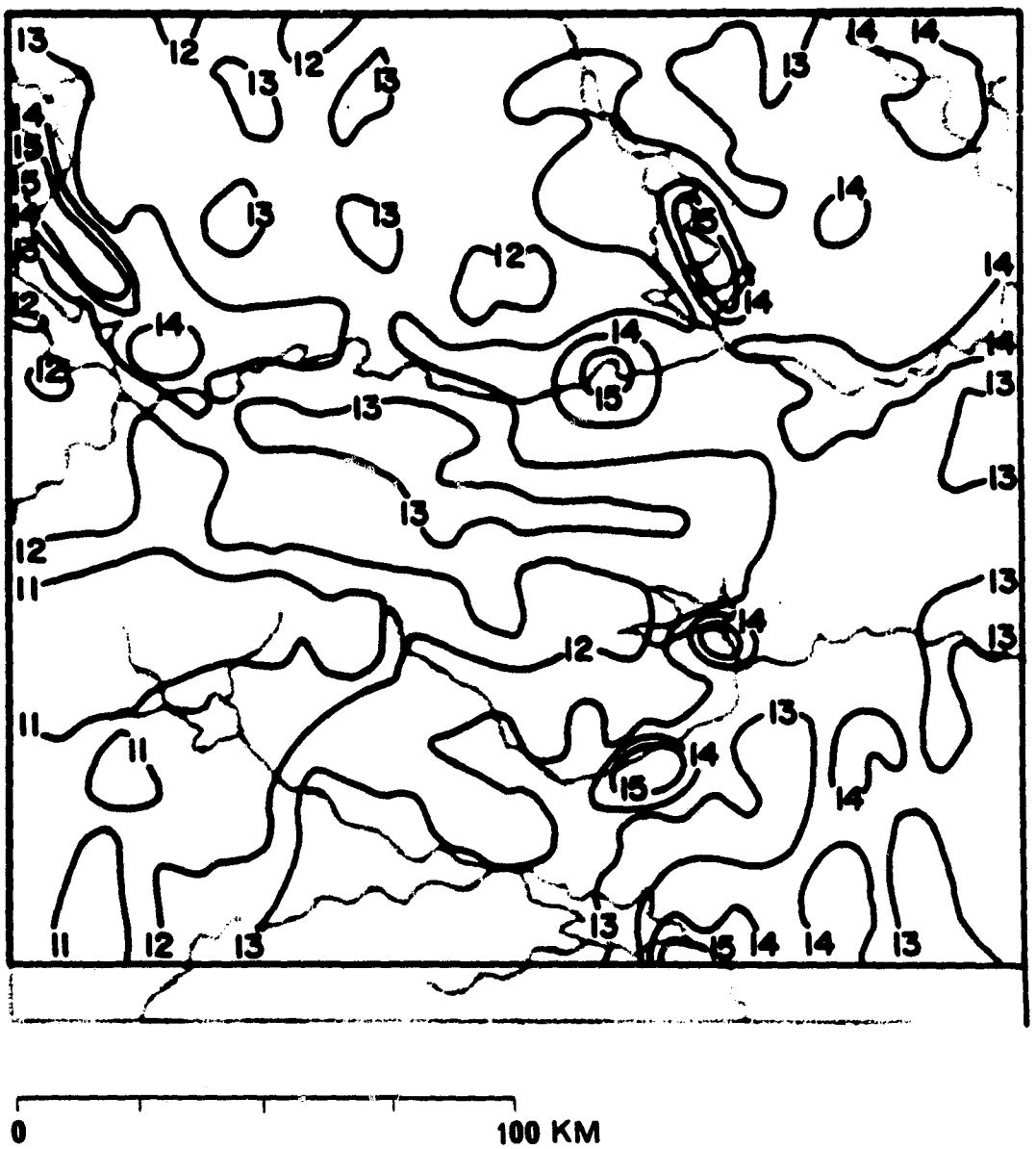

Figure 4.15B: Kansas-case HCMM image, 0823Z, 27 July 1978. Contours as in Fig. 4.3A.

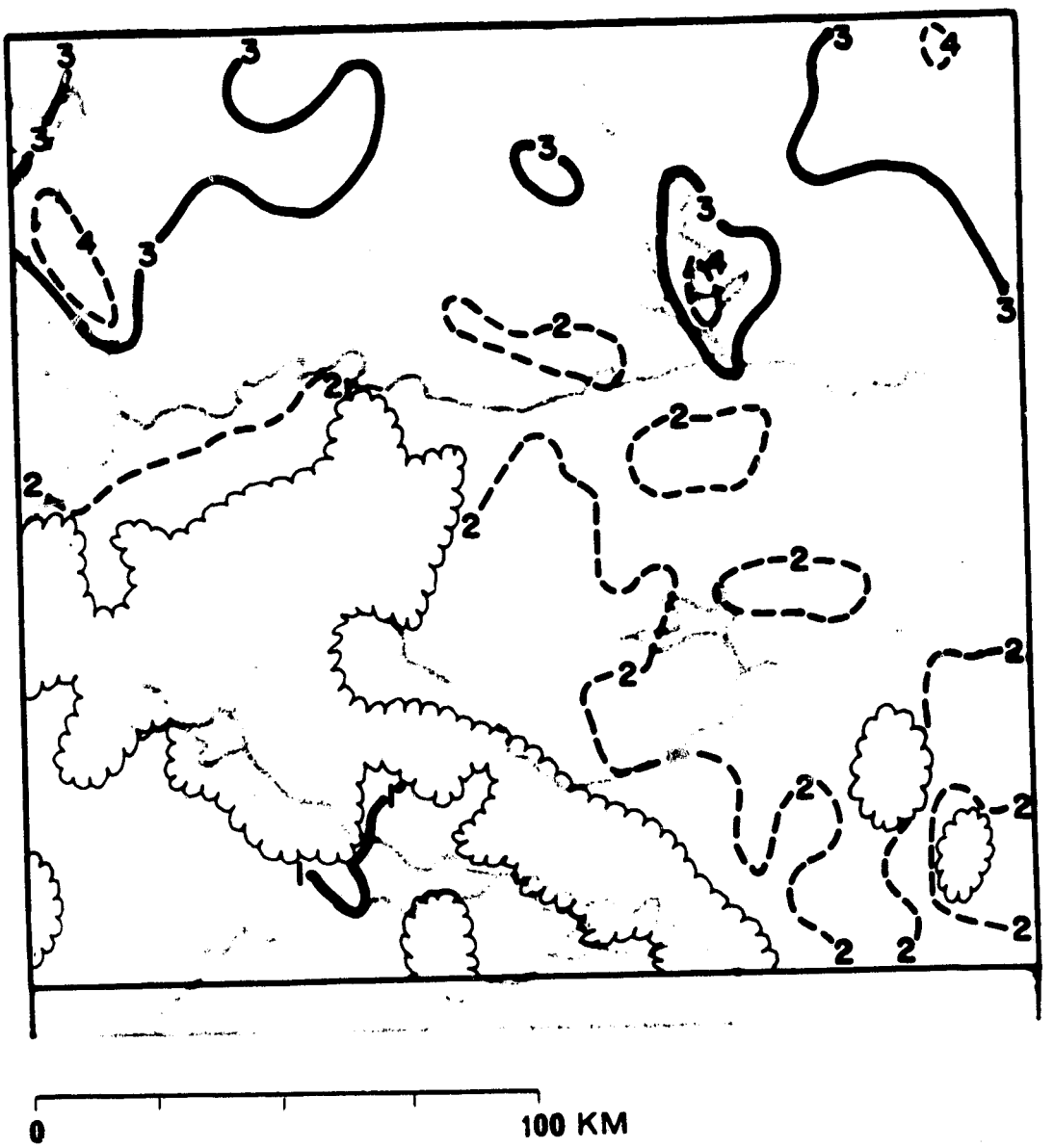

Figure 4.16: Kansas-case moisture availability (M) diagnosed from HCMM data. Contours as in Fig. 4.4.

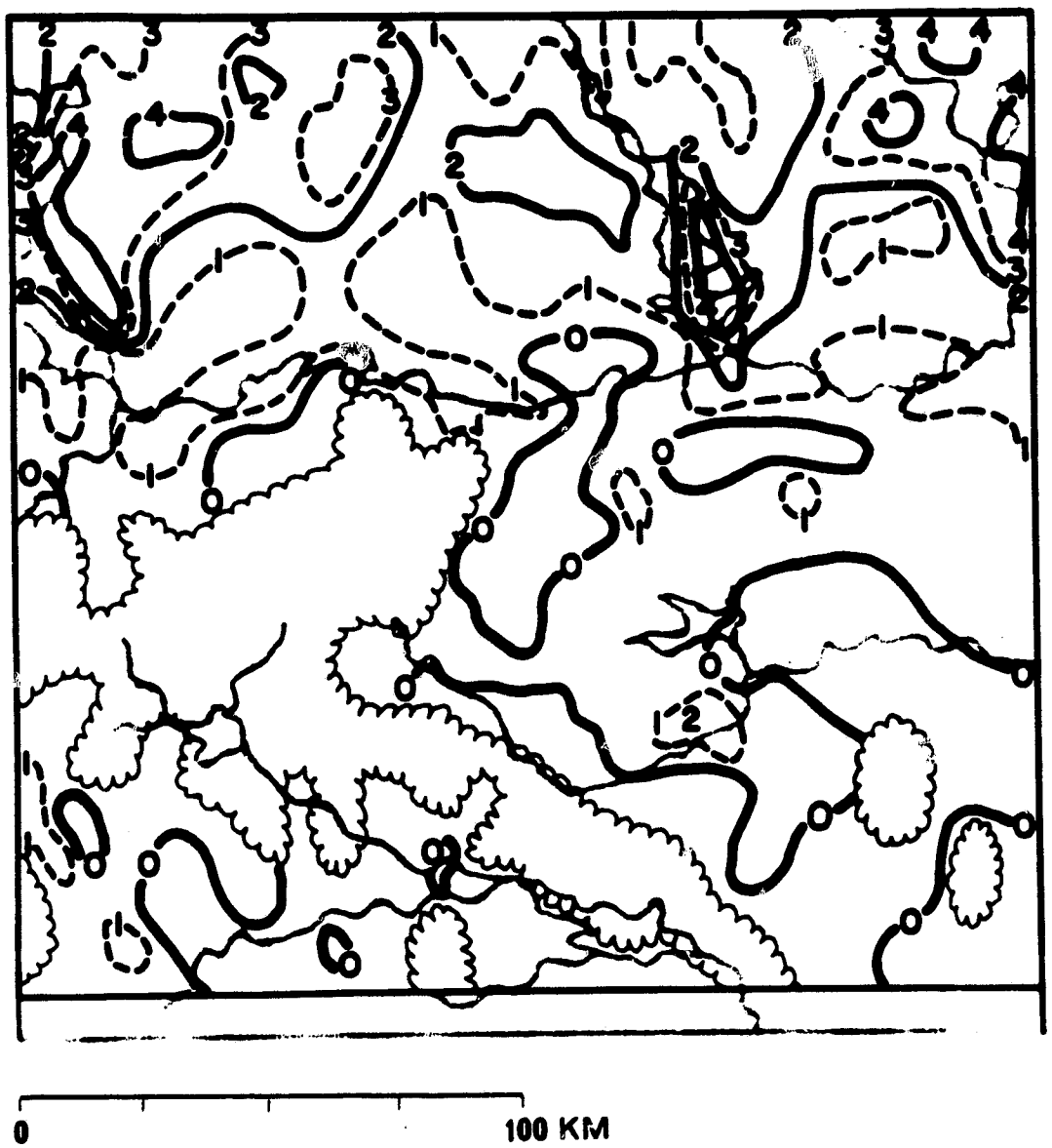

Figure 4.17: Kansas-case thermal inertia (P) diagnosed from HCMM data. Contour interval: 0.01 cal cm^{-1} K^{-1} $sec^{-1/2}$.

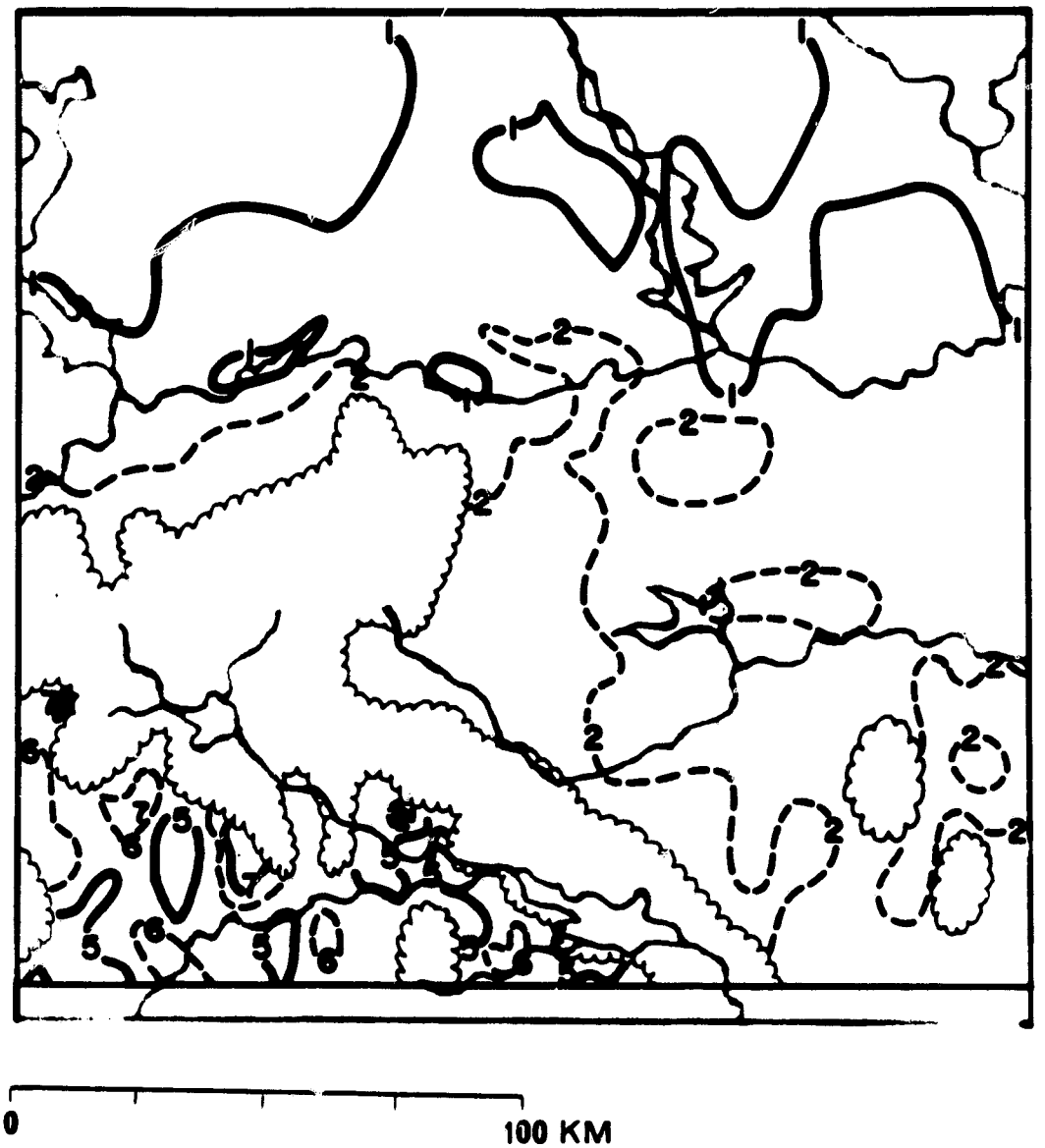

Figure 4.18: Kansas-case heat flux (H_o) diagnosed from HCMM data. Contours in W m^{-2}.

1: 0.15	2: 0.20	3: 0.25	4: 0.30
5: 0.35	6: 0.40	7: 0.45	

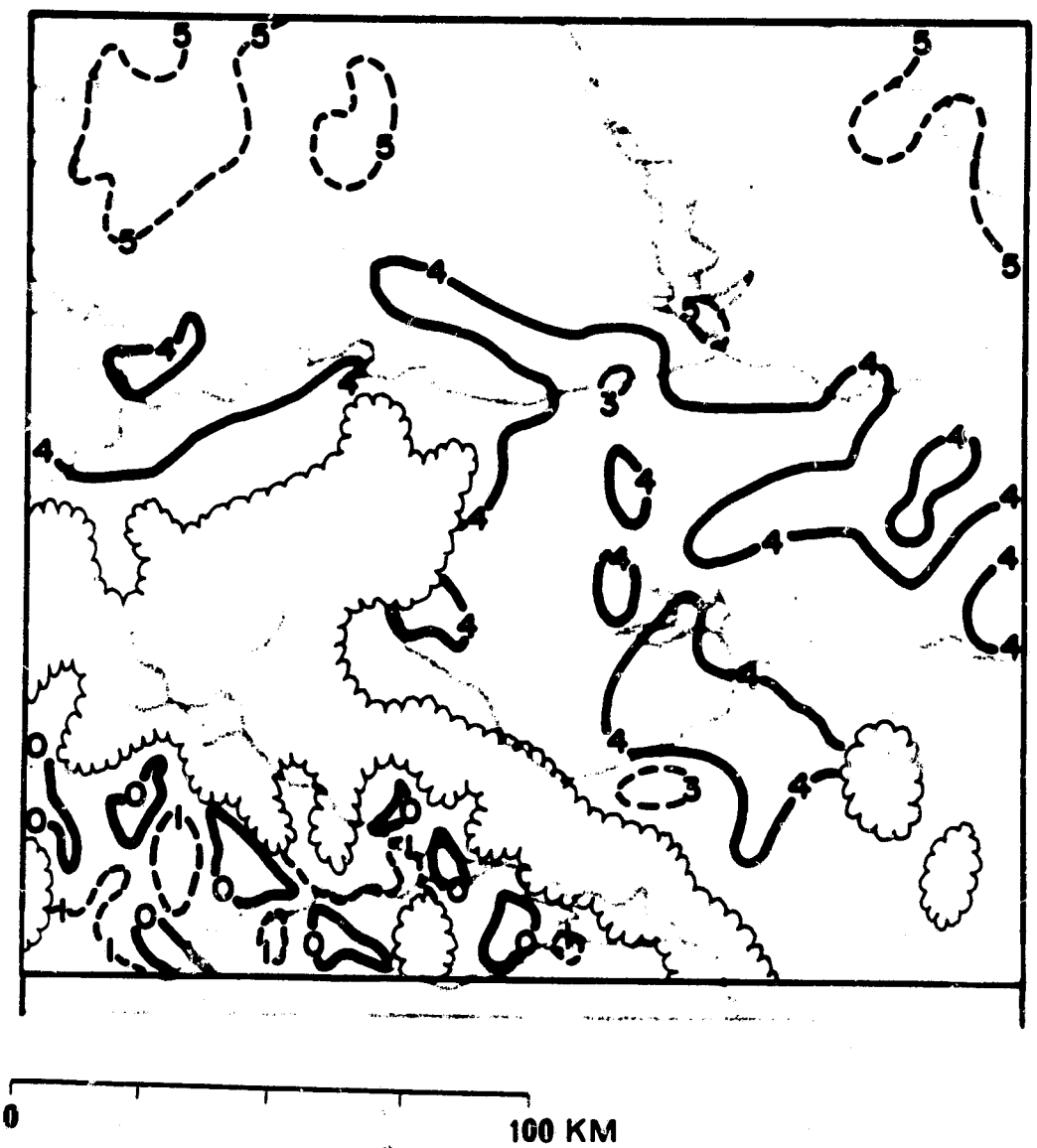

Figure 4.19: Kansas-case total evaporation (E) diagnosed from HCMM data. A special model run using 32 (M, P) pairs was used to produce this diagnosis.

1: 0.35 cm	1: 0.40 cm	2: 0.45 cm
3: 0.50 cm	4: 0.55 cm	5: 0.60 cm

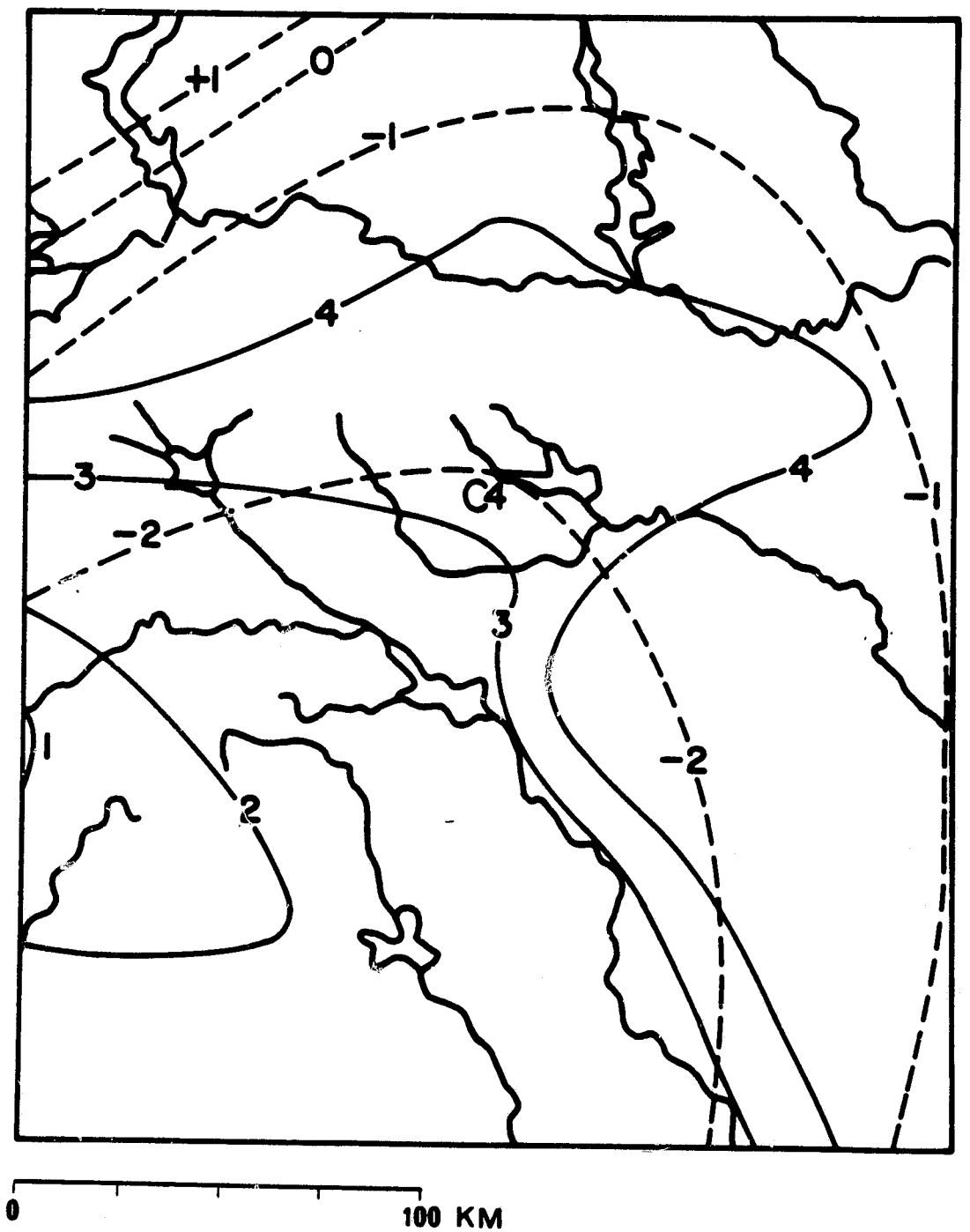

Figure 4.20: Three-week antecedent rainfall and crop moisture index for the Kansas case GOES domain. Contours as in Fig. 4.2.

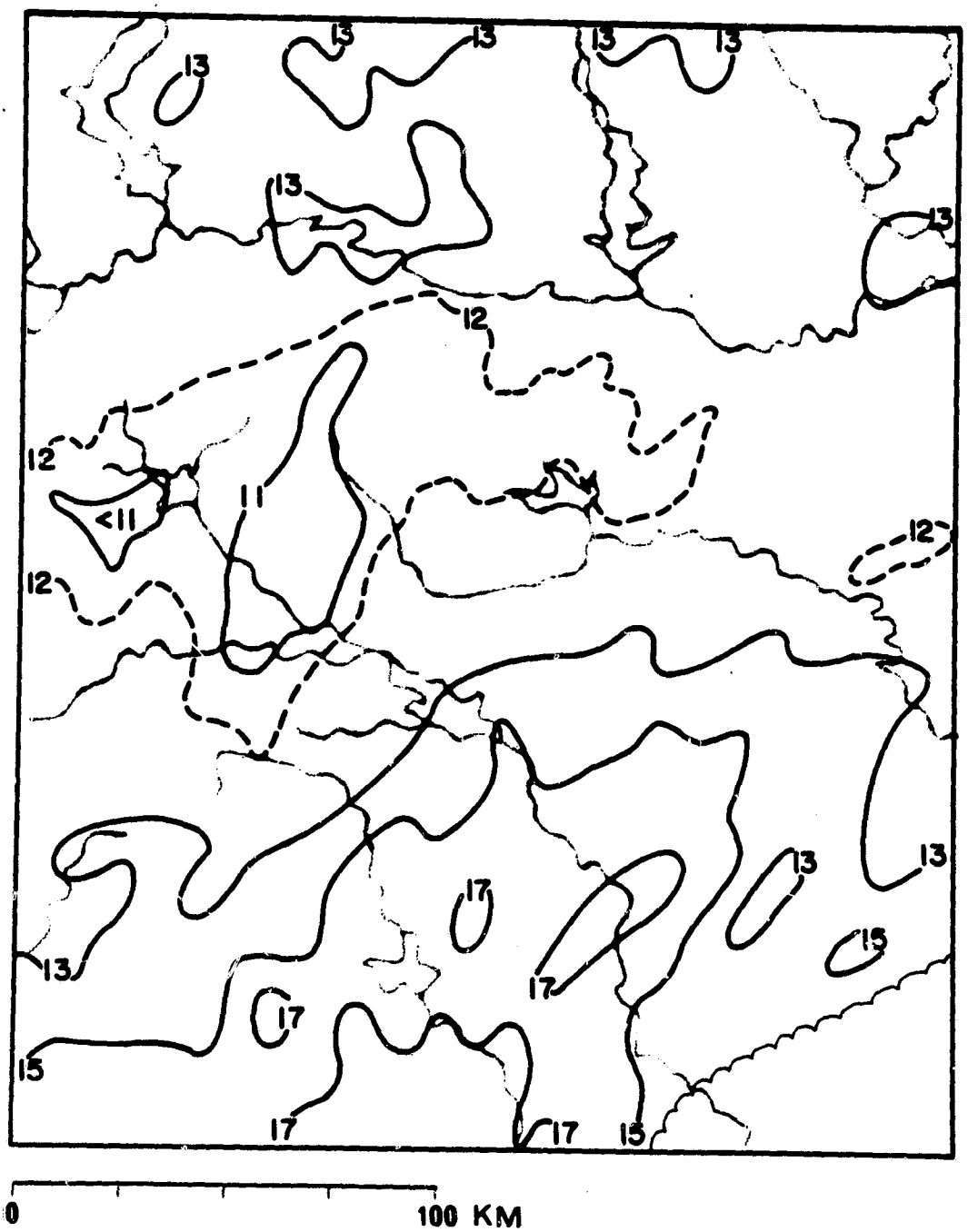

Figure 4.21A: Kansas-case GOES image, 1100Z, 27 July 1978. Contours as in Fig. 4.3A.

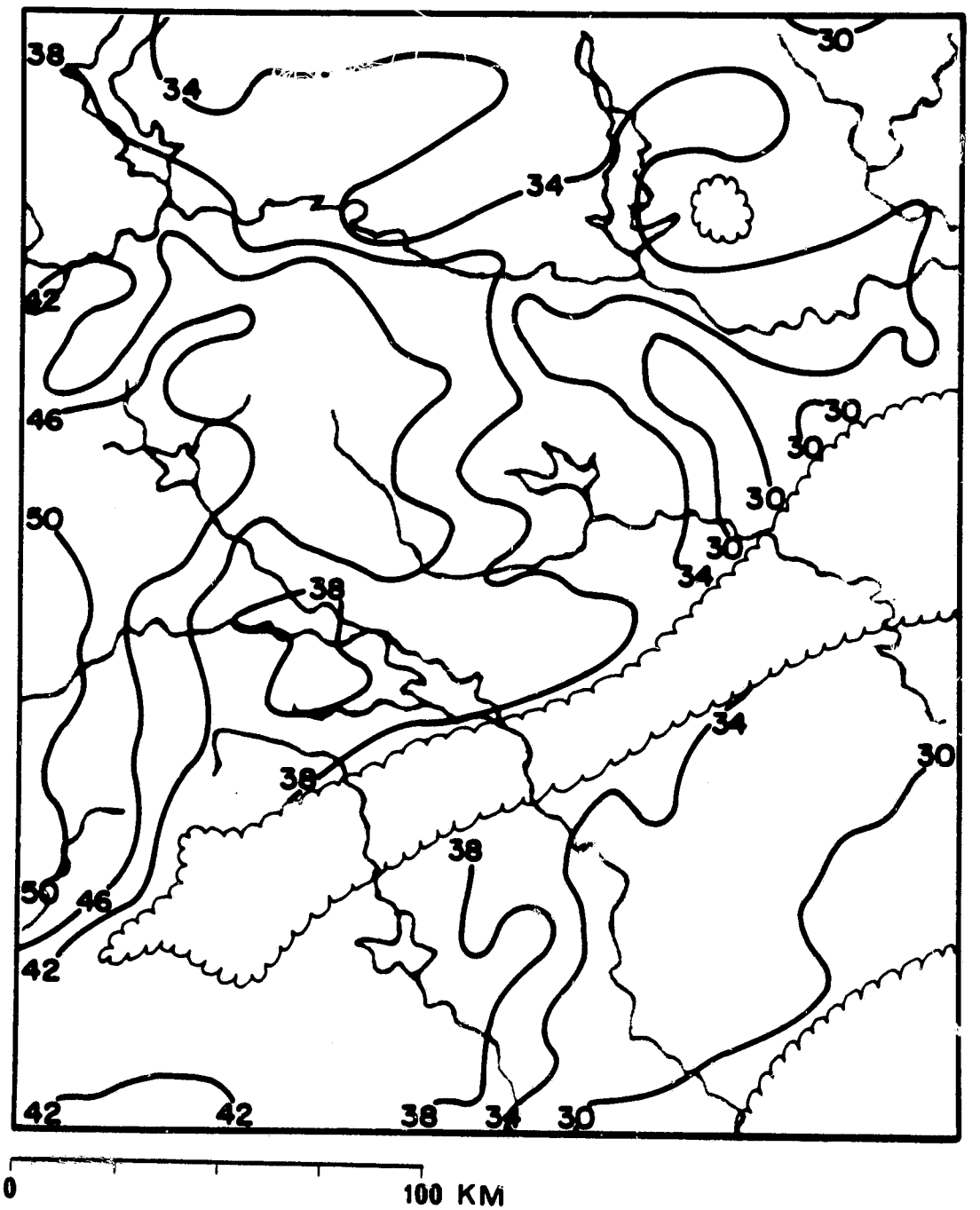

Figure 4.21B: Kansas-case GOES image, 2000Z, 27 July 1978. Contours as in Fig. 4.3A.

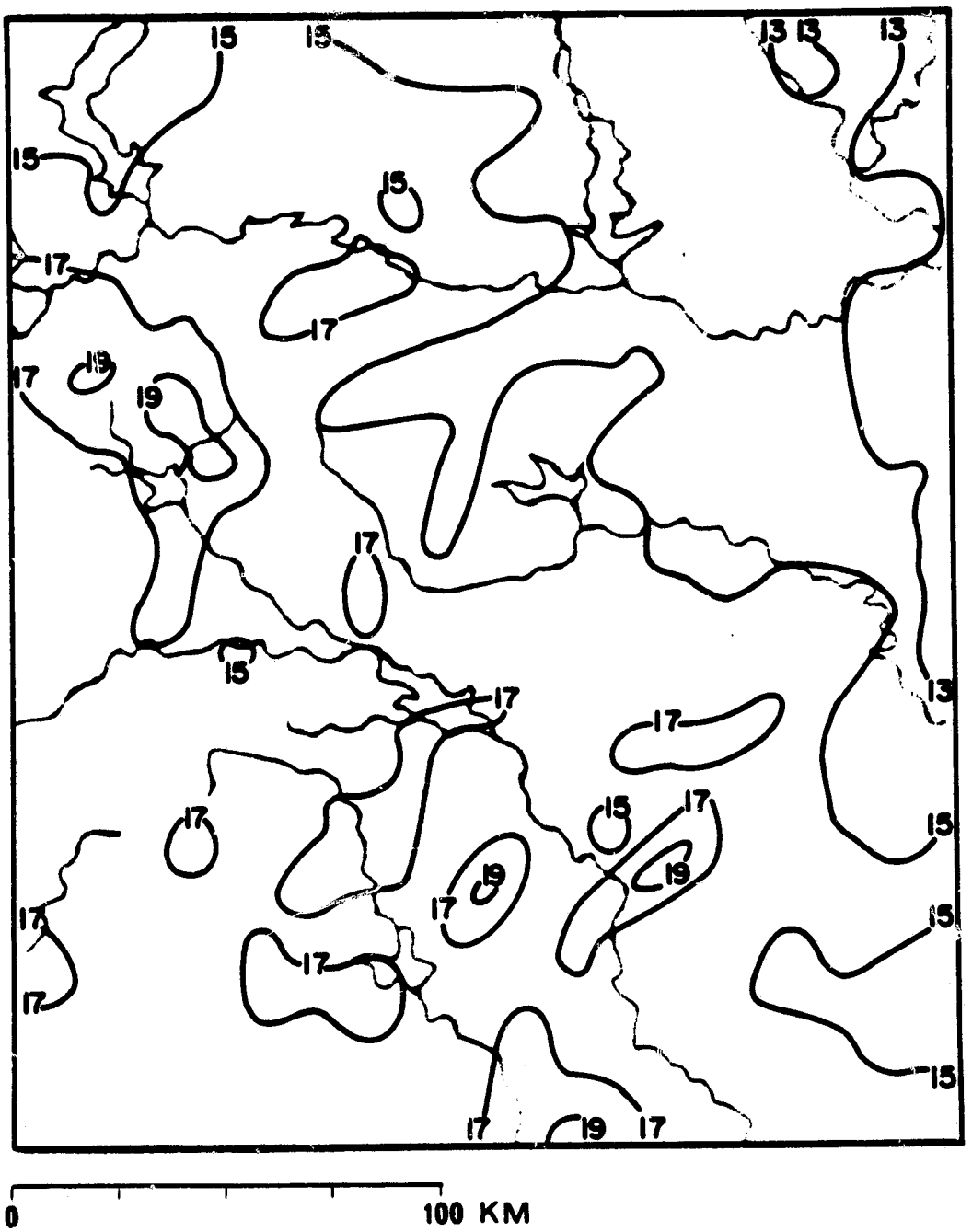

0 100 KM

Figure 4.21C: Kansas-case GOES image, 0900Z, 28 July 1978. Contours as in Fig. 4.3A.

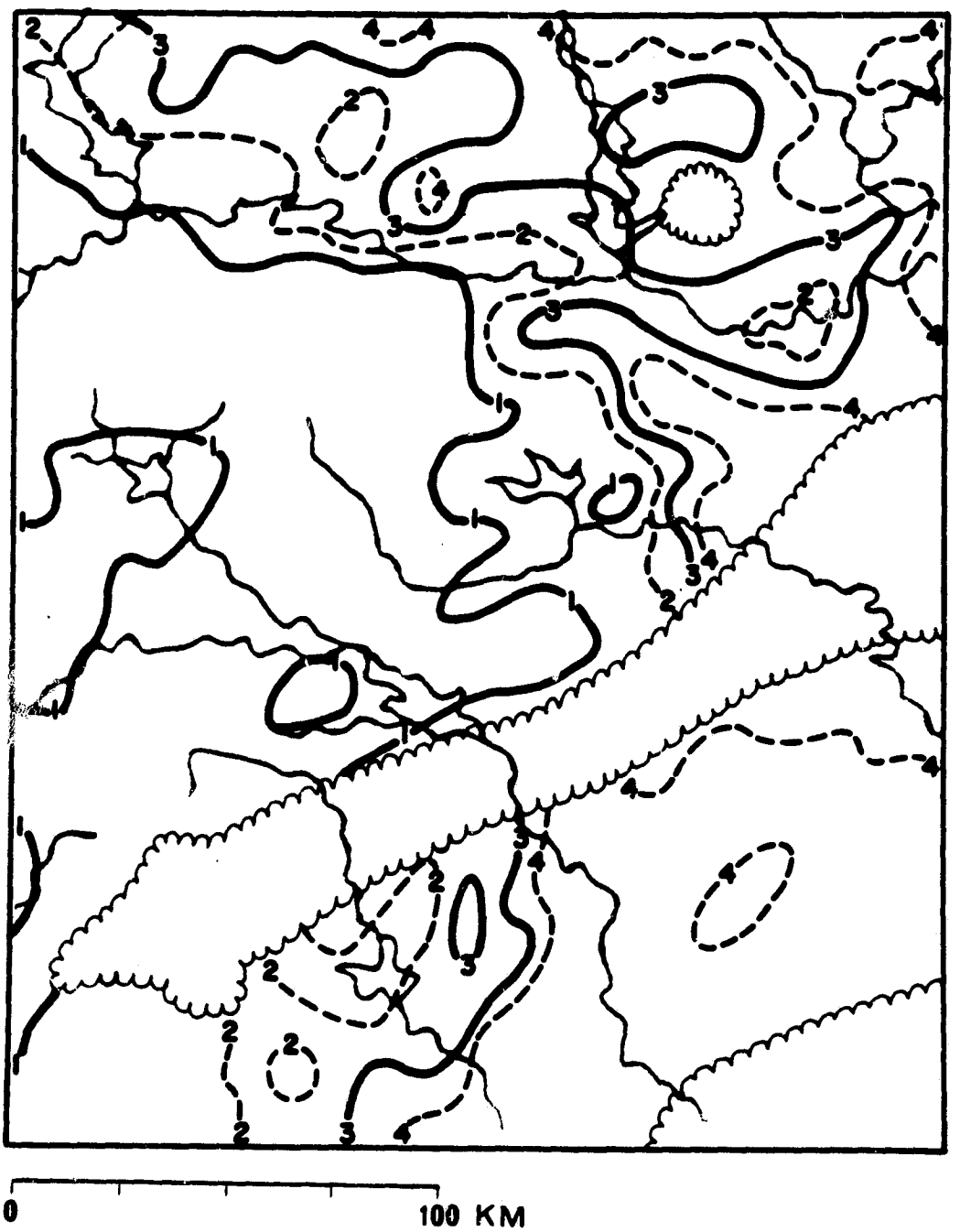

Figure 4.22: Kansas-case moisture availability (M) diagnosed d from GOES data. Contours as in Fig. 4.4.

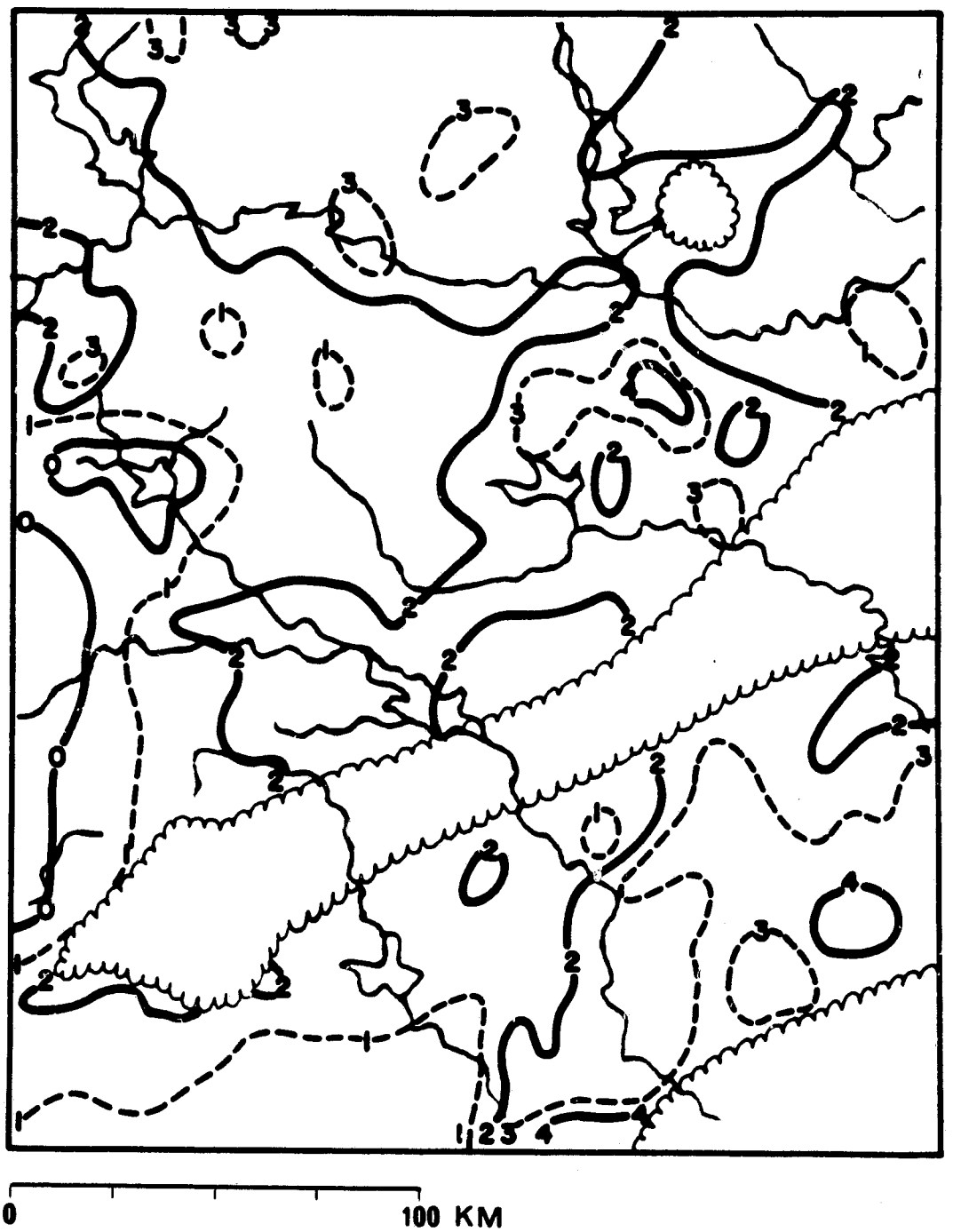

Figure 4.23: Kansas-case thermal inertia (P) diagnosed from GOES data. Contours as in Fig. 4.5.

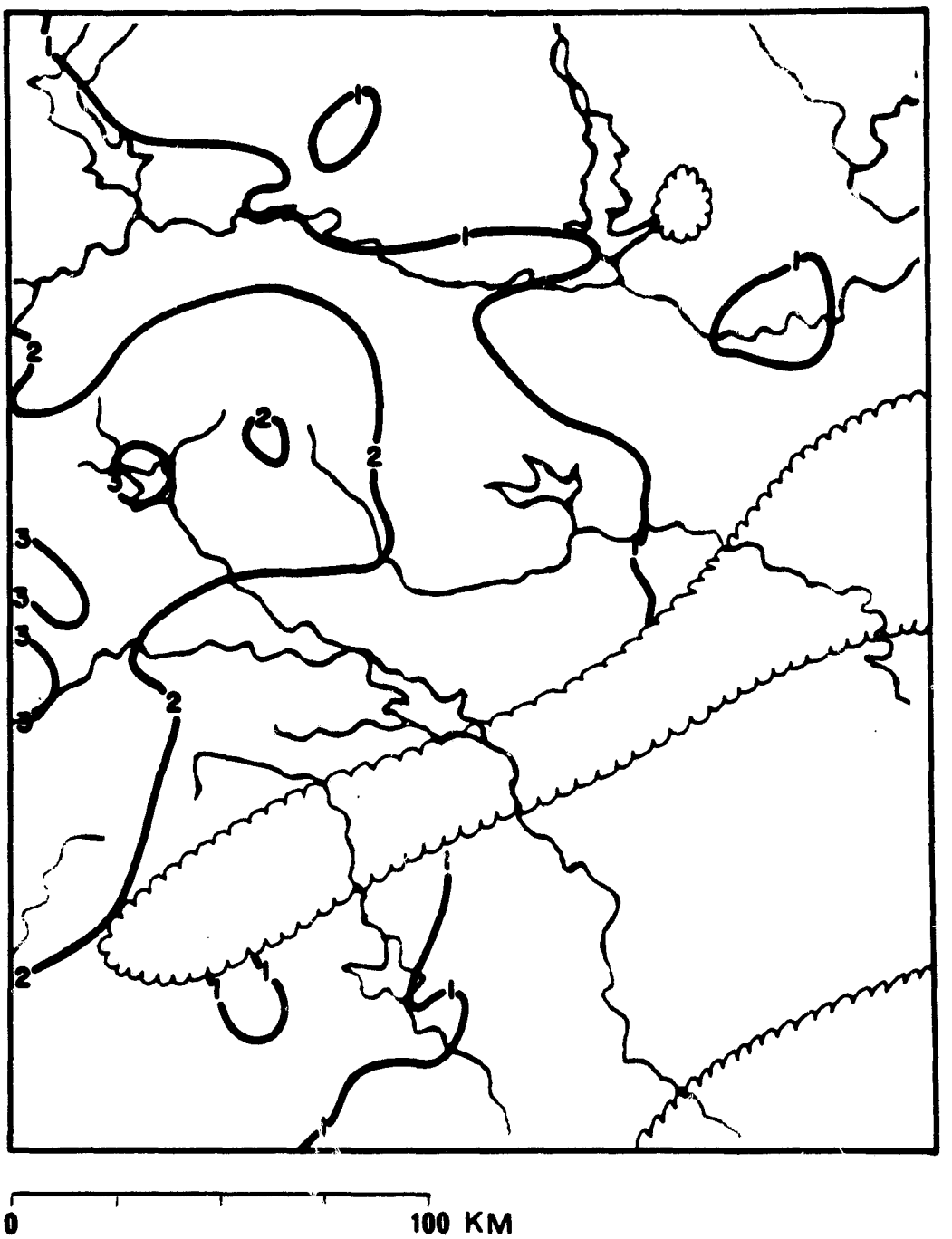

Figure 4.24: Kansas-case heat flux (H_o) diagnosed from GOES data. Contours in W m^{-2}.

0: 0.05 1: 0.15 2: 0.25 3: 0.35 4: 0.45

Note that contour 1 of Fig. 4.18 corresponds to contour 1 of this figure; contour 7 of Fig. 4.18 corresponds to contour 4 of this figure.

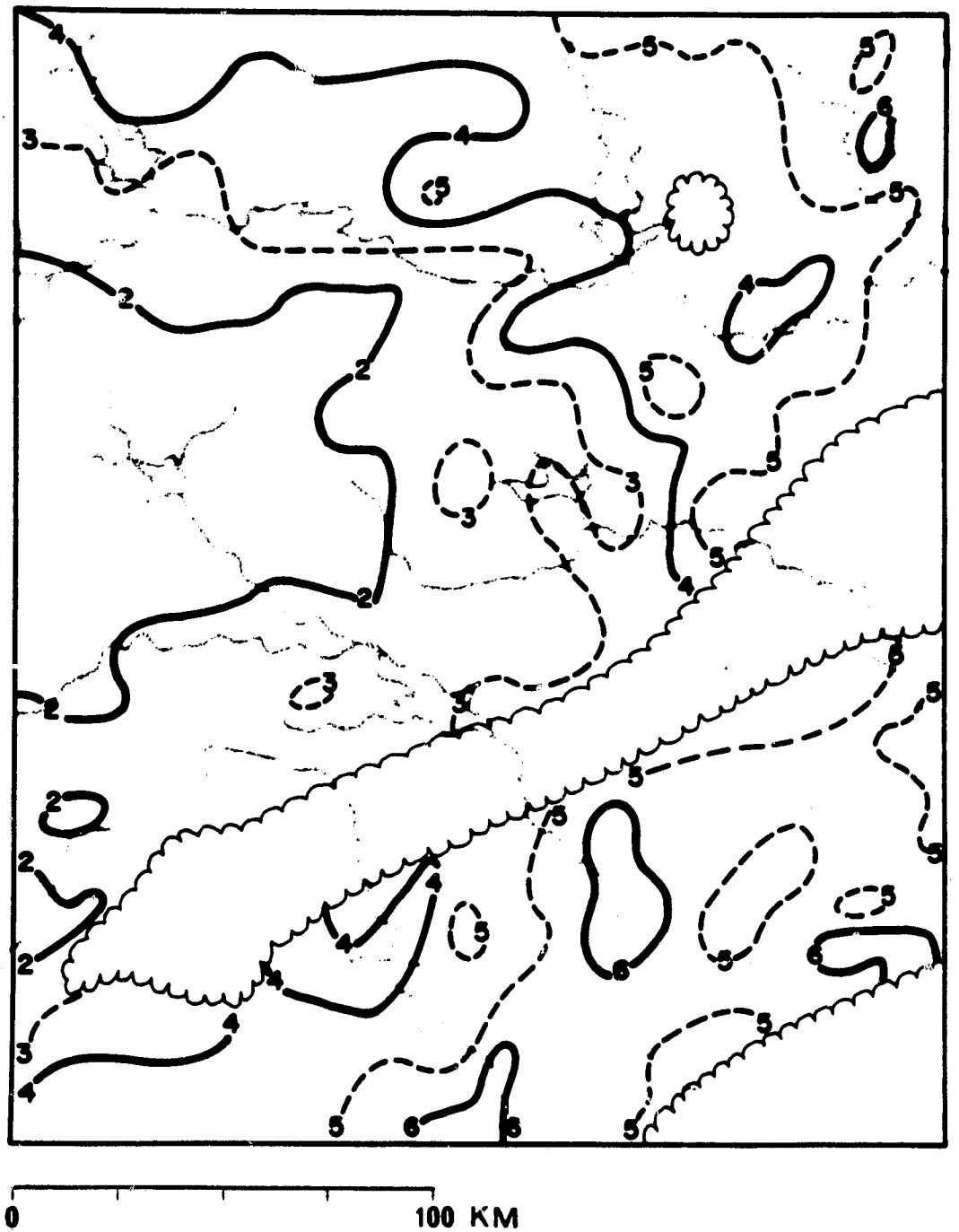

Figure 4.25: Kansas-case total evaporation (E) diagnosed from GOES data. Contour interval: 0.10 cm.

5.0 CONCLUSIONS AND SUGGESTIONS FOR FUTURE RESEARCH

5.1 CONCLUSIONS

The following conclusions can be drawn:

1) Both the GOES method and CD can be used for regional-scale studies
2) Three GOES images are required for the GOES method. The optimal image times are:
    a) about 90 min after sunrise
    b) the time of maximum surface temperature
    c) around midnight

    There is some flexibility in the choice of image times, particularly in the choice of the third image time.
3) The superior resolution of HCMM is important, even on the regional scale. Significant features can be resovled via CD which are invisible to the GOES method.
4) The superior resolution of HCMM enables CD with only two images to equal or exceed the performance of the GOES method with three images.
5) Relative diagnoses of M, P, and H_o can be obtained from either method. The ability to diagnose E has not been satisfactorally demonstrated. Although the E fields produced by both methods appear qualitatively reasonable in most areas and are probably adequate, there are some inconsistencies that need to be explained.

6) Neither method may produce quantitatively correct output fields. The diagnosed M fields exaggerate naturally-occurring contrasts. The same type of error probably occurs in the E and H_o fields. Analysis of error in the P fields is complicated by the difficulty of defining P in a vegetative canopy. Negative and near-zero values of P are certainly incorrect.

7) The present work must be considered a preliminary study. The development of the GOES method is far from complete.

5.2 LIMITATIONS OF THE METHOD: DISCUSSION AND SUGGESTIONS FOR FUTURE RESEARCH

Considerable research is needed in defining and measuring surface parameters in vegetative canopies. Diagnoses of these parameters must remain tentative until more is known about them. The difficulties encountered in defining and measuring surface temperature have been discussed (Section 3.4). Several other questions involving vegetative canopies must be addressed:

1) How is P defined in a vegetative canopy where the radiating surface is a significant distance above the solid ground surface? How is the temperature of the radiating surface influenced by heat transport to and from the region below?

2) To what extent is the temperature of the effective radiating surface affected by ventilation, when the radiating surface is at some distance above the ground in a canopy?

3) Does M vary significantly during the day as plant stomata open and close in response to a variety of stresses?

4) Does E vary significantly as plant stomata open and close? Is any significant part of such variation independent of the variation of M?

These and similar questions need to be answered through further observations in vegetated areas. Significant input into the research effort must be provided by plant physiologists. The research will be neither easy nor inexpensive.

To date, neither CD nor the GOES method has been attempted on an autumn or winter case. The numerical considerations cited in Section 3.4 suggest that some difficulty may be encountered in diagnosing the surface parameters from autumn or winter imagery, even if the question of the thermal and radiative properties of snow is ignored. The daily range of surface temperature may be reduced to the point that the errors inherent in the model overwhelm the information in the satellite images. The numerical model has been demonstrated successfully on simulated autumn initial conditions. The question of whether regression equations obtained from such initializations are adequately stable to permit the mapping of satellite images into M, P, H_o, and/or E fields has not yet been addressed.

The superior resolution of HCMM proved to be of value even in the regional-scale studies (Section 4). The ability to resolve a feature like the Ohio River is certainly worthwhile. HCMM is no longer operating, however, and there is no likelihood that a similar mission will be launched in the near future. The CD algorithm could be tested on TIROS-N imagery or on other thermal-IR

imagery from polar-orbiting platforms. Although TIROS-N has poorer resolution than HCMM, its resolution (1 km) is distinctly superior to the resolution of GOES. The question of whether the superior resolution adequately compensates for the paucity of overpass times is one that can only be answered by experiment.

Hybrid methods could also be attempted to take advantage of the availability of GOES imagery while retaining the superior resolution of polar-orbiter imagery. On a day when a polar-orbiter image pair is available, for example, one GOES image could be used -- probably the early-morning image -- to provide the three images needed for the GOES method. On a day with a single polar-orbiter overpass, two GOES images could be combined with the single polar-orbiter image. It is not known whether differences in image quality or calibration are large enough to prevent the mixing of image sources in the GOES method, nor is it known whether the difference in resolution between GOES and polar-orbiter imagery will make the two types incompatible.

The image differencing done in the GOES method has a theoretical deficiency which was not realized until after the completion of the case studies presented in Section 4. Image subtraction is a valid technique only under the conditions cited in Section 3.5. The assumption of similar soundings at all points in the domain is crucial. If clear skies and light winds prevail during the night, this assumption is likely to fail. Cold-air drainage will produce local pockets of anomalously cold air at the surface; just above these shallow cold layers, there will be no horizontal contrast.

These shallow cold pockets are definitely large enough to be resolved by HCMM; some are resolvable by GOES.[1] This error in the subtraction procedure is maximized by selecting a morning image time near sunrise; the error decreases as the morning image time is made later. Unfortunately, a later morning image time increases the numerical difficulties cited in Section 3.4. The trade-off between inaccuracies and numerical difficulties could be investigated, but only if some form of ground truth is available. Preliminary evidence indicates that the numerical difficulties are the more serious. There is no evidence of degradation of performance attributable to cold pockets in either of the case studies in Section 4.

The subtraction step could be bypassed, and all three temperatures could be used as predictors in a modified GOES procedure. If this were done, the number of coefficients in the regression equations would increase, increasing the risk of overfitting the data (Section 3.4 and Appendix I). Also, the underlying problem would not be addressed. The model would still be initialized with only one sounding. The method would implicitly assume that the

[1] An extreme example of this phenomenon is presented by Schlegel and Butch (1980). They found that the nocturnal temperature drop is greatly exaggerated in the Barrens, a notorious cold-air drainage location near State College, PA. Minimum temperatures in the Barrens are much lower than minima at Penn State University on clear, calm nights. Daytime maxima in the two locations are comparable. Much of this anomaly is explained by cold-air drainage into the bowl-shaped valley. The thermal properties of the sandy soil and stunted vegetation cannot alone account for an effect of the magnitude of the cold anomaly of the Barrens.

sounding was identical at all points in the region: a more stringent assumption than the assumption of similar-shaped soundings. However, the quality of the output might be improved. A test of a three-temperature GOES method is desirable, but should not be given high priority. Unless a new idea is forthcoming, the error in the subtraction algorithm will probably have to be accepted.

The one-dimensional boundary-layer model used in CD and the GOES method has proved to be adequate in diagnosing M, P, H_o, and E from HCMM and GOES imagery in several different studies. Work is presently in progress to add several improvements to the model:

1) constant temperature advection,

2) improved daytime boundary-layer winds,

3) better subsurface heat storage and flux parameterization.

These improvements should be documented by Rose in 1983.

Both CD and the GOES method use a simple polynomial regression equation in two variables to invert the model. Results have been qualitatively satisfying but quantitatively dubious. This inadequacy may be related to the physical response of surface temperature to M and P -- a response which is apparently modeled quite well.

Diurnal surface temperature rise and fall are extremely sensitive to small changes of M and P when M and P both have relatively low values. For high values of M and P, diurnal temperature rise and fall are rather insensitive to changes in M and P. Note the data in Table 5.1, taken from a model simulation of the Kansas case

Table 5.1

Model surface temperatures generated for the Kansas case (27 July 1978) for selected initial values of M and P

M	P	SIMULATED SFC TEMPERATURES (K) AT SIMULATED GOES TIMES LST 0800	1400	2300	DTD	DTN
0.05	0.0125	303.21	332.37	292.89	29.16	39.50
0.35	0.0125	299.61	317.39	289.45	17.78	27.94
0.05	0.0500	296.62	322.52	300.18	25.90	22.34
0.35	0.0500	295.75	313.87	296.57	18.12	17.3
0.65	0.0875	294.10	308.74	296.91	14.64	11.83
0.95	0.0875	293.75	307.59	296.66	13.84	10.93
0.65	0.1250	293.89	307.07	297.50	13.18	9.57
0.95	0.1250	293.59	306.16	297.28	12.60	8.91

(4.2). When the model is inverted, the sensitivities are also inverted. Let ΔT be an appropriate measure of diurnal temperature rise or fall. Then, $\frac{\partial M}{\partial \Delta T}$ and $\frac{\partial P}{\partial \Delta T}$ are very small for large ΔT, and rather large for small values of ΔT. It is difficult to obtain a single polynomial in temperature or temperature-change which matches the behavior of M or P at both ends of the temperature or temperature-change range. A piecewise-polynomial interpolating function may fit the data more successfully than a global least-squares approximating polynomial. The piecewise interpolant need not match the model-output globally. For example, a cubic spline interpolant can fit data very well, providing only a single predictor is used. If M were to be diagnosed from morning temperature change only, with

P-dependence suppressed in the model, a cubic spline could be used in place of a regression equation in the single predictand DTD. The extension of the concept of cubic splines to two dimensions is beyond the competence of the present author. However, it might be possible to fit an augmented model-output data set by piecewise-linear functions (see Appendix II). More than 16 (M, P) pairs would probably have to be used in the model simulation. The problem of replacing the regression routine by piecewise-polynomial interpolants is worth pursuing. See Appendix II, Section 3 for a possible piecewise-linear interpolation method.

The chief impediment to the operational use of CD or the GOES method is the acquisition and alignment of satellite subimages. To obtain one aligned subimage of a target area, a technician must spend one half to one full working day searching for recognizable geographic features on the satellite image. The task is exceptionally difficult on night imagery, where the contrast between land and ocean is minimal. Until the procedure for obtaining aligned subimages is expedited, real-time applications will be nearly impossible, and ongoing studies of several regions will be economically infeasible. High priority should be placed on developing a fully-automated procedure for selecting and aligning subimages for GOES and other infrared satellite imagery.

Although the GOES method is not yet ready for real-time operational use, work is currently being done on the time evolution of the historical M anomaly in the Kansas case (Section 4.3) (Rose, 1983). Other potential applications of the GOES method

include the preparation of M, P, and possibly H_o and E fields for use by mesoscale numerical weather prediction models. If the subimage acquisition problem can be solved, the GOES method could provide surface parameters for operational NWP; a pilot study should be done.

5.3 FUTURE RESEARCH: A PLAN OF ACTION

Remote sensing of soil and surface parameters is potentially very valuable. The GOES method has been shown to diagnose several soil and surface parameters with some skill, using weather-satellite imagery. The future usefulness of this technique depends on the results of further research. This author recommends pursuing the following course:

As the top priority, solve the subimage acquisition and alignment problem. Operational work cannot proceed as long as acquisition of usable data is extremely tedious and difficult.

If funding and outside expertise can be found, the study of the micrometeorology of plant canopies should also be given high priority. It is hard to model a quantity which is poorly understood, using data of unknown quality and a method designed for conditions different from the ones which actually prevail.

Applications of the GOES method and pilot studies of its uses should be given intermediate priority.

Intermediate priority also should be given to improving the regression algorithm or replacing it with piecewise-polynomial functions.

Studies of TIROS-N and hybrid methods should receive high priority when the image acquisition problem is solved. The use of TIROS-N data in the CD method should be attempted as soon as data become available. Large-scale evaluation of TIROS-N and hybrid methods must wait for the solution to the image acquisition and alignment problem, for economic reasons.

Low priority should be given to the incorporation of improvements into the model and the systematic evaluation of the image-differencing technique. Until the micrometeorology of plant canopies is understood, it will be difficult to evaluate the results of "improving" the model or to evaluate image-differencing. Preliminary experiments with "improvements" in the model indicate that uncertainties in the GOES method overwhelm any improvements resulting from added sophistication in the numerical model. The time for major improvements in the model is after ground-truth becomes available, not before.

There is little doubt that surface parameters will eventually be diagnosed via some form of remote sensing. Whether operational diagnoses can be achieved by the GOES method, using geostationary observation platforms, remains to be seen. Whether the GOES method or one of its successors is eventually adopted, the experience gained in the development of CD and the GOES method will be valuable.

BIBLIOGRAPHY

Carlson, T.N. and F.E. Boland, 1978: Analysis of urban-rural canopy using a surface heat flux/temperature model. J. Appl. Met., 17: 998-1013.

Carlson, T.N., and D.C. di Cristofaro, 1981: The effects of surface heat flux on plume spread and concentration: an assessment based on remote measurements. Remote Sensing of the Environment, 11: 385-392.

Carlson, T.N., J.K. Dodd, S.G. Benjamin, and J.N. Cooper, 1981: Satellite estimation of surface energy balance, moisture availability, and thermal inertia. J. Appl. Met., 20: 67-87.

Conte, S.D., and de Boor, C., 1972: Elementary Numerical Analysis, 2nd ed., McGraw Hill Book Co., New York, NY, Ch. 4, pp. 191-273.

Davis, P.J., 1963, 1975: Interpolation and Approximation. Dover Press, New York, NY, xiv + 393 pages. 1975 reprint of 1963 book.

Dejace, J. and Megier, J., 1979: Mapping thermal inertia, soil moisture, and evaporation from aircraft day and night thermal data. Proc. of the 13th Internat. Symp. on Remote Sensing of the Environ., Environmental Research Institute of Michigan, Ann Arbor, pp. 1015-1027.

Dodd, J.K., 1979: Determination of surface characteristics and energy budget over an urban-rural area using satellite data and a boundary-layer model. MS Thesis, Department of Meteorology, The Pennsylvania State University.

Espenshade, E.B. and J.L. Morrison, ed., 1978: Goode's World Atlas, 15th Ed., Rand McNally, Chicago, p. 76-77, 116-117, 104-105, 120-121.

Forsythe, G.E., M.A. Malcolm, and C.B. Moler, 1977: Computer Methods for Mathematical Computations. Prentice-Hall, Englewood Cliffs, NJ 07623, Ch. 2, pp. 10-29.

Goody, R.M., 1964: Atmospheric Radiation I: Theoretical Basis. Oxford University Press, pp. 29-31.

Kocin, P.J., 1979: Remote Estimation of Surface Moisture Over a Watershed, MS Thesis, Department of Meteorology, The Pennsylvania State University.

Price, J.C., 1980. The potential of remotely sensed thermal infrared data to infer surface soil moisture and evaporation. Water Resources Research, 16: 787-795.

Price, J.C., 1982a: On the use of satellite data to infer surface fluxes at meteorological scales. J. Appl. Met. (in press).

Price, J.C., 1982b: Estimation of regional scale evapotranspiration through analysis of satellite thermal infrared data. Submitted for publication.

Rose, F., 1983: MS Thesis; research in progress. Department of Meteorology, The Pennsylvania State University.

Rosema, A. and J.H. Bijleveld, P. Reininger and G. Tassone, K. Blyth and R.J. Gurney, 1978: "Tell-us," a combined surface temperature, soil moisture, and evaporation mapping approach. Proc. of the 12th Int. Symp. on Remote Sensing of the Environ., Environmental Research Institute of Michigan, Ann Arbor.

Ryan, T.A., Jr., B.L. Joiner, and B.F. Ryan, 1976. MINITAB Student Handbook. Duxbury Press, North Scituate, MA, IX + 341 pages.

Schlegel, J. and G. Butch, 1980: The Barrens: Pennsylvania's year-round deep-freeze. Bull. AMS 61: 1368-1373.

Schmugge, T., B. Blanchard, A. Anderson, and J. Wang, 1978: Soil moisture sensing with aircraft observations of the diurnal range of surface temperature. Water Resource Bull., 14: 169-178.

Sellers, W.D., 1965: Physical Climatology. University of Chicago Press, Chicago, IL, pp. 134-140.

Short, N.M., P.D. Lowman, Jr., S.C. Freden, and W.A. Finch, 1976: Mission to Earth: LANDSAT Views the World. NASA SP-360, Govt. Printing Office, Washington, DC, ix + 459 pages.

Wetzel, P.J. and Atlas, D., 1981: Inference of precipitation through thermal infrared measurements of soil moisture. Precipitation Measurements from Space Workshop Report, 1981, Atlas, D. and Thiele, O.W., Ed., Goddard Laboratory for Atmospheric Sciences, Goddard Space Flight Center, Greenbelt, MD, pp. D-170 to D-172.

Williams, D.L. and B.L. Barker, 1973: Kansas Land Use Patterns, Summer 1973. Space Technology Laboratories, University of Kansas in coop with Planning Division, Kansas Department of Econ. Devel.

APPENDIX I: NUMERICAL ANALYSIS

Much of the work in this thesis involves approximations. The satellite data and model output are approximate; they contain error. This appendix discusses:

1) theoretical implications of approximation
2) the role of approximation in the GOES method
3) possible effects of approximation

A formal numerical analysis of the GOES method is not attempted. Basic principles of numerical analysis will be presented and applied to the GOES method. Awareness of these principles can suggest ways of reducing numerical errors in the GOES method.

The important topic of floating-point arithmetic will not be discussed, since the numerical model used in the GOES method is relatively simple and stable. The interested reader is referred to Chapter 2 of Forsythe, Malcolm, and Moler (1977). Section I.1 considers the problem of approximating derivatives, and applies its results to the problem of approximating temperature derivatives with GOES data. Section I.2 deals with regression: approximating one function by a simpler one, when only limited data of uncertain quality are available.

I.1 NUMERICAL APPROXIMATION OF DERIVATIVES

Assume that it is desirable to estimate the time derivative of temperature at a specific time: 0945 local time, for example.

The simplest and best approach would be to use the centered-difference approximation to the derivative:

$$\frac{\partial T}{\partial T} = \frac{T_2 - T_1}{t_2 - t_1} \tag{I.1}$$

where T_1 and T_2 are temperatures measured at times t_1 and t_2, respectively. Times t_1 and t_2 are selected such that:

$$\frac{1}{2}\,(t_1 + t_2) = 0945\ . \tag{I.2}$$

This approximation is equivalent to approximating the graph of $T(t)$ from t_1 to t_2 by a straight line.

Assume that the actual temperatures are as follows:

Time	Temperature	
0930	300.0 K	(I.3)
1000	301.0 K	

The actual value of the derivative:

$$\frac{\partial T}{\partial t} = 2.00\ \text{K/hr} \tag{I.4}$$

Now, assume that satellite imagery or computer output is available, but that either contain random error of up to 0.3 K. This corresponds to a 0.1 percent error in absolute temperature, not unreasonable for a temperature computed from narrow-band IR reception by a satellite. The available data are:

Time	Temperature Range	
0930	$299.7\ \text{K} \leq T_1 \leq 300.3\ \text{K}$	(I.5)
1000	$300.7\ \text{K} \leq T_2 \leq 301.3\ \text{K}$	

The derivative computed from this data could fall anywhere in the range: 0.8 K/hr to 3.2 K/hr. An estimate that crude would have little or no practical value.

Consider the following data, containing the same uncertainty:

Time	Temperature Range (K)	
0730	$295.7 \leq T_1 \leq 296.3$	(I.6)
1200	$204.7 \leq T_2 \leq 305.3$	

The computed value of $\frac{\partial T}{\partial t}$ falls in the range: 1.87 K/hr to 2.31 K/hr. This estimate is useful.

The above is an example of the problem of subtraction of nearly-equal approximate quantities. The relative error in the quantities can be greatly magnified. Finite-difference approximation of derivatives is a numerically sensitive process because of this property of subtraction.

An implicit assumption was made in the discussion of the second set of data: we assumed that the time derivative of temperature remained essentially constant for several hours. There is no *a priori* justification for that assumption; in fact, it is unlikely to be strictly true. Conte and De Boor (1972) demonstrate that the centered-difference approximation to $\frac{\partial T}{\partial t}$ has an error:

$$E = \left(-\frac{h^2}{6}\right) \left(\frac{\partial^3 T}{\partial t^3}\bigg|_{t=t^*}\right) \tag{I.7}$$

where

$$|t_2 - t_1| = 2h \tag{I.8}$$

t* is some (unknown) time in the interval (t_1, t_2), and T(t) must have three time derivatives throughout the interval. The error increases as the square of the time interval between observations.

There is a trade-off between the accuracy of the centered-difference formulation and the numerical error introduced by subtraction of nearly-equal approximate quantities. In the situation encountered in this thesis, the errors from the subtraction are the more serious.

I.2 REGRESSION, CURVE-FITTING, AND APPROXIMATE DATA

Curve-fitting is a common problem in science. An experiment or simulation provides data, and the investigator wishes to express the data as a mathematical function. However:

1) The data are not available for all possible experimental conditions.

2) The data invariably contain some error or uncertainty.

The investigator would like to obtain a mathematical result of general applicability which is consistent with the experimental or simuluated data. She is willing to accept a function which merely approximates the data collected from one series of experiments or simulations if that function will provide a good fit to data from similar experiments or simulations.

The one-dimensional case will be considered here: Given a set of ordered pairs $\{(x_i, y_i)\}$, determine a function $y = f(x)$ that corresponds to these ordered pairs in some fashion which can be called a 'best fit.' The description is intentionally vague, at this point. Similar results can be obtained for n-dimensional spaces. The interested reader should consult intermediate to advanced numerical analysis or approximation theory texts (example: Davis, 1965). The n-dimensional case can be proved using the techniques of Hilbert space.

There exists a polynomial $y = p(x)$ of degree at most n, which passes through any n + 1 points (x_o, y_o), (x_1, y_1) ..., (x_n, y_n) where $x_0 < x_1 < \ldots < x_n$. It is not clear that p(x) is the best polynomial representation of the data. Consider Figure I.1 (Figure 4.8 from Conte and De Boor (1972)). It is exceedingly unlikely that any investigator would use a tenth-degree polynomial to fit this data, even though there is a tenth degree polynomial that interpolates it perfectly. Instead, a linear function was selected in Conte and de Boor. The investigator would assume that the small, seemingly random deviations from the straight line in Figure I.1 represent error; she would discount the possibility that the universe incorporates tenth-degree corrections to linear relationships.

Linear regression and least-squares curve fitting are formal techniques for defining and obtaining a 'best fit' to data. Both methods attempt to fit data by minimizing the sum of the squares

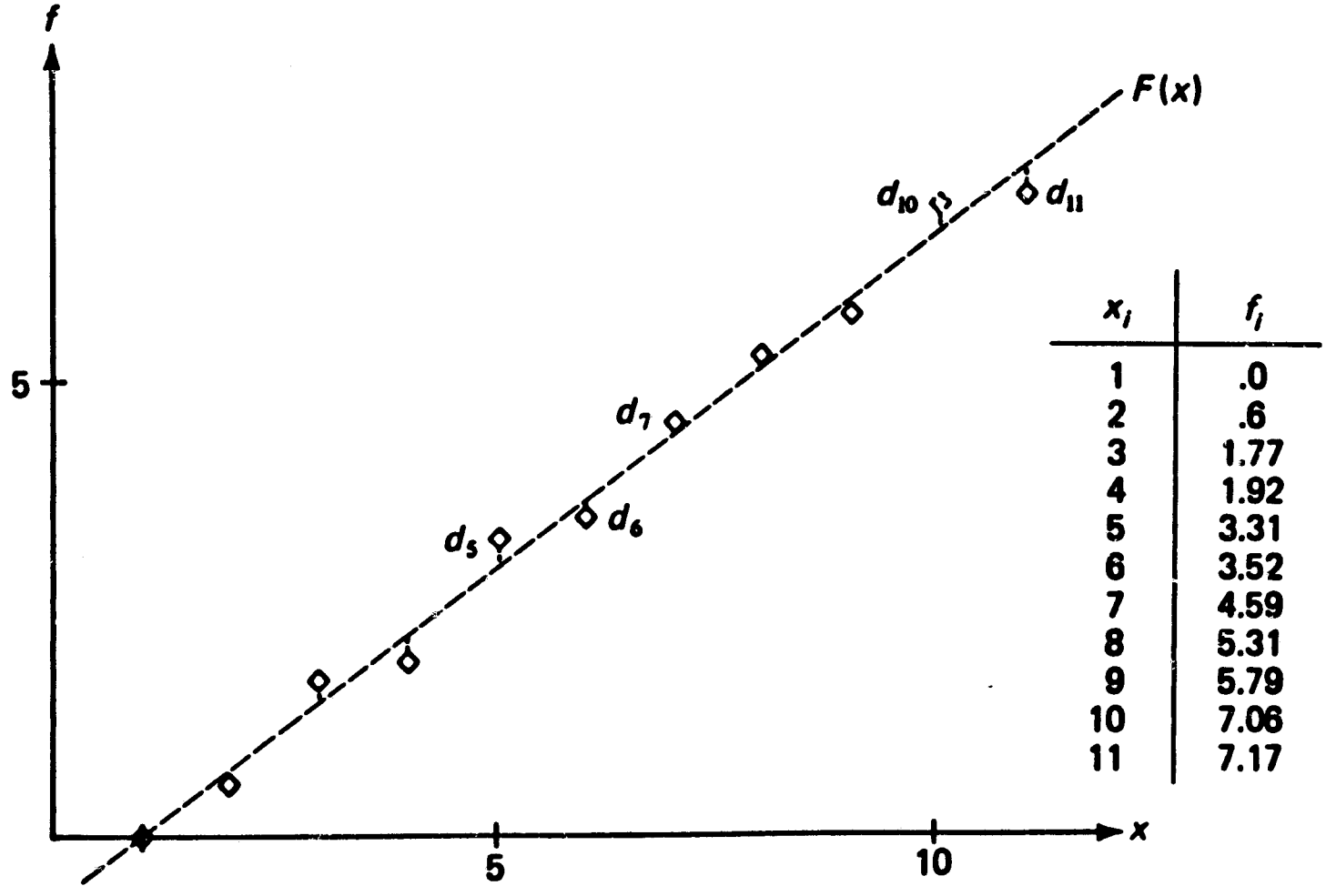

x_i	f_i
1	.0
2	.6
3	1.77
4	1.92
5	3.31
6	3.52
7	4.59
8	5.31
9	5.79
10	7.06
11	7.17

Least-squares straight-line approximation to certain data.

Figure I.1: Conte and De Boor (1972), Fig. 4.8.

of the 'error,' or distance from a data point to the best-fit curve. Multi-variable linear regression approximates the data via a linear equation in many unknowns. Curve-fitting approximates the data via a function, generally nonlinear, selected from a family of simple functions. A commonly-used family of functions is the polynomials; trigonometric functions or exponentials are sometimes used. Since the polynomials form a linear space, curve-fitting by polynomials is mathematically equivalent to multi-variable linear regression.

One hardly needs mathematical formalism to deal with Figure I.1. Consider, however, example 4.21 from Conte and de Boor (1972), presented in Table I.1. Twenty-one data points are available. These data are to be fit by a polynomial. A 20th-degree polynomial can, in principle, be found to interpolate the data. The interpolating polynomial, once obtained, would have a least-squares error of zero. However, the 20th-degree polynomial could not be found using simple algorithms on a computer. Computer truncation error would contaminate the result. Even if the 20th-degree polynomial could be obtained, it would be a poor choice as an approximant. The data in Table I.1 happens to be the values of e^x, rounded to the nearest 0.01. If this data were the result of a numerical simulation and the approximating polynomial were to be used as a mathematical model of this growth, the approximant would be expected to resemble e^x as closely as possible. e^x is a very smooth function. The twentieth degree interpolant to the rounded values of e^x is unlikely to be as smooth. Without computing the interpolating polynomial, it is not even possible to determine if it is monotonic on the interval (-1.0, 1.0).

Table I.1: Conte and De Boor (1972), Table 4.3.

Computer results for Example 4.21

x_n	f_n	$p_3^*(x_n)$	$f_n - p_3^*(x_n)$	$p_4^*(x_n)$	$f_n - p_4^*(x_n)$	e^{x_n}
−1.0	0.370	0.36387	6.130E−03	0.37115	−1.154E−03	0.36788
−0.9	0.410	0.40874	1.263E−03	0.40874	1.263E−03	0.40657
−0.8	0.450	0.45481	−4.806E−03	0.45097	−9.719E−04	0.44933
−0.7	0.500	0.50315	−3.148E−03	0.49804	1.964E−03	0.49659
−0.6	0.550	0.55484	−4.836E−03	0.55021	−2.134E−04	0.54881
−0.5	0.610	0.61094	−9.436E−04	0.60789	2.108E−03	0.60653
−0.4	0.670	0.67254	−2.542E−03	0.67156	−1.565E−03	0.67032
−0.3	0.740	0.74070	−7.045E−04	0.74183	−1.832E−03	0.74082
−0.2	0.820	0.81650	3.497E−03	0.81940	6.029E−04	0.81873
−0.1	0.900	0.90101	−1.010E−03	0.90507	−5.070E−03	0.90484
0.0	1.000	0.99530	4.701E−03	0.99976	2.358E−04	1.00000
0.1	1.110	1.10044	9.558E−03	1.10450	5.499E−03	1.10517
0.2	1.220	1.21751	2.490E−03	1.22040	−4.045E−04	1.22140
0.3	1.350	1.34758	2.422E−03	1.34871	1.294E−03	1.34986
0.4	1.490	1.49172	−1.717E−03	1.49074	−7.399E−04	1.49182
0.5	1.650	1.65100	−1.000E−03	1.64795	2.052E−03	1.64872
0.6	1.820	1.82650	−6.499E−03	1.82188	−1.876E−03	1.82212
0.7	2.010	2.01929	−9.287E−03	2.01418	−4.176E−03	2.01375
0.8	2.230	2.23044	−4.368E−04	2.22660	3.397E−03	2.22554
0.9	2.460	2.46102	−1.020E−03	2.46102	−1.020E−03	2.45960
1.0	2.720	2.71211	7.890E−03	2.71939	6.061E−04	2.71828

The interpolant would be a very poor choice of function for extrapolation outside the interval (-1, 1). It would probably not represent the derivative of e^x well. The twentieth degree interpolating polynomial overfits the data; it faithfully reproduces the noise in the data so well that the signal tends to be obscured.

What degree of polynomial best fits the data? The pragmatist would examine Figure I.2, after Conti and de Boor (1972), Figure 4.9. Graphs (a), (b), and (c) are relatively smooth. Graph (a) certainly has a linear component, although it does exhibit some curvature. Graphs (b) and (c) resemble a quadratic and a cubic, respectively. In each case, the error graph resembles a polynomial of degree one higher than the degree of least-squares approximating polynomial whose error is being graphed. Graph (d) displays considerable oscillation, but the relative maxima at -1, 0.1, and 1 suggest a quartic component. Graphs (e) and (f) show virtually no regular pattern; they are pure noise. The fourth-degree polynomial (error graph (e)) fits the data as well as it can be fit. Note that 21 data points were used to obtain a fourth-degree polynomial. Five points uniquely determine a quartic.

The threshold at which overfitting begins depends on:

1) the quality of the data
2) The underlying function or physical law governing the data

The more error the data contains, the more likely that overfitting will occur. To minimize the squares the distance between

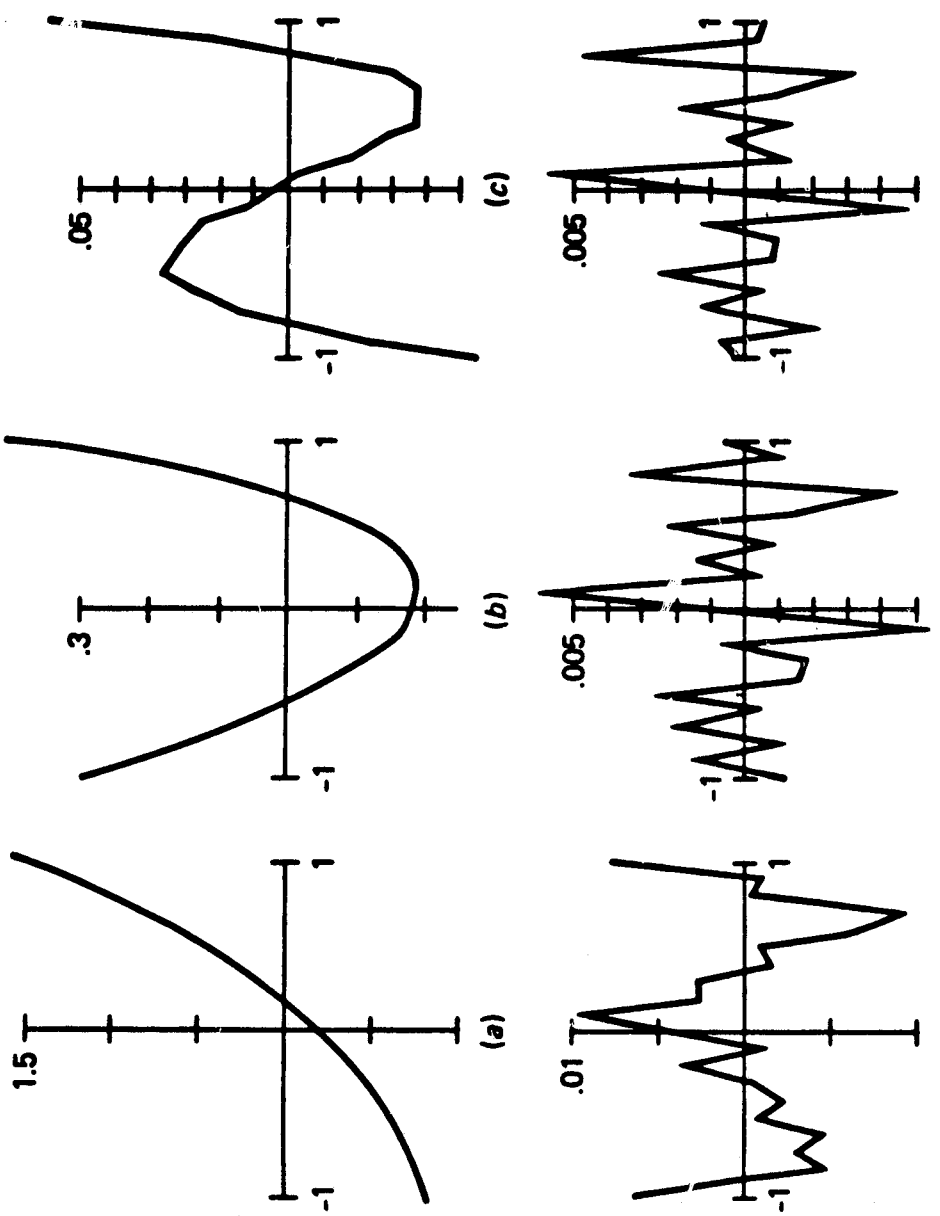

The error in the least-squares approximation to the data of Example 4.21 by polynomials of degree (a) zero, (b) one, (c) two, (d) three, (e) four, (f) five.

Figure I.2: Conte and De Boor (1972), Fig. 4.9.

the data points and the approximating curve, the curve will be adjusted toward the data points. If the data points are scattered due to random errors, the curve may tend to oscillate away from the underlying function in order to approach the error-laden data points. By using a lower-degree polynomial as the least-squares approximant, this oscillatory behavior is suppressed. The number of local maxima, local minima, and inflection points of a polynomial is limited by the degree of the polynomial. The data is fit less well in this case, but the underlying function and its derivatives are fit better.

Sensitivity studies on the original (Carlson and Boland, 1978) model indicate that M and P vary smoothly as functions of day and night temperature. Model output probably contains errors on the order of 1 K. Overfitting the model output by a polynomial is a real possiblility. Regression equations of high degree or regressions using many temperatures as predictors should be avoided. Another possible course of action, piecewise-linear interpolation in two variables, is presented in Appendix II.

APPENDIX II: PIECEWISE LINEAR INTERPOLATION IN TWO DIMENSIONS

II.1 THEORETICAL OVERVIEW

Piecewise-polynomial interpolation is an alternative to global least-squares regression for mathematically inverting the numerical model in the GOES method. The simplest case of piecewise-polynomial interpolation is piecewise-linear interpolation. Piecewise-linear interpolation has the advantage of simplicity over higher-order methods. However, to obtain an equivalent degree of fit to the data, additional data points will be needed. Thus, more than 16 (M, P) pairs may be needed in a piecewise-linear interpolation scheme. Model computation time is proportional to the number of (M, P) pairs.

Consider a piecewise-linear interpolation scheme for diagnosing M from the two variables (predictors) DTD and DTN. M can be considered to be a function of the two variables DTD and DTN. If M(DTD, DTN) is multi-valued, this scheme and the regression scheme will fail. Therefore, assume that M(DTD, DTN) is single-valued. M(DTD, DTN) is a surface in (DTD, DTN, M) space. A piecewise-linear approximation to this surface consists of a number of planar segments lying "close" to the surface. A piecewise-linear interpolant to the surface at n specified (DTD, DTN) pairs is a

set of planar segments intersecting the M(DTD, DTN) surface at each of the n specified (DTD, DTN) values. If M(DTD, DTN) is not multi-valued, each planar segment can be expressed as an equation of the form:

$$M = a_i DTD + b_i DTN + c_i \qquad \text{(II.1)}$$

The ith equation will be valid over the ith planar segment.

Piecewise-linear interpolation in two dimensions, unlike global polynomial interpolation in one dimension, is not unique. Given a set of n (DTD, DTN, M) ordered triplets, where $n > 3$, there are, in general, several sets of planar segments interpolating the set of points.[1] A reasonable set of linear functions must be selected. Consider Figure II-1. Assume that the 16 points graphed in the (DTD, DTN) plane represented 16 data points from a model run.[2] Each point is associated with an M value, which is not plotted.

I now address the problem of selecting the linear functions. Note that three points determine a plane. To find a piecewise-linear interpolant to the function M(DTD, DTN) over the domain defined by the points shown in Figure II.1A, it is sufficient to

---

[1] Global polynomial interpolation in higher-dimensional spaces is unique, if the correct number of points is chosen. Linear interpolation with two predictors is unique if three data points are chosen.

[2] Sixteen data points from an actual model run are presented in Figure II-2. Note that the data points are close together at low values of DTD and DTN. The M and P values used in the model run were M and P values appropriate for the regression routine. To obtain a more uniform distribution of data points in the (DTD, DTN) plane for a piecewise-linear interpolation routine, different M and P values should be selected.

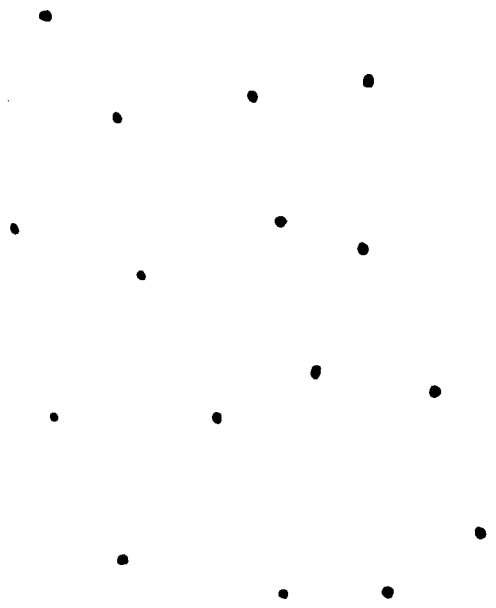

A

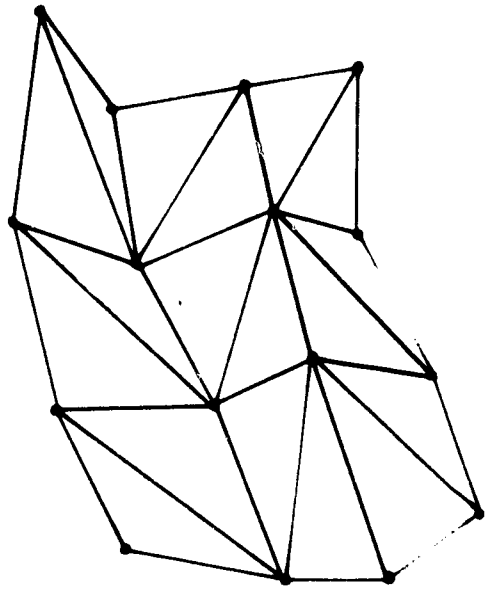

B

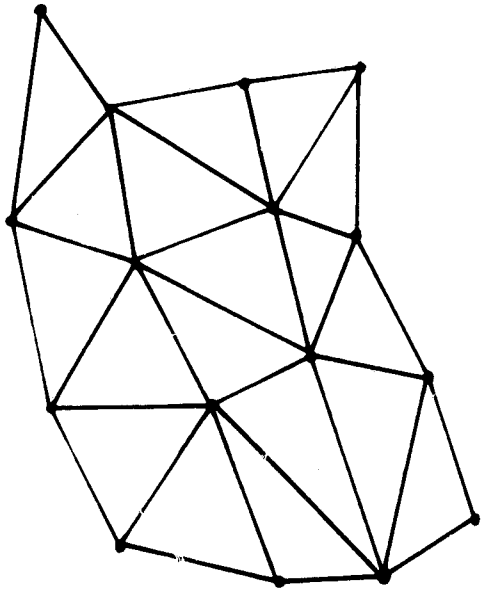

C

A: A set of points

B: A poor triangulation

C: A better triangulation

Figure II.1: An example of triangulation.

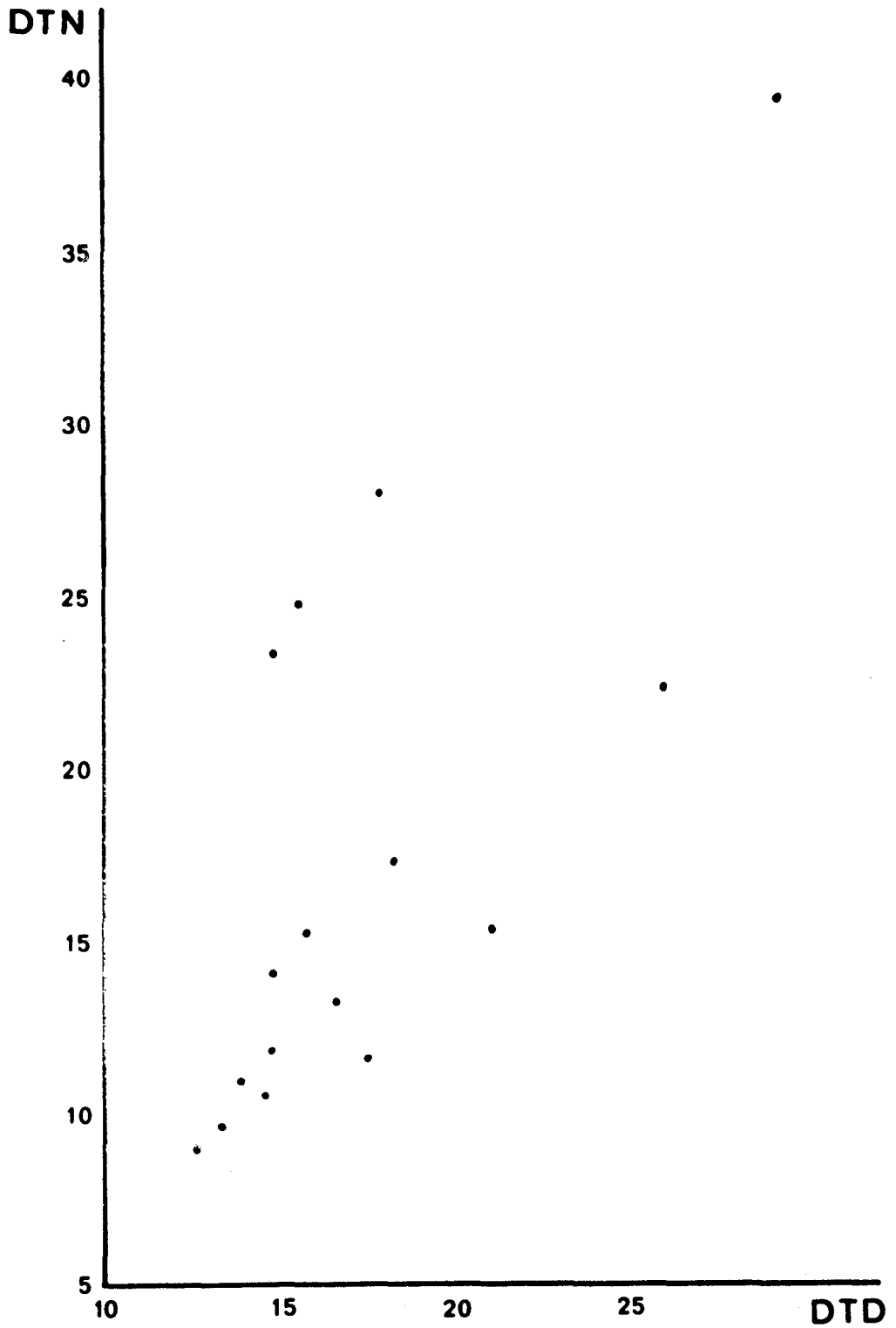

Figure II.2: Sixteen (DTD, DTN) pairs from a model simulation of the Kansas case (Section 4.3). Model initialization time was 0400 local time. Simulated GOES times were 0800, 1400, and 2300 local time.

break up that domain into triangles and find planar functions over each triangle. Two ways of triangulating the region are presented in Figures II.1B and II.1C. The pattern shown in Figure II.1C is preferred, since the largest angle in each triangle is as small as possible. Once the region has been triangulated, the functions are relatively easy to find. At each vertex, (DTD, DTN, M) are known. Combine the three ordered triplets to obtain an equation of the form of Eq. II.1.

When this is done for all the triangles in the region, a piecewise-linear interpolant for M(DTD, DTN) over the domain will have been generated. Note that the interpolant is continuous at all points in the domain, but its derivatives fail to exist at the intersection of triangles. Since we have little interest in the derivatives of M with respect to DTD or DTN, we can accept the result.

II.2 PRACTICAL CONSIDERATIONS

In the example of II.1, the domain contained 16 (DTD, DTN) points. These points determined 18 triangles. The number of triangles needed to triangulate the domain increases faster than the number of data points included in the domain. We will assume that a fast algorithm for obtaining the coefficients a_i, b_i and c_i in Eq. II.1 is available. The main practical problems are:

1) triangulating the region efficiently
2) given a (DTD, DTN) pair from satellite data, selecting the triangle containing the (DTD, DTN) pair quickly

The second problem cannot be finessed via lookup tables as was done in the GOES method and CD. Lookup tables could be used in those methods because:

1) a global regression equation was used
2) the variables DTD and DTN never appeared together in a term in the global equation

The piecewise-linear method meets the second criterion, but fails to meet the first. Since the domain is divided into irregular triangles and not rectangles, there is no hope of developing a simple lookup-table algorithm.

The region could be triangulated interactively, if desired. After the model has completed execution, the (DTD, DTN) data points could be displayed graphically. The operator could then enter triplets of points, defining triangles. The resulting triangles could then be displayed on the graphics terminal for verification. An option to delete points from the domain should be provided, since the model may generate several nearly coincident (DTD, DTN) pairs at high values of M and P. Another alternative would be automated selection of triangles. The automated selection could be preceded by an interactive opportunity to delete points from the domain, and followed by an interactive opportunity to revise the computer's choices. If a sufficiently robust triangulation routine can be developed, the entire triangulation procedure could be automated.

The efficiency of selecting the proper triangle (and thus the proper coefficients a_i, b_i, and c_i) will depend on the data structure used to store the triangles, and the amount of storage space that can be used for redundant information. Since 16384 (DTD, DTN) pairs must be processed per image, storage should be sacrificed to improve efficiency. The triangle-selector and output-field builder should be combined: they should be in the same job step. All desired output fields should be built concurrently, to avoid the necessity for searching more than once for the triangle containing a particular (DTD, DTN) value. For four output variables, 2K (2048 bytes) of storage will be needed to hold output fields. Storage requirements for the piecewise-linear approximant should be modest: 12 coefficients plus four output variables, or 64 bytes per triangle. The data structure used to select the proper triangle can occupy most of the remaining core, if needed.

The piecewise-linear inversion method should run considerably slower than the global regression-equation inversion method. No estimate is possible until the details of the triangle selection method are specified. Since the current inversion method takes on the order of 1-2 minutes per output field, a factor of five loss in efficiency is barely tolerable. There is reason to hope that the loss in efficiency will be less than a factor of five.

Higher-degree piecewise-polynomial interpolants can be defined over a two-dimensional domain, but they have little or no

applicability to the problem at hand. Higher-order interpolants would produce better approximations to the output variables with fewer (DTD, DTN) pairs from the model. However, higher-order methods suffer from two flaws:

1) One must be very careful to obtain a piecewise-polynomial approximation which is continuous at all points in the domain, and one which is never multi-valued
2) The computation time required per (DTD, DTN) pair from the satellite data rises rapidly with increasing degree of polynomial approximant

The first flaw probably can be overcome by careful programming. The second flaw appears to be unremovable. Piecewise-polynomial interpolants of degree higher than one may be practical on main-frame computers or vector-processors, but they are not practical on minicomputers.

II.3 A PIECEWISE-LINEAR INTERPOLATION ALGORITHM

The problem of selecting the triangle containing a particular (DTD, DTN) pair from satellite data is the key problem in the practical piecewise-linear algorithm. It may be possible to side-step this problem though the use of a very large lookup table, which would be built during interactive selection of triangles. The large amount of time needed to initialize the lookup table can be hidden from the user if asynchronous I/O or multitasking is used.

Under most circumstances, DTD and DTN will have ranges of less than 50 K. Since DTD and DTN have inherent uncertainties of $\pm$ 0.4 K due to the method of storing satellite images on tape (Section 3.6), little additional uncertainty would be introduced into the method by mapping DTD and DTN into the integers from 1 to 128. This mapping can be done by utility program MYCONR2, already part of the GOES method library. Alternatively, a specialized version of MYCONR2 could be written to map DTD and DTN into the integers with a minimum of additional error, using information about the original range of temperatures on the input (magnetic-tape) satellite images. The output from the specialized version of MYCONR2 could be two-byte integers instead of one-byte integers, to facilitate the use of the integer values as indices into an array. The integer-DTD and integer-DTN fields would be written to disk as DEFINE FILE files, using the same record-numbering as is used to store the DTD and DTN fields (the record sizes would differ).

(DTD, DTN) pairs generated by the numerical model would be displayed on the graphics terminal. Each (DTD, DTN) point would be represented by a distinguishing character and would be shown on the screen in its proper position in the DTD-DTN plane. While this display is being constructed, an auxiliary task would be clearing (setting to zero) a 128 by 128 array (16 K bytes) for use as the triangle-finding lookup table. This array will represent the region of DTD-DTN space of relevance to the GOES method.

After the array is cleared and all data points have been displayed, the interactive selection of triangles would begin. At this point, asynchronous I/O or multitasking becomes essential. The following description assumes multitasking. Task A, the main task, will interact with the user and accept the triangulation of the region. Task B, the subtask, will incorporate the selected triangulation into the lookup table.[1]

Task A requests the user to input the first triangle by typing the distinguishing characters of the three vertices. Task A then plots the triangle on the graphics terminal, and asks the user to accept or reject it. When the first triangle is accepted, the multitasking begins. Task A attaches Task B, and passes Task B the coordinates of the vertices of the first triangle. Task B, being able to count, knows that the vertices it has received are the vertices of the first triangle. Task B begins to fill all locations in the array corresponding to points on the edges and interior of this triangle with the integer 1 (one-byte integer, to save storage). When Task B has completed its work on triangle 1, it increments its triangle-counter, signals Task A, and goes to sleep.

---

[1] If asynchronous I/O were used, the actions performed by Task B would be interleaved with the terminal I/O in Task A. Task B actions would begin when the START I/O instruction to READ the terminal was issued. The terminal I/O event flags would be checked (and WAIT state entered, if necessary) on completion of Task B's work. Multitasking is preferred over asynchronous I/O, since multitasking simplifies the coding of efficiently-overlapping routines.

Meanwhile, Task A is asking the user to input the vertices of the second triangle. When the vertices are input, displayed, and accepted, Task A will:

1) wait for Task B's signal, if it has not been received

2) wake-up Task B and pass it the new set of vertices

3) ask the user for the next triangle

This procedure will continue until the region is completely triangulated. The user will inform Task A that the last triangle has been entered. Task A will then wait for Task B to finish setting the array locations representing the last triangle. When Task B signals, Task A will detach Task B. At this point, the 128 by 128 array could be written to disk if it is to be saved. The array is now ready to be used to locate triangles.

The linear equations for M, P, H_o, and E can be computed by Task A or by Task B during the above procedure (let the faster routine do the extra work), or they can be computed and stored after the triangulation has been completed (if storage is severaly limited). The index-numbers of the coefficients must match the index-numbers of the triangles used by Task B.

The output fields can now be generated. Under the current image-storing convention, all imagery used in the GOES method is stored in 128 by 128 arrays on disk. Each horizontal line of the image is stored in one logical record of a disk file; an image file consists of 128 data records and a control record. DTD, DTN, M, P, H_o, and E are stored as REAL*4 variables: four bytes of storage per pixel. The integer-DTD and integer-DTN fields will be

INTEGER*2 fields: two bytes per pixel. All eight fields plus the lookup table must be simultaneously resident in core. The storage requirements are:

Lookup table:	16 K	16 K
REAL*4 record:	1/2 K each	3 K
INTEGER record:	1/4 K each	1/2 K

Total storage for these fields: 19 1/2 K.

(Note that only one record of each disk file must be resident at any one time, but that the entire lookup table must be resident at all times.) Additional storage for the piecewise-linear coefficients will depend on the number of triangles used. Assume that 64 triangles are used -- probably more than will ever be used in an actual case. For each triangle, assume that three coefficients are stored for each of the four output variables. These coefficients must be REAL*4 variables. The storage requirement for the coefficients is 3*4*4*64 = 3072, or 3 K bytes. If the vertices of the triangles are to be stored, they will occupy under 1 K if stored as REAL*4, or under 1/2 K if stored as integers (coded as the integer-DTD and integer-DTN fields are coded). This additional storage requirement brings the total storage for all arrays to 23 K or 23 1/2 K of the vertices are kept; 22 1/2 K if they are discarded. The code required to perform the piecewise-linear approximation should easily fit in 4 K, allowing the job to run in a 28 K partition. (If the partition size is 32 K, an additional margin of safety exists).

The output fields are produced by a simple algorithm. A (DTD, DTN) pair is selected from the temperature-difference input files. The corresponding integer-DTD, integer-DTN pair is also selected. The (integer-DTD, integer-DTN) pair is used as an index into the lookup table. The single byte returned from the lookup table is expanded into a two-byte integer via an EQUIVALENCE statement. If this integer is zero, the (DTD, DTN) pair represents out-of-range values and is treated accordingly. If the integer is nonzero, it is the sequence number of the triangle containing the (DTD, DTN) pair. The proper coefficients are obtained for each output variable from the tables of coefficients. The output values for the four output variables are obtained by substituting the (DTD, DTN) values into the appropriate equations of the form of Eq. II-1.

Considerable care in coding will be necessary if this peicewise-linear interpolation and evaluation routine is to be implemented on a minicomputer with 32 K of storage available. The total storage requirement for the entire procedure is likely to exceed 32 K. Assume that the routine is to be implemented on the PSU Meteorology Department PDP 11/34 system. During the triangulation phase, the Grinnell driver and graphics routines will have to be resident. The DTD, DTN, M, P, H_o, and E fields will not be needed. During the output-field generation phase, the various fields will have to be resident, but the graphics package will not be needed. The lookup table and the coefficient tables will be needed at all

times. An overlay structure will have to be devised to meet these requirements; appropriate sections of code must also be overlaid. It may also be necessary to force the system to allocate the absolute minimum input and output buffer space. In particular, it may be necessary to output the four computed fields without buffering, even at the cost of extra I/O time. Unbuffered I/O probably will not be needed if the available region size is 32 K (no system overhead).

If the piecewise-linear algorithm is implemented as described above, the execution time will not seem to be much longer than the execution time for the current regression algorithm. The evaluation step (done for each output variable) entails three table lookups (to get the coefficients), two multiply instructions, and two additions. One two-dimensional table-lookup is needed (to find the triangle) for each pixel; one fourth of this overhead can be assigned to the computation of each of the four output fields. The regression routine presently uses two table lookups and one addition per pixel per output field. The computation time for the piecewise-linear routine would be approximately three times that of the regression routine. There would, however, be a savings of 512 disk reads. The DTD and DTN fields will have to be read only once each, not four times (saving 768 reads), and the new integer fields will have to be read (costing 256 reads). The initialization of the triangulation lookup table will be lengthy. However, the subjective computation time will be negligible. Most of the computation time

required for the initialization of the table will be concealed in the time spent in the interactive inputting of the triangles. The initialization will be done while the computer is waiting for the user to respond to requests for vertices. The user, busy thinking about vertices and typing on the keyboard, will be unaware of the time required for initialization of the large array. An automated procedure could be devised to select the triangles; however, if this were done, the user would become painfully aware of the length of time required to initialize the large array. The user would also lose the option to delete points and the ability to select triangles of nonoptimal shape that are desirable for other reasons.